ELSEVIER

Coordination Chemistry Reviews
170 (1998) 141–202

COORDINATION CHEMISTRY REVIEWS

Diruthenium and diosmium tetracarboxylates: synthesis, physical properties and applications

Manuel A.S. Aquino *

Department of Chemistry, St. Francis Xavier University, P.O. Box 5000, Antigonish, NS, Canada B2G 2W5

Received 20 August 1997; accepted 30 November 1997

Contents

1. Chemical abbreviations . . . 142
2. Introduction . . . 143
3. Synthesis . . . 144
   3.1. Diruthenium(II,III) complexes . . . 144
   3.2. Diruthenium(II,II) complexes . . . 145
   3.3. Diruthenium(III,III) complexes . . . 145
   3.4. Diosmium(II,III) and (III,III) complexes . . . 146
4. Crystal structures . . . 146
5. Electronic structure and spectra . . . 158
6. Vibrational spectroscopy . . . 163
7. Electron spin resonance . . . 165
8. Electrochemistry . . . 167
9. Kinetics and thermodynamics . . . 170
10. Other physical measurements . . . 172
11. Magnetic susceptibility . . . 176
   11.1. Diruthenium(II,III) systems . . . 176
   11.2. Diruthenium(II,II) systems . . . 182
   11.3. Diosmium(III,III) and (II,III) systems . . . 184
12. Mesogenic properties . . . 186
13. Anti-tumour properties . . . 188
14. Catalytic applications . . . 190
15. Conclusion . . . 191
16. Addendum . . . 191
Appendix . . . 192
References . . . 199

* Tel: +1 902 867 5336; Fax: +1 902 867 2414; e-mail: maquino@stfx.ca

PII S0010-8545(97)00079-9

Abstract

Dimetal tetracarboxylates, $[M_2(O_2CR)_4]^n$, have received much coverage in the literature. The metals include Cr, Mo, W, Tc, Re, Ru, Os, Co, Rh, Ir, Ni and Cu with *n* ranging from −2 to +4 (0 to +2 being most common). Diruthenium and diosmium tetracarboxylates form two of the younger families of these ubiquitous compounds and are known to exist as homovalent Ru_2(II,II) and Os_2(III,III) and mixed-valent Ru_2(II,III) and Os_2(II,III) species. This paper will provide a comprehensive review of these complexes and include such things as their discovery, synthesis and crystal structures; electronic, vibrational (IR and Raman), ESR and photoelectron spectroscopy; magnetic susceptibility; electrochemistry; kinetics; calorimetry; theoretical calculations such as SCF-Xα-SW and CASSCF; and more recent studies of their mesomorphic behaviour and biological and catalytic applications. The ruthenium compounds, in particular, have shown a potential application as liquid crystals. Current work (including this author's) is also focused on the development of linear chains involving these metal carboxylate units and bidentate bridges with the view to developing ferromagnetic materials and conductive polymers.

There have been no previous reviews on ruthenium (and osmium) carboxylates *per se*. Cotton and Walton give them some coverage in the context of metal–metal bonds in Multiple Bonds Between Metal Atoms (2nd ed., 1993) however the direct coverage of $Ru_2(O_2CR)_4$ and $Os_2(O_2CR)_4$ type complexes is cursory and dispersed throughout the book. As well, the coverage is only comprehensive through December 1990 with some references from 1991. The current review will be complete through to mid-1997.

1. Chemical Abbreviations

Me	methyl
Et	ethyl
Pr^n	*n*-propyl
Bu^n	*n*-butyl
Ph	phenyl
asp^-	aspirinate anion
dpf^-	diphenylformamidinate anion
fhp^-	6-fluoro-2-hydroxypyridinate anion
$mand^-$	mandelate anion
$2\text{-}PBZ^-$	2-phenylbenzoate anion
DCE	1,2-dichloroethane
DCM	dichloromethane
DM-DCNQI	bis(2,5-dimethyl-*N*,*N*′-dicyanoquinonediimine)
DMF	*N*,*N*-dimethylformamide
DMSO	dimethylsulphoxide
MeIm	*N*-methylimidazole
nitPh	2-phenyl-4,4,5,5-tetramethyl-4,5-dihydro-1*H*-imidazolyl-1-oxy-3-oxide
phz	phenazine
py	pyridine

pyz pyrazine
tempo 2,2,6,6-tetramethylpiperidine-*N*-oxyl

2. Introduction

Of all the dinuclear coordination compounds formed by the transition metals, some of the more ubiquitous are the dimetal tetracarboxylates, $[M_2(\mu\text{-}O_2CR)_4]^{n+}$ [1]. The metal (in various oxidation states) can include Cr, Mo, W, Tc, Re, Ru, Os, Co, Rh, Ir, Ni and Cu. R in most cases is an alkyl or substituted alkyl group but can also include alkoxy and aryl derivatives. The structure (for M = Ru) is shown in Fig. 1 and consists of two metals (all have metal–metal bonds except for the copper derivatives) bridged by four carboxylates which give a "lantern" or "paddle-wheel" type geometry of essentially core D_{4h} symmetry.

One of the youngest and potentially most interesting family of these compounds involve ruthenium and osmium. The ruthenium compounds are known to exist as homovalent $Ru_2(\mu\text{-}O_2CR)_4$ (Ru_2(II,II)) (Fig. 1) and as mixed-valent $[Ru_2(\mu\text{-}O_2CR)_4]^+$ (Ru_2(II,III)) in which the odd electron is delocalised between the metals and the complex can, in effect, be formulated as $Ru_2(II\frac{1}{2},II\frac{1}{2})$. The osmium complexes exist as Os_2(III,III), and mixed-valent Os_2(II,III).

Interest in these compounds, particularly the mixed-valent species, centres around their unique magnetic properties and unusual stability. The Ru_2(II,III) species contain three unpaired electrons due to an accidental near-degeneracy of the two highest lying occupied molecular orbitals, the π^* and δ^*, to give a $\sigma^2\pi^4\delta^2(\pi^*\delta^*)^3$ configuration. This quartet ground-state could potentially be exploited in the design of molecular magnetic materials. Linear chain materials can be easily constructed due to the lability of the axial positions which could readily incorporate a bridging ligand.

Also of growing interest are the liquid-crystalline properties of both Ru_2(II,II) and Ru_2(II,III) compounds in which the R groups are long-chain saturated and unsaturated fatty acids. The field of transition-metal containing liquid crystals (TMLC's) or metallomesogens is in its infancy but TMLC's have already proven themselves to be superior to their organic cousins due to the enhanced magnetic

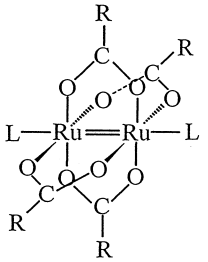

Fig. 1. Typical "lantern" structure of an $Ru_2(\mu\text{-}O_2CR)_4L_2$ adduct.

and electronic properties unique to metal ions. Ru_2(II,III) tetracarboxylates have become the first "mixed-valent" metallomesogens.

There have been no reviews of ruthenium and osmium carboxylates in the past, only overviews of their properties in the context of metal–metal bonding [2–4]. This review will attempt to draw together the steadily growing information on these compounds and in the first few sections give a comprehensive synopsis of the structural and physico-chemical properties of diruthenium and diosmium tetracarboxylates. The final sections will put these properties into the context of the current interests and applications mentioned above. A comprehensive Appendix A is also included to ease the locating of a particular complex and its relevant references. The reaction chemistry of these compounds as starting materials in the conversion to products *other than* different tetracarboxylate derivatives will not be discussed here.

3. Synthesis

3.1. Diruthenium(II,III) complexes

The first reported synthesis of a diruthenium or diosmium tetracarboxylate was reported in 1966 by Stephenson and Wilkinson [5]. They obtained the mixed-valent $Ru_2(\mu\text{-}O_2CR)_4Cl$ compound, with R = Me, Et or Pr^n, by refluxing $RuCl_3 \cdot 3H_2O$ in the appropriate carboxylic acid/acid anhydride mixtures. This synthesis was improved upon in 1973 by Wilkinson's group [6] by the addition of LiCl and oxygen to the reaction mixture. This gave yields of 80% or greater and is the method of choice to this day. An alternate technique involved the reaction of a diruthenium(III,IV) chloride intermediate with acetic acid in a steel container [7], but, the yields were not as good. Once the chloride salt has been made the bridging carboxylates can be exchanged by simply refluxing the $Ru_2(\mu\text{-}O_2CR)_4Cl$ complex in the desired carboxylic acid or solvent containing the acid or acid salt [8– 19].

Since the $Ru_2(\mu\text{-}O_2CR)_4Cl$ compounds all possess a polymeric or chain-like structure (see Section 3) in which chlorides bridge adjacent dimers it was sought to synthesize diadducts in which isolated dimers are present with two axially coordinated ligands. In many cases these ligands were solvent molecules. Diadducts of the type $[Ru_2(\mu\text{-}O_2CR)_4L_2]X$ can be synthesized from the $Ru_2(\mu\text{-}O_2CR)_4Cl$ compounds using cation exchange techniques [20,21] or by removing Cl^- as AgCl, thus leaving the axial positions open to coordination by the ligand, L [13,14,22–27] (Eq. (1)).

$$Ru_2(\mu\text{-}O_2CR)_4Cl + Ag^+ \xrightarrow[H_2O]{PF_6^-} [Ru_2(\mu\text{-}O_2CR)_4(H_2O)_2]PF_6 + AgCl \qquad (1)$$

The axial ligands include: H_2O [20,25–27], $OPPh_3$ [14,19,22,23], THF [13,14,22], pyridine [14], MeOH [10], Cl^- [20], DMSO [27] and DMF [27]. Complexes with mixed axial ligands have also been prepared such as $Ru_2(\mu\text{-}O_2CR)_4(SCN)(OPPh_3)$ [28].

3.2. Diruthenium(II,II) complexes

The air-sensitive Ru_2(II,II) complexes proved somewhat more difficult to synthesize than the mixed-valent complexes and it wasn't until 1984 that the neutral $Ru_2(\mu\text{-}O_2CCH_3)_4(THF)_2$ adduct was prepared and characterized [29]. This complex was prepared by the addition of the Grignard reagent Me_3SiCH_2MgCl (which acts as a one-electron reductant) to $[Ru_2(\mu\text{-}O_2CCH_3)_4]Cl$ in THF. Subsequent Ru_2(II,II) complexes were prepared via a more direct route involving the refluxing of a H_2 reduced "blue solution" of $RuCl_3 \cdot 3H_2O$ in the presence of excess alkali-metal carboxylate [30,31].

$Ru_2(\mu\text{-}O_2CCF_3)_4$ adducts could not be synthesized by either of the above routes and required prolonged reflux of $Ru_2(\mu\text{-}O_2CCH_3)_4$ in $CF_3CO_2H/(CF_3CO)_2O$ mixtures in the presence of excess $Na(O_2CCF_3)$. In essence this is a modified carboxylic acid exchange reaction.

Four additional methods have been employed, for preparing specific compounds, with varying degrees of success. The first involves preparation of $Ru_2(\mu\text{-}O_2CPr^n)_4$ by the reduction of $Ru_2(\mu\text{-}O_2CPr^n)_4Cl$ in methanol/water using $CrCl_2$ [32]. The second method involved conversion of a tetra-aspirinato complex $Ru_2(\mu\text{-asp})_4Cl$ to the nitrosyl adduct $[Ru_2(\mu\text{-asp})_4(NO)] \cdot 4H_2O$ by heating the former at 70 °C in methanol in the presence of $AgNO_3$ [12]. Another preparation reacts $Ru_2(\mu\text{-}O_2CCH_3)_4Cl$ with L-mandelic acid to give $Ru_2(\mu\text{-L-mand})_4 \cdot 2H_2O$ [33]. In all three of the above cases further $Ru_2(\mu\text{-}O_2CR)_4$ complexes could be formed using a carboxylate exchange process. Recently a fourth route has been used to prepare an adamantylcarboxylato diruthenium(II,II) complex which involves the reaction of 1-adamantylcarboxylic acid with $K_3Ru_2(CO_3)_4$ in a (1:4) methanol/water solution [34]. In these last two syntheses the method of reduction is not entirely clear but appears to involve a disproportionation reaction (for example see Eq. (2)).

$$6Ru_2(\mu\text{-mand})_4Cl + 8H_2O \rightarrow 3Ru_2(\mu\text{-mand})_4 + 2[Ru_3O(\mu\text{-mand})_6(H_2O)_3]Cl + HCl \quad (2)$$

In the latter case an $Ru_2(\mu\text{-adamantyl})_4(CO_3)$ intermediate is presumably formed and disproportionates rapidly [34].

The vast majority of Ru_2(II,II) complexes exist as diadducts of the form $Ru_2(\mu\text{-}O_2CR)_4L_2$, where L = THF [29–31], H_2O [21,30], benzoic acid [8], NO [31,35], MeOH [34] and tempo [36] (tempo = 2,2,6,6-tetramethylpiperidine-*N*-oxyl). A diadduct with mixed ligands, $[Ru_2(\mu\text{-}O_2CCPh_3)_4(H_2O)(EtOH)] \cdot 2EtOH$, has been prepared by carboxylate exchange using $Ru_2(\mu\text{-mand})_4(H_2O)_2$ as the starting material [37].

3.3. Diruthenium(III,III) complexes

To date, no Ru_2(III,III) tetracarboxylate has been synthesized. An early report of two hexacarboxylatodiruthenium(III,III) complexes $[Ru_2(\mu\text{-}O_2CCH_3)_4(O_2CCH_3)_2] \cdot H_2O$ and $[Ru_2(\mu\text{-}O_2CCH_3)_2(\mu\text{-}O_2CCF_3)_2(O_2CCF_3)_2]$ [26,38] was later

proven in error and the compounds were reformulated by Cotton *et al.* as $[Ru_2(\mu\text{-}O_2CCH_3)_4(O_2CCH_3)_2H]\cdot 0.7H_2O$ and $Ru_2(\mu\text{-}O_2CCF_3)_4(O_2CCF_3)$, respectively [11], both Ru_2(II,III) species. Analogous complexes in which both rutheniums exist in the 3+ oxidation state have been synthesized recently. Two of these are the *N*,*N*′-diphenylformamidinato (dpf) dimer, $Ru_2(\mu\text{-dpf})_4(C{\equiv}CC_6H_5)_2$ [39] and the edge-sharing bioctahedral $[Ru_2(\mu\text{-}O_2CC_6H_4\text{-}p\text{-}X)_4(1\text{-MeIm})_4](ClO_4)_2$ where X = OMe or Me and 1-MeIm = 1-methylimidazole [40].

3.4. Diosmium(II,III) and (III,III) complexes

Unlike the diruthenium tetracarboxylates, diosmium tetracarboxylates were not synthesized until 1981 [41] and the literature on them has remained sparse. The preparation of $Os_2(\mu\text{-}O_2CCH_3)_4Cl_2$, an Os_2(III,III) complex, was achieved by reacting Na_2OsCl_6 in an acetic acid/acetic anhydride solution containing some HCl. As with the ruthenium analogues, carboxylate exchange can be afforded by refluxing $Os_2(\mu\text{-}O_2CCH_3)_4Cl_2$ in the desired carboxylic acid [42,43]. The bromide salts of the tetrapropionate and tetrabutyrate-bridged species have also been prepared [44].

The first mixed-valent diosmium complexes were synthesized in 1984 by reducing $Os_2(\mu\text{-}O_2CR)_4Cl_2$ (R = Et or Pr^n) using cobaltocene as the reducing agent. This reaction produces $[(\eta^5\text{-}C_5H_5)_2Co][Os_2(\mu\text{-}O_2CR)_4Cl_2]$ [45]. Unlike the diruthenium analogues, the diosmium complexes are virtually insoluble in most solvents.

4. Crystal structures

The first crystal structure of a diruthenium tetracarboxylate was elucidated by Cotton *et al.* in 1969 [46]. The complex, $Ru_2(\mu\text{-}O_2CPr^n)_4Cl$, was found to have a Ru–Ru bond length of 2.281(4) Å. It was also found that the chloride ions served as bridges, linking together adjacent $[Ru_2(\mu\text{-}O_2CPr^n)_4]^+$ units in an infinite zigzag chain (Fig. 2).

To date, there have been over 50 structures of Ru_2(II,III) and Ru_2(II,II) complexes reported. Only four structures exist for Os_2(III,III) species and no structure has yet been published for a mixed-valent diosmium tetracarboxylate. The X-ray crystallographic and structural parameters for these complexes are given in Table 1. All of the Ru_2(II,III) compounds of the type $Ru_2(\mu\text{-}O_2CR)_4X$ (where X = halide) show a linear or bent chain structure. Which of these forms the chain will assume is not predictable from the nature (e.g. steric bulk) of the R substituent, since complexes with R = Pr^n, Ph, C_6H_4-*p*-OMe and $[(CH_3)(C{=}CH_2)]$ [15,46,53,54] display bent, zigzag chains (cf. Fig. 2) with Ru–Cl–Ru bond angles ranging from 117.8° to 125.4° while complexes with R = CH_3, Et and C[(Me)(Ph)$_2$] [16,20,48–50] manifest linear chains. The complex with R = H and X = Br^- is exceedingly bent with Ru–Br–Ru = 110° [47]. Other structurally characterized chain compounds containing anionic bridges other than halides, including $[Ru_2(\mu\text{-}O_2CCH_3)_4(O_2CCH_3)]H\cdot 0.7H_2O$ [11], $[Ru_2(\mu\text{-}O_2CCH_3)_4(HPhPO_2)_2]H$ and $[Ru_2(\mu\text{-}O_2CCH_3)_4(HPhPO_3H)_2]H\cdot H_2O$ [24], contain significant hydrogen bonding that link together axial acetate, phenylphosphi-

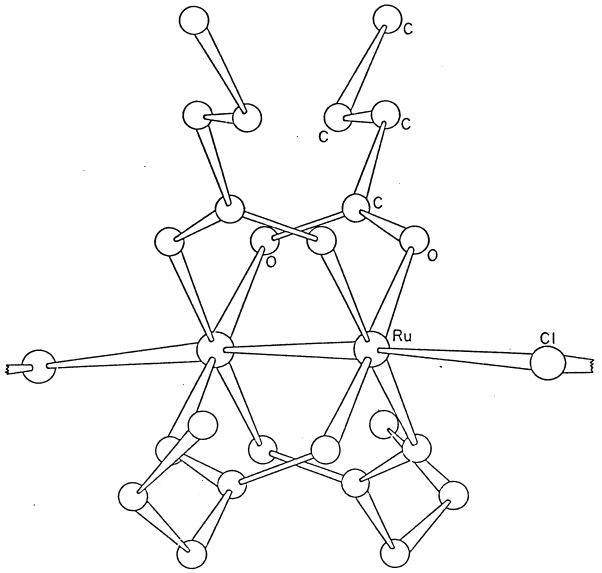

Fig. 2. Structure of the $[Ru_2(\mu\text{-}O_2CPr^n)_4Cl]$ chain complex. Adapted from Ref. [46].

nate and phenylphosphonate groups on neighbouring dimer units forming essentially linear chains (Fig. 3(a)). An example of a chain compound in which there are distinct bonds between the bridging ligand and adjacent dimers is $[Ru_2(\mu\text{-}O_2CEt)_4(O_2CEt)]$ [11]. Here one of the propionates spans the dimer units leading to an infinite linear chain (Fig. 3(b)). Similarly, $[Ru_2(\mu\text{-}O_2CPh)_4(O_2CPh)]\cdot(HO_2CPh)$ [8] and $[Ru_2(\mu\text{-}O_2CCF_3)_4(O_2CCF_3)]$ [11] contain interdimer bridging carboxylates that lead to linear chains. Another category of polymers contain neutral linkers. Both $[Ru_2(\mu\text{-}O_2CEt)_4(phz)](BF_4)$ [21] and $[Ru_2(\mu\text{-}O_2CBu^t)_4(nitPh)](BF_4)$ [52] have a bent chain structure. The reasons for this in the former are not clear and have been attributed to intermolecular packing forces. In the latter case the nature of the nitPh bridge forces the chain to be non-linear (Fig. 4).

Recently the structures of four non-polymeric chlorotetracarboxylates have been reported with various solvent molecules occupying the second axial position. These include $Ru_2(\mu\text{-}O_2CCH(CH_3)_2)_4(Cl)(THF)$, $Ru_2(\mu\text{-}O_2CC(CH_3)_3)_4(Cl)(H_2O)$ [18], $Ru_2(\mu\text{-}O_2CCH(CH_3)_2)_4(Cl)(OPPh_3)$ [28] and $[Ru_2(\mu\text{-}O_2CC_4H_4N)_4(Cl)\text{-}(THF)]\cdot THF\cdot H_2O$ [17] where $(O_2CC_4H_4N)^- =$ pyrrole-2-carboxylate (Fig. 5). The R group in all these cases is rather bulky but this in itself does not explain the reason for the lack of polymer formation [28]. Structures for the non-polymeric diadducts of the form $[Ru_2(\mu\text{-}O_2CR)_4L_2]^{+/0}$ where L is often solvent are more frequent and exist for both Ru_2(II,III), where the counterion is often BF_4^- or PF_6^-, and Ru_2(II,II) states (Fig. 6).

The Ru–Ru bond lengths in all of the Ru_2(II,III) complexes display only small deviations with the nature of both the bridging carboxylate and the axial

Table 1
X-ray crystal structure data for diruthenium and diosmium tetracarboxylates

$M_2(\mu\text{-}O_2CR)_4L_n$	Crystal system	Space group	Z	M–M (Å)	M–O (Å)	M–O (Å)	M–L (Å)	Ref.
Ru_2(II,III) compounds								
$Ru_2(\mu\text{-}O_2CH)_4Br$	monoclinic	$P2_1/c$	4	2.2899(7) 2.2901(7)	2.023(5) 2.024(5) 2.027(5) 2.023(4)	2.030(5) 2.025(5) 2.024(5) 2.028(5)	2.7170(8) 2.7313(9)	[47]
$K[Ru_2(\mu\text{-}O_2CH)_4Cl_2]$	tetragonal	$P4_2/n$	4	2.290(1)	2.016(5) 2.034(5)	2.010(5) 2.024(5)	2.517(2)	[20]
$Ru_2(\mu\text{-}O_2CCH_3)_4Cl$	monoclinic	C2/c	4	2.281(3)	2.03(1) 2.03(1)	2.04(1) 2.01(1)	2.571(4)	[48]
$Ru_2(\mu\text{-}O_2CCH_3)_4Cl$	monoclinic	C2/m	2	2.287(2)	2.019(5)	2.014(5)	2.577(1)	[49]
$Ru_2(\mu\text{-}O_2CCH_3)_4Cl \cdot 2H_2O$	monoclinic	C2/m	2	2.267(1)	2.016(4)	2.022(4)	2.566(1)	[20]
$Cs[Ru_2(\mu\text{-}O_2CCH_3)_4Cl_2]$	tetragonal	$P4_2/m$	4	2.286(2)	2.02(1) 2.02(1)	2.02(1) 2.01(1)	2.521(4)	[20]
$[Ru_2(\mu\text{-}O_2CCH_3)_4(H_2O)_2](BF_4)$	monoclinic	Cc	4	2.248(1)	2.02(2) 2.06(2) 1.90(2) 1.99(2)	2.05(2) 2.02(2) 2.01(2) 1.97(2)	2.34(1) 2.27(1)	[20]
$[Ru_2(\mu\text{-}O_2CCH_3)_4(H_2O)_2](BF_4)$[a]	monoclinic	C2/c	4	2.248(1)	2.008(5) 2.025(5)	1.998(6) 2.002(6)	2.310(6)	[50]
$[Ru_2(\mu\text{-}O_2CCH_3)_4(H_2O)_2](PF_6) \cdot 3H_2O$	monoclinic	C2/c	4	2.2648(9)	2.023(4) 2.039(3)	2.018(4) 2.026(3)	2.279(4)	[27]

$[Ru_2(\mu\text{-}O_2CCH_3)_4(DMSO)_2](PF_6)$	triclinic	$P\bar{1}$	2	2.274(1) 2.268(1)	2.017(5) 2.035(5) 2.024(5) 2.028(5)	2.025(5) 2.025(5) 2.017(5) 2.030(5)	2.240(5) 2.243(5)	[27]
$[Ru_2(\mu\text{-}O_2CCH_3)_4(DMF)_2](PF_6)$	orthorhombic	$P2_12_12_1$	4	2.262(3)	1.999(14) 2.003(13) 2.004(13) 2.009(13)	1.998(12) 2.002(13) 2.005(14) 2.015(12)	2.22(2) 2.22(2)	[27]
$[Ru_2(\mu\text{-}O_2CCH_3)_4(DMF)_2](PF_6)\cdot DMF$	monoclinic	$P2_1/c$	4	2.265(2)	2.021(13) 2.052(13) 2.009(13) 2.023(14)	2.009(14) 2.00(2) 2.006(13) 1.969(14)	2.229(14) 2.229(13)	[27]
$[Ru_2(\mu\text{-}O_2CCH_3)_4(OPPh_3)_2](PF_6)\cdot DCE$	triclinic	$P\bar{1}$	2	2.267(1)	2.014(6) 2.018(6)	2.018(6) 2.030(6)	2.227(4)	[23]
$[Ru_2(\mu\text{-}O_2CCH_3)_4(CH_3CO_2)]H\cdot 0.7H_2O$[b]	triclinic	$P\bar{1}$	2	2.265(1)	2.018(5) average		2.243(6) average	[38,11]
$[Ru_2(\mu\text{-}O_2CCH_3)_4(HPhPO_2)_2]H$	triclinic	P1	1	2.272(1)	2.026(2) 2.026(2)	2.021(2) 2.017(2)	2.214(2)	[24]
$[Ru_2(\mu\text{-}O_2CCH_3)_4(PhPO_3H)_2]H\cdot H_2O$	monoclinic	$P2_1$	2	2.267(2)	2.03(1) 1.99(1) 2.03(1) 2.04(1)	1.99(1) 2.02(1) 2.04(1) 2.01(1)	2.24(1) 2.22(1)	[24]
$Ru_2(\mu\text{-}O_2CEt)_4Cl$	tetragonal	$I\bar{4}$	2	2.292(7)	1.92(3)	2.04(2)	2.566(4)	[20]
$Ru_2(\mu\text{-}O_2CEt)_4Cl$[c]	tetragonal	I4/m	2	2.274(9)	2.013(7)		2.575(7)	[50]
$Ru_2(\mu\text{-}O_2CEt)_4(O_2CEt)$	orthorhombic	$P2_12_12_1$	4	2.273(1)	2.013(12) 2.032(12) 1.995(12) 2.010(13)	2.026(15) 2.008(13) 2.017(15) 1.979(10)	2.157(10) 2.172(10)	[11]

Table 1 (*continued*)

$M_2(\mu\text{-}O_2CR)_4L_n$	Crystal system	Space group	Z	M–M (Å)	M–O (Å)	M–O (Å)	M–L (Å)	Ref.
$[Ru_2(\mu\text{-}O_2CEt)_4(phz)](BF_4)$	triclinic	$P\bar{1}$	2	2.2756(6)	2.011(5) 2.010(4)	2.016(5) 2.027(4)	2.436(4)	[21]
				2.2747(7)	2.009(3) 2.013(4)	2.015(3) 2.004(4)	2.443(5)	
$Ru_2(\mu\text{-}O_2CPr^n)_4Cl$	tetragonal	$I\bar{4}2m$	8	2.281(4)	2.04(2) 1.96(2)	2.00(2) 2.00(2)	2.587(5)	[46]
$Ru_2(\mu\text{-}O_2CCH(CH_3)_2)_4(Cl)(THF)$	monoclinic	$P2_1/m$	2	2.272(2)	2.00(1)	2.02(2)	2.445(6) (Ru–Cl)	[18]
					2.00(2)	2.01(1)		
					2.00(1)	2.02(2)	2.37(2) (Ru–THF)	
					2.00(2)	2.01(2)		
$Ru_2(\mu\text{-}O_2CCH(CH_3)_2)_4(Cl)(OPPh_3)$	monoclinic	$P2_1/n$	4	2.279(1)	2.030(8)	2.004(8)	2.490(4) (Ru–Cl)	[28]
					2.022(8)	2.027(8)		
					2.036(7)	2.001(8)	2.249(9) (Ru–$OPPh_3$)	
					2.029(7)	2.016(9)		
$Ru_2(\mu\text{-}O_2CBu^t)_4(Cl)(H_2O)$	triclinic	$P\bar{1}$	1	2.274(2)	2.021(6)	2.014(7)	2.486(7) (Ru–Cl/O)	[18]
					2.024(7)	2.018(7)		
$[Ru_2(\mu\text{-}O_2CBu^t)_4(tempo)_2]$- $[Ru_2(\mu\text{-}O_2CBu^t)_4(H_2O)_2](BF_4)$	triclinic	$P\bar{1}$	1	2.273(1)	2.026(3)	2.028(3)	2.184(3) (Ru–tempo)	[51]
				(tempo)	2.015(3)	2.016(3)		
				2.260(1)	2.018(3)	2.019(3)	2.247(4) (Ru–OH_2)	
				(H_2O)	2.024(3)	2.014(3)		
$[Ru_2(\mu\text{-}O_2CBu^t)_4(nitPh)]_n(BF_4)_n \cdot$ 2n benzene	monoclinic	$P2_1/n$	4	2.266(1)	2.017(8)	2.012(8)	2.264(8)	[52]

					2.011(8)	2.015(8)		
					2.009(8)	2.018(7)	2.236(8)	
					2.020(8)	2.010(8)		
$Ru_2(\mu\text{-}O_2C(CH_3)C{=}CH_2)_4Cl$	monoclinic	$P2_1/a$	4	2.287(1)	2.024(5)	2.006(5)	2.555(2)	[15]
					2.015(5)	2.026(5)		
				2.290(1)	2.011(4)	2.018(5)	2.572(2)	
					2.018(5)	2.022(5)		
$Ru_2(\mu\text{-}O_2CPh)_4Cl$	monoclinic	C2/c	4	2.290(1)	2.021(4)	2.021(4)	2.532(1)	[53]
					2.011(4)	2.021(4)		
$[Ru_2(\mu\text{-}O_2CPh)_4(O_2CPh)]\cdot(HO_2CPh)$	triclinic	$P\bar{1}$	2	2.277(1)	1.999(3)	2.020(3)	2.244(3)	[8]
					2.012(3)	2.002(3)		
				2.278(1)	2.001(3)	2.021(3)	2.214(3)	
					2.013(3)	2.014(3)		
$Ru_2(\mu\text{-}O_2CC_6H_4\text{-}p\text{-}OMe)_4Cl\cdot 0.25H_2O$	triclinic	$P\bar{1}$	4	2.284(1)	2.024(5)	2.024(5)	2.554(2)	[54]
					2.014(5)	2.025(5)		
				2.290(1)	2.031(7)	2.014(7)	2.583(2)	
					2.009(7)	2.006(7)		
					2.012(5)	2.005(5)	2.563(2)	
					2.017(5)	2.020(5)		
				2.283(2)	2.018(7)	2.023(5)	2.568(3)	
					2.034(7)	2.011(5)		
$[Ru_2(\mu\text{-}O_2CC_6H_4\text{-}p\text{-}Bu^t)_4(THF)_2]OH$	monoclinic	C2/c	4	2.260(1)	2.015(9)	2.010(7)	2.247(8)	[13]
					2.007(8)	2.011(7)		
$[Ru_2(\mu\text{-}O_2C\text{-}p\text{-}tolyl)_4(THF)_2](BF_4)$	monoclinic	C2/m	2	2.2618(16)	2.013(3)	2.017(4)*	2.258(6)	[55]
$[Ru_2(\mu\text{-}O_2CPh)_4(C_2H_5OH)_2]$-	triclinic	P1	2	2.272(2)	2.005(8)	2.024(8)	2.270(9)	[25]
$[Ru_2(\mu\text{-}O_2CPh)_4(HSO_4)_2]$							(HSO_4)	
				(HSO_4)	2.017(8)	2.107(8)?		
				2.265(2)	2.01(1)	2.014(9)	2.234(9)	
							(C_2H_5OH)	
				(C_2H_5OH)	2.00(1)	2.012(9)		

Table 1 (*continued*)

$M_2(\mu\text{-}O_2CR)_4L_n$	Crystal system	Space group	Z	M–M (Å)	M–O (Å)	M–O (Å)	M–L (Å)	Ref.
$Ru_2(\mu\text{-}O_2CC(CH_3)(Ph)_2)_4Cl$	tetragonal	$P\bar{4}2_1c$	2	2.2893(9)	2.029(6)	2.031(5)	2.5016(6)	[16]
$[Ru_2(\mu\text{-}O_2CC_4H_4N)_4Cl(THF)]\cdot THF\cdot H_2O$, $(O_2CC_4H_4N)^- =$ pyrrole-2-carboxylate	triclinic	$P\bar{1}$	2	2.268(1)	2.036(7)	2.007(7)	2.523(3) (Ru–Cl)	[17]
					2.022(7)	2.005(7)		
					2.029(9)	2.011(9)	2.249(9) (Ru–O)	
					2.027(9)	2.004(9)		
$[Ru_2(\mu\text{-}O_2CC_4H_3S)_4(OPPh_3)_2](BF_4)\cdot 2H_2O$, $(O_2CC_4H_3S)^- =$ thiophene-2-carboxylate	monoclinic	C2/c	4	2.275(1)	2.031(6)	2.014(8)	2.216(7)	[19]
					2.020(6)	2.024(8)		
$Ru_2(\mu\text{-}O_2CCF_3)_4(O_2CCF_3)$	monoclinic	C2/c	4	2.278(1)	2.029(7)	2.015(7)	2.157(10)	[11]
					2.012(7)	2.028(8)		
$[RuCl(MeCN)_4(PPh_3)]$-$[Ru_2(\mu\text{-}O_2CC_6H_4\text{-}p\text{-}OMe)_4Cl_2]$	monoclinic	$P2_1/c$	4	2.299(1)	2.024(6)	2.022(6)	2.508(3)	[56]
					2.031(6)	2.025(6)		
					2.016(6)	2.023(6)	2.493(3)	
					2.022(7)	1.999(6)		
Ru_2(II,II) compounds								
$Ru_2(\mu\text{-}O_2CCH_3)_4(H_2O)_2$	monoclinic	C2/c	8	2.262(3)	2.079(4)	2.072(4)	2.335(4)	[30]
					2.054(4)	2.068(4)		
$Ru_2(\mu\text{-}O_2CCH_3)_4(THF)_2$	orthorhombic	Pbcn	4	2.261(3)	2.060(5)	2.063(5)	2.391(5)	[29]
					2.061(5)	2.057(5)		[30]
$Ru_2(\mu\text{-}O_2CEt)_4((CH_3)_2CO)_2$	triclinic	$P\bar{1}$	1	2.260(3)	2.075(4)	2.056(4)	2.363(5)	[30]
					2.062(4)	2.077(4)		
$Ru_2(\mu\text{-}O_2CEt)_4(NO)_2^c$	monoclinic	$P2_1/a$	2	2.515(4)	2.047(6)	2.056(6)	1.781(7)	[31]
					2.041(5)	2.065(5)		

$Ru_2(\mu\text{-}O_2CCF_3)_4(NO)_2$[d]	monoclinic	C2/c	4	2.532(4)	2.060(7) 2.053(7)	2.062(7) 2.060(7)	1.844(21) 1.786(19)	[31]
$Ru_2(\mu\text{-}O_2CCF_3)_4(THF)_2$	triclinic	$P\bar{1}$	1	2.276(3)	2.070(6) 2.076(6)	2.072(6) 2.072(6)	2.268(6)	[31]
$Ru_2(\mu\text{-}O_2CCF_3)_4(tempo)_2$ 201 K	triclinic	$P\bar{1}$	2	2.300(2)	2.066(3) 2.066(5)	2.083(3) 2.056(5)	2.136(5)	[42]
293 K				2.293(1)	2.059(2) 2.073(5)	2.077(2) 2.062(5)	2.162(4)	
$Ru_2(\mu\text{-}O_2CPh)_4(HO_2CPh)_2$	monoclinic	$P2_1/n$	2	2.263(1)	2.044(2) 2.062(2)	2.059(2) 2.048(2)	2.355(3)	[8]
$[Ru_2(\mu\text{-}O_2CC(Ph)_3)_4(H_2O)\text{-}(C_2H_5OH)]\cdot 2C_2H_5OH$	monoclinic	C2/c	4	2.252(2)	2.079(7) 2.073(7)	2.061(8) 2.064(7)	2.35(1) 2.35(1)	[37]
$Ru_2(\mu\text{-L-}O_2CCH(OH)C_6H_5)_4(H_2O)_2$ $(L\text{-}O_2CCH(OH)C_6H_5)^- =$ L-mandelate	monoclinic	$P2_1$	4	2.266(1) 2.265(1)	2.078(8) 2.061(9) 2.048(9) 2.043(8) 2.085(9) 2.060(8) 2.056(8) 2.045(8)	2.038(9) 2.074(9) 2.079(9) 2.075(9) 2.055(9) 2.076(9) 2.104(8) 2.071(9)	2.366(9) 2.330(9) 2.369(9) 2.332(9)	[33]
$Ru_2(\mu\text{-}O_2C\text{-}p\text{-tolyl})_4(THF)_2\cdot 2THF$	triclinic	$P\bar{1}$	2	2.2689(11)	2.0702(22) 2.0570(22)	2.0578(22) 2.0692(22)	2.3696(24)	[55]
$Ru_2(\mu\text{-}O_2C\text{-}p\text{-tolyl})_4(MeCN)_2\cdot 3MeCN$	monoclinic	C2/c	4	2.2757(10)	2.061(4) 2.066(4)	2.056(4) 2.067(4)	2.331(5)	[55]
$[Ru_2(\mu\text{-}O_2CC_{10}H_{15})_4(CH_3OH)_2]\cdot 2CH_3OH$, $C_{10}H_{15}=$ 1-adamantyl	monoclinic	$P2_1/c$	2	2.2809(9)	2.015(7)	2.023(6)	2.287(5)	[21]

Table 1 (*continued*)

$M_2(\mu\text{-}O_2CR)_4L_n$	Crystal system	Space group	Z	M–M (Å)	M–O (Å)	M–O (Å)	M–L (Å)	Ref.
					2.019(7)	2.011(6)		
$[RuCl(MeCN)_3(PPh_3)_2]_2$-$[Ru_2(\mu\text{-}O_2CC_6H_4\text{-}p\text{-}OMe)_4Cl_2]$	monoclinic	$P2_1/c$	2	2.291(2)	2.041(10)	2.010(10)	2.528(4)	[56]
					2.017(10)	2.017(9)		
Os_2(III,III) compounds								
$Os_2(\mu\text{-}O_2CCH_3)_4Cl_2$	monoclinic	$P2_1/n$	2	2.314(1)	2.004(7) 2.006(7)	2.017(6) 2.009(7)	2.448(2)	[57]
$Os_2(\mu\text{-}O_2CEt)_4Cl_2$	monoclinic	$P2_1/n$	2	2.316(1)	2.014(10) 2.008(11)	2.028(10) 2.006(11)	2.430(5)	[57]
$Os_2(\mu\text{-}O_2CPr^n)_4Cl_2$	monoclinic	$P2_1/n$	2	2.301(1)	2.018(8) 2.015(8)	1.996(7) 2.022(8)	2.417(3)	[42] [43]
$Os_2(\mu\text{-2-PBZ})_4Cl_2$-(2-PBZ = 2-phenyl-benzoate)	triclinic	$P\bar{1}$	2	2.3173(6)	2.01(3)	–	2.386(3)	[58]
				2.3180(7)	(average)	–	2.375(4)	

[a] Correction of the previous structure from Ref. [20].
[b] Reformulation of $[Ru_2(\mu\text{-}O_2CCH_3)_4(CH_3CO_2H)_2]$ from Ref. [38].
[c] Correction of previous structure from Ref. [20].
[d] Formally Ru_2(I,I) compounds.

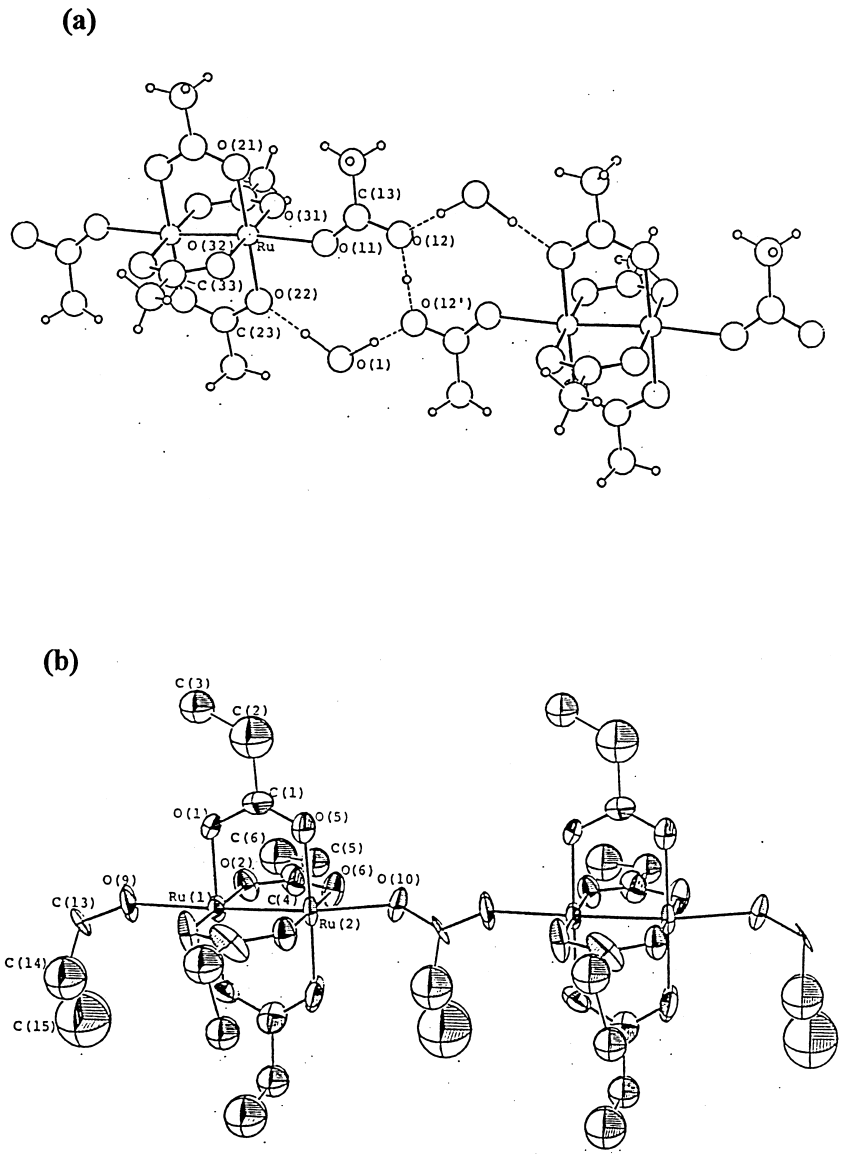

Fig. 3. (a) Structure of two hydrogen bonded $Ru_2(\mu\text{-}O_2CCH_3)_4 \cdot (O_2CCH_3)_2H \cdot 0.7H_2O$ molecules. (b) Structure of two $Ru_2(\mu\text{-}O_2CEt)_4(O_2CEt)$ molecules linked in an infinite chain. Adapted from Ref. [11].

ligand [27]. The bond lengths range from 2.248 to 2.292 Å. In general the $Ru_2(\mu\text{-}O_2CR)_4X$ chain compounds exhibit slightly longer Ru–Ru bonds (2.267–2.292 Å) than the $Ru_2(\mu\text{-}O_2CR)_4L_2$ diadducts (2.248–2.275 Å). The invariance in the Ru–Ru bond distance with the nature of the axial donor is explained by the fact that the metal–axial ligand bond formed produces a predominantly ligand

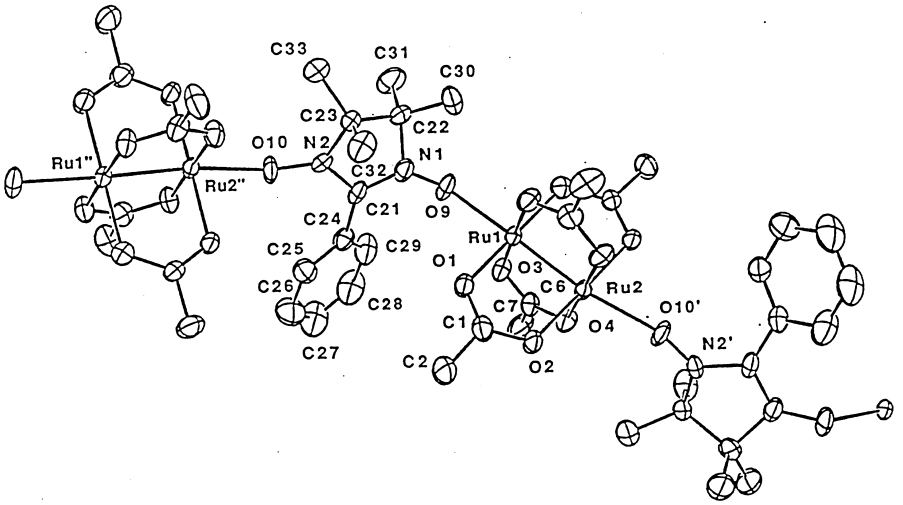

Fig. 4. Chain structure of $\{[Ru_2(\mu\text{-}O_2CBu^t)_4(nitPh)](BF_4)\}_n$. Adapted from Ref. [52].

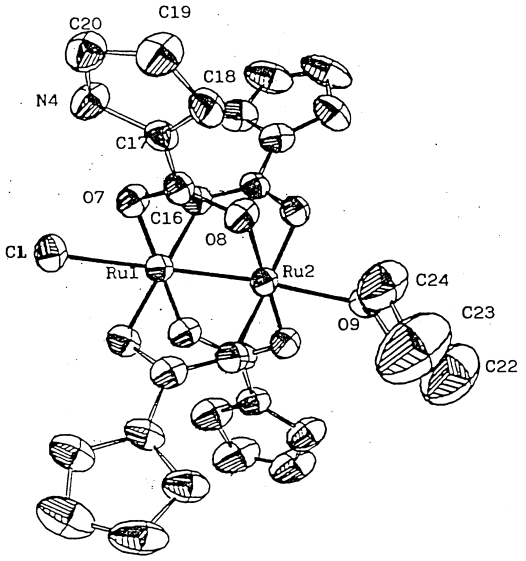

Fig. 5. Structure of $Ru_2(\mu\text{-}O_2CC_4H_4N)_4(Cl)(THF)$. Adapted from Ref. [17].

based (>70% of the electron density) σ, σ* molecular orbital pair. The population density of the HOMO π* and δ* orbitals are not affected significantly so as to increase (or decrease) the bond length [27,59,60] (see also Section 4 on Electronic Structure). The Ru–L bonds of similar axial donors also display similar bond lengths. For example, Ru–Cl bonds range from 2.45–2.59 Å, with the shorter ones corresponding to those in the diadducts such as $K[Ru_2(\mu\text{-}O_2CH)_4Cl_2]$ (Ru–Cl=

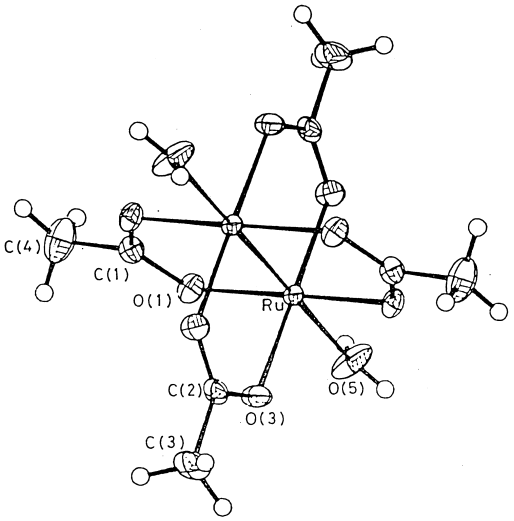

Fig. 6. Structure of $Ru_2(\mu\text{-}O_2CCH_3)_4(H_2O)_2$. Adapted from Ref. [30].

2.517(2) Å) [20] and $[Ru_2(\mu\text{-}O_2CCH(CH_3)_2)_4](Cl)(THF)$ (Ru–Cl = 2.445(6) Å) where only one Ru–Cl bond exists and the longer bonds occurring in the chain compounds such as $Ru_2(\mu\text{-}O_2CPr^n)_4Cl$ (Ru–Cl = 2.587(5) Å) [46] and $Ru_2(\mu\text{-}O_2CCH_3)_4Cl$ (Ru–Cl = 2.577(1) Å) [49] where the Cl^- acts as a bridging ligand. Most of the diadducts involve oxygen-donor ligands such as H_2O, DMF or $OPPh_3$ and consequently the Ru–L bond lengths fall into a relatively narrow range (2.22–2.37 Å). Other than the halides Cl^-, Br^-, or O-donors the only other type of axial donors found in structurally characterized Ru_2(II,III) complexes involve the nitrogen-donors phenazine (phz), in the chain compound $[Ru_2(\mu\text{-}O_2CEt)_4(phz)](BF_4)$ (Ru–N = 2.44 Å) [21], and MeCN, in the Ru_2(II,II) complex $Ru_2(\mu\text{-}O_2C\text{-}p\text{-}tolyl)_4(MeCN)_2 \cdot 3MeCN$ [55]. Crystal structures exist for $Ru_2(\mu\text{-}O_2CEt)_4(NO)_2$ and $Ru_2(\mu\text{-}O_2CCF_3)_4(NO)_2$ [31] but these I will designate formally as Ru_2(I,I) compounds (see below). It has been documented that reaction of the diruthenium tetracarboxylate core with some N-donors and P-donors such as pyridine, acetonitrile, isocyanides or PPh_3, which also display significant π-acid properties, leads to a substitution of the bridging carboxylates and a breakdown of the lantern structure [5,6,14,31]. Another Ru_2(II,II) acetonitrile complex, $[Ru_2(\mu\text{-}O_2CCH_3)_4](MeCN)_2$ [30], some dipyridine adducts [14,61] and two chain compounds involving N-donors, $[Ru_2(\mu\text{-}O_2CR)_4$(DM-DCNQI)] (R = H, CH_3, Et, Pr^n and Ph and DM-DCNQI = bis(2,5-dimethyl-*N*,*N*′-dicyanoquinonediimine)) [62–65] and $[Ru_2(\mu\text{-}O_2CCH_3)_4(pz)](BPh_4)$ (pz = pyrazine) [26], have been reported but not structurally characterized.

The Ru–Ru and Ru–L bond lengths in the Ru_2(II,II) complexes display a remarkable insensitivity to the nature of L and the R group. The Ru_2(II,II) compounds show, on average, only a small lengthening of their Ru–Ru bonds over their oxidized

Ru_2(II,III) cousins. For example, for $Ru_2(\mu\text{-}O_2CCH_3)_4(H_2O)_2$ (Fig. 6) Ru–Ru = 2.262 Å, whereas for $[Ru_2(\mu\text{-}O_2CCH_3)_4(H_2O)_2](BF_4)$ Ru–Ru = 2.248 Å. This is likely due to population/depopulation of a δ* orbital which has only a small effect on the Ru–Ru bond length and which is compensated for by the decrease/increase in the electrostatic repulsion between the metals. The Ru–OH_2 bonds are quite similar, being 2.335 Å in the reduced compound and 2.310 Å in the mixed-valent species.

The bridging carboxylate oxygen to metal bond distances are relatively invariant of the substituent R group, ranging from 1.96 Å in $Ru_2(\mu\text{-}O_2CPr^n)_4Cl$ [46] to 2.052 Å in $[Ru_2(\mu\text{-}O_2CCH_3)_4(DMF)_2](PF_6)\cdot DMF$ [27] for Ru_2(II,III) type complexes and from 2.043 Å in $Ru_2(\mu$-L-mandelate$)_4(H_2O)_2$ to 2.104 Å in this same Ru_2(II,II) complex. The bonds are slightly longer in the reduced complexes due to the increase in antibonding character at the metal centres as mentioned and a decrease in the electrostatic attraction between the ruthenium and the carboxylate oxygen.

Two interesting structures have been determined in which NO^+ is the axial ligand [31]. $Ru_2(\mu\text{-}O_2CC_2H_5)_4(NO)_2$ and $Ru_2(\mu\text{-}O_2CCF_3)_4(NO)_2$ have substantially longer Ru–Ru bonds (2.515 and 2.532 Å, respectively) than any other Ru_2(II,II) complex which is consistent with the filling of the π* orbital and a diamagnetic ground-state. It was therefore postulated that these compounds contain a Ru_2(I,I) core. (This can also be viewed as a strong antiferromagnetic interaction between the Ru_2^{4+} centre and a radical $NO^{\cdot}$. Since the magnetic orbital is primarily metal based it amounts to, in essence, a Ru_2^{2+} centre with axial NO^+ ligands.)

A complex containing chiral carboxylate bridges was formed from the reaction of $Ru_2(\mu\text{-}O_2CCH_3)_4Cl$ and L-mandelic acid. This yielded, surprisingly, the reduced $[Ru_2(\mu\text{-L-}O_2CCH(OH)C_6H_5)_4]\cdot 2H_2O$ species which was structurally characterized and found to contain the four bridging mandelate ligands with their *S* conformations maintained [33].

Only four Os_2(III,III) compounds have been characterized using X-ray crystallography: $Os_2(\mu\text{-}O_2CR)_4Cl_2$ (R = Me, Et and Pr^n) [43,57] and $Os_2(\mu\text{-2-PBZ})_4Cl_2$ where 2-PBZ = 2-phenylbenzoic acid [58]. The first three complexes all crystallize in the monoclinic space group, $P2_1/c$, and have very similar Os–Os bond lengths (≈2.31 Å) and Os–O(bridge) bond lengths (≈2.01 Å). The fourth complex crystallizes in a triclinic $P\bar{1}$ space group but has similar Os–Os and Os–O(bridge) bond lengths. The Os–Cl bonds do tend to decrease slightly in length with increasing length of R: 2.448 Å for R = Me, 2.430 Å for R = Et, 2.417 Å for R = Pr^n and 2.381(average) Å for R = 2-phenylbenzene. The structure of the phenylbenzoate derivative is shown in Fig. 7.

5. Electronic structure and spectra

It was noticed at a very early stage [5] that the mixed-valent Ru_2(II,III) complexes had surprisingly high magnetic moments, 3.6–4.4 B.M. per dimer. The elucidation of the electronic structure has gone through a series of steps since the early 1970s. Early qualitative molecular orbital schemes using $Re_2Cl_8^{2-}$ as a model placed the

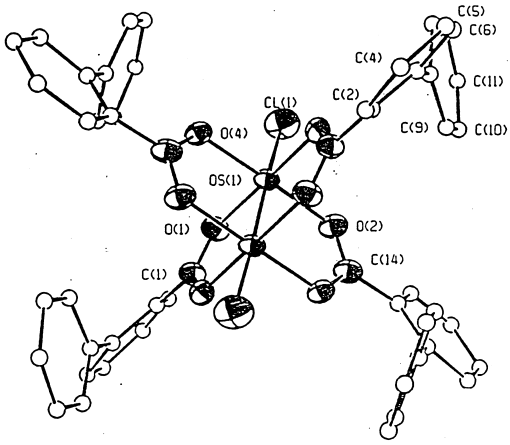

Fig. 7. Structure of $Os_2(\mu\text{-}2\text{-}PBZ)_4Cl_2$. Reproduced with permission from Ref. [58].

three unpaired electrons into closely spaced $b_{1u}(\delta^*)$, $a_{2u}(\sigma_n')$ and $a_{1g}(\sigma_n)$ orbitals under D_{4h} symmetry for the $Ru_2(\mu\text{-}O_2CR)_4Cl$ species [46,66].

Most of the mixed-valent complexes display electronic transitions at 23 500 and 32 250 cm^{-1} which were originally assigned to $b_{2g}\rightarrow a_{1g}$ or $b_{2g}\rightarrow a_{2u}$ and $b_{2g}\rightarrow b_{1u}$ respectively [46] as well as bands in the near-infrared at $\approx$10 400 and 9000 cm^{-1} which were assigned to $a_{2u}\rightarrow b_{1u}$ and $a_{1g}\rightarrow b_{1u}$ transitions [66]. This was later clarified by Clark and Franks [67] whose resonance Raman work led them to the electron configuration $a_{1g}\ (\sigma)^2\ e_u\ (\pi)^4\ b_{2g}\ (\delta)^2\ b_{1u}\ (\delta^*)^1\ e_g\ (\pi^*)^2$.

A thorough theoretical analysis of the electronic structure of $[Ru_2(\mu\text{-}O_2CR)_4]^+$ complexes was provided in the late 1970s by Norman and coworkers [59,68]. In this study detailed SCF-Xα-SW calculations were performed on $[Ru_2(\mu\text{-}O_2CH)_4Cl_2]^-$, $[Ru_2(\mu\text{-}O_2CH)_4]^+$ and $Ru_2(\mu\text{-}O_2CH)_4$. For the Ru_2(II,III) species they postulated a $\sigma^2\pi^4\delta^2\pi^{*2}\delta^{*1}$ configuration (Fig. 8); the "high-spin", $S=3/2$, configuration being favoured due to the close spacing of the π^* and δ^* orbitals. The ordering $\delta^*<\pi^*$, which would be expected if the bonding were entirely metal–metal in nature, is not seen here. Since there is a downward shift of metal 4d levels with respect to the ligand levels, as well as the influence of the carboxylate ligands and, to a lesser extent the axial ligands, the ordering is reversed; $\pi^*<\delta^*$. Norman emphasizes that the major contribution to this ordering is that the δ^* d-orbital combination interacts significantly with low lying carboxylate orbitals whereas the π^* orbital does not. The axial ligand influence is the opposite to that of the carboxylates but the effect is predicted to be much smaller (which has been shown by Norman for $[Ru_2(\mu\text{-}O_2CH)_4Cl_2]^-$) and a restoration of the $\delta^*<\pi^*$ ordering is not predicted.

Experimentally, the near-degeneracy has only been lifted by changing the carboxylate bridges to N,N- or N,O-donor chelates. For example, in the reduced $Ru_2[\mu\text{-}(p\text{-}CH_3C_6H_4)NNN(p\text{-}CH_3C_6H_4)]_4$ complex the δ^* orbital lies much higher than the π^* leading to a *diamagnetic* $\sigma^2\pi^4\delta^2\pi^{*4}$ ground-state configuration [69]. At

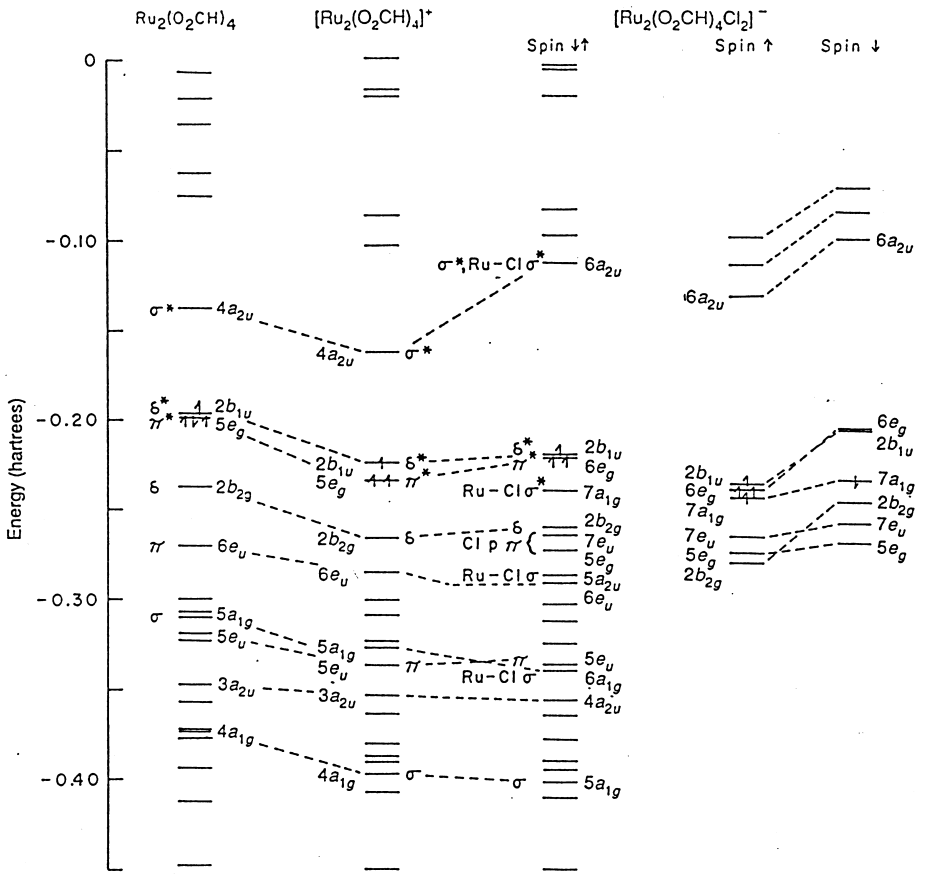

Fig. 8. Theoretically calculated molecular orbital energies for $Ru_2(\mu\text{-}O_2CH)_4$, $Ru_2(\mu-O_2CH)_4^+$ and $Ru_2(\mu-O_2CH)_4Cl_2^-$ using the SCF-Xα-SW method. Reproduced with permission from Ref. [59].

the other extreme, $Ru_2(\mu\text{-fhp})_4$ ($fhp^- = 6$-fluoro-2-hydroxypyridinate), has $\pi^* > \delta^*$ and a $\sigma^2\pi^4\delta^2\delta^{*2}\pi^{*2}$ configuration yielding two unpaired electrons [70]. Influencing the orbital ordering of tetracarboxylate-bridged species, simply by varying the nature of the axial ligands, has been attempted [27] but has, as yet, not met with success.

The consequences of the near-degeneracy and hence the half-filled π^* and δ^* energy levels leads to an increase in stability of the mixed-valent $[Ru_2(\mu\text{-}O_2CR)_4]^+$ species relative to the reduced $Ru_2(\mu\text{-}O_2CR)_4$ complex (see Fig. 8). A (weak) trans effect was predicted with the Cl^- ligand weakening the $Ru^{2.5}$–$Ru^{2.5}$ bond more than H_2O. This has been supported by the fact that the Ru–Ru bond is 0.038 Å longer in $Cs[Ru_2(\mu\text{-}O_2CCH_3)_4Cl_2]$ (2.286 Å) [20] versus $[Ru_2(\mu\text{-}O_2CCH_3)_4(H_2O)_2](BF_4)$ (2.248 Å) [20,50] or 0.021 Å longer than in $[Ru_2(\mu\text{-}O_2CCH_3)_4(H_2O)_2](PF_6)\cdot 3H_2O$ [27].

Diffuse reflectance spectra of $Ru_2(\mu\text{-}O_2CCH_3)_4Cl$ performed by Clark and Franks [67] showed a major band at $\approx 21\,700\ cm^{-1}$ and a minor band at $17\,850\ cm^{-1}$. In

solution only one major band is seen at $\approx 23\,500\ cm^{-1}$. All of these bands were originally assigned to a $\delta \rightarrow \delta^*$ transition. However, Norman's subsequent calculations assigned the major band to an allowed (Ru–O, $Ru_2\pi \rightarrow Ru_2\pi^*$) transition with the π orbital mainly of Ru–O bonding character but with a significant Ru–Ru π bonding contribution. This is the accepted assignment today. The near-IR bands seen in solution by earlier workers at 10 400 and 9000 cm^{-1} were tentatively assigned to $\delta \rightarrow \delta^*$ ($b_{2g} \rightarrow b_{1u}$) and $\delta \rightarrow \pi^*$ ($b_{2g} \rightarrow e_g$) transitions, respectively.

A year later Martin *et al.* [49] performed single-crystal polarized optical spectroscopy on $Ru_2(\mu\text{-}O_2CCH_3)_4Cl$ (Fig. 9). Some of the bands previously predicted by Norman *et al.* for $[Ru_2(\mu\text{-}O_2CCH_3)_4Cl_2]^-$ were seen here. In particular they saw a *z*-polarized (dipole-allowed) band around 21 000 cm^{-1} closely corresponding to that observed and predicted by Norman. A weak dipole-allowed band at 17 800 cm^{-1} appears to be a Cl (a_{2u})$\rightarrow\pi^*(e_g)$ (*x*,*y* polarized) band predicted to lie at 18 700 cm^{-1} although the intensity was stronger than expected. Finally a broad *x*,*y* polarized band at 22 500 cm^{-1} correlates to a composite of the calculated 23 000 and 24 700 cm^{-1} bands which are $O \rightarrow \pi^*$ and $O \rightarrow \delta^*$ transitions, respectively.

Subsequent studies by Clark and Ferris [71] using resonance Raman techniques confirmed the band at $\approx 21\,000\ cm^{-1}$ to be a dipole-allowed *z*-polarized $O(\pi) \rightarrow \pi^*$ ($e_u \rightarrow e_g$) transition. A magnetic study by Telser and Drago [60] also supported Norman's MO scheme using $Ru_2(\mu\text{-}O_2CR)_4X$ (R = Me, Et, Pr^n; X = Cl^- and Br^-).

A definitive 1987–88 study by Gray *et al.* [72,73] confirmed the assignment of a *z*-polarized band at 9000 cm^{-1} as a $\delta \rightarrow \delta^*$ transition using single-crystal polarized spectroscopy. A new band at $\approx 6900\ cm^{-1}$ ($\epsilon = 1$–$5 M^{-1}\ cm^{-1}$) which had *x*,*y* polarization was assigned to a spin-forbidden $\pi^* \rightarrow \delta^*$ transition. Also, bands at 5048 and 1600 cm^{-1} (from resonance Raman) were tentatively assigned to "spin-flip" transitions within the $(\pi^*\delta^*)^3$ orbital manifold. This study was extended into the

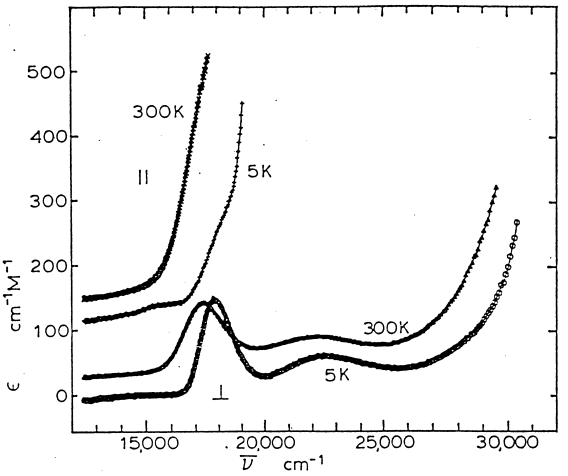

Fig. 9. Polarized single-crystal spectra of $Ru_2(\mu\text{-}O_2CCH_3)_4Cl$. Adapted from Ref. [49].

visible and ultraviolet using both solution and single crystal data [73] for $Ru_2(\mu\text{-}O_2CR)_4Cl$ (R = Me and Et) and $Ru_2(\mu\text{-}O_2CR)_4Br$ ($R = Pr^n$). A summary of the major bands and their current assignments for $Ru_2(\mu\text{-}O_2CCH_3)_4Cl$ are given in Table 2.

The situation for diosmium tetracarboxylates is somewhat more complicated. Early studies on $Os_2(\mu\text{-}O_2CR)_4Cl_2$ ($R = Pr^n$) indicated a μ_{eff} that varied with temperature (i.e. $\mu_{eff} = 1.15$ B.M. per Os at 300 K and 1.02 B.M. per Os at 188 K). It was concluded that a significant antiferromagnetic interaction existed between the Os atoms and that there was an appreciable population of a spin triplet state at higher temperatures suggesting an electronic configuration of $\sigma^2\pi^4\delta^2\pi^{*2}$ or $\sigma^2\pi^4\delta^2\delta^{*1}\pi^{*1}$ at the higher temperatures with the singlet ground-state, $\sigma^2\pi^4\delta^2\delta^{*2}$, more favoured at lower temperatures [42,43]. This is supported by the previous SCF-Xα-SW calculations on $[Ru_2(\mu\text{-}O_2CH)_4]^+$ which indicate a near degenerate HOMO of π* and δ* orbitals.

Electronic spectra (solid-state reflectance due to insolubility) show broad bands in the UV at $\sim 38\,500\ cm^{-1}$ and 27 000–28 000 cm^{-1} for $Os_2(\mu\text{-}O_2CCH_3)_4Cl_2$ and $Os_2(\mu\text{-}O_2CCH_2Cl)_4Cl_2$. A solution spectrum ($CH_2Cl_2$) was obtained for $Os_2(\mu\text{-}O_2CPr^n)_4Cl_2$ and bands at 44 800 cm^{-1} ($\epsilon = 15\,800 M^{-1}\ cm^{-1}$), 38 500 cm^{-1} (shoulder), 36 000 cm^{-1} ($\epsilon = 6100 M^{-1}\ cm^{-1}$), 27 800 cm^{-1} (shoulder) and 25 500 cm^{-1} ($\epsilon = 10\,400 M^{-1}\ cm^{-1}$) were observed. No attempts were made to assign these bands.

Spectroelectrochemically generated $[Os_2(\mu\text{-}O_2CR)_4Cl_2]^-$ where R = Et and Pr^n show a series of peaks in the UV–vis region [45]. Some assignments were presented

Table 2
Electronic transitions in $Ru_2(\mu\text{-}O_2CCH_3)_4Cl$[a]

Band energy (cm^{-1})	Calculated from Ref. [59][b]	Assignment(s)	Selection rule	Ref.
31 000	–	$\pi(Cl)\rightarrow\pi^*(Ru_2)$	–	[73]
22 500	23 000	$n(O)\rightarrow\pi^*(Ru_2)$, ($1a_{1u}\rightarrow 6e_g$)	*x*,*y*	[49,59]
	24 700	$n(O)\rightarrow\delta^*(Ru_2)$, ($4e_g\rightarrow 2b_{1u}$)		
22 200	–	$\pi(Ru\text{–}O, Ru_2)\rightarrow\sigma^*(Ru\text{–}O)$ ($6e_u\rightarrow 4b_{2u}$ or $5b_{1g}$)	*x*,*y*	[73]
21 000–21 700	19 900	$\pi(Ru\text{–}O, Ru_2)\rightarrow\pi^*(Ru_2)$	*z*	[49,59,67,71,72]
23 500 (soln.)		($6e_u\rightarrow 6e_g$)		
17 600–17 800	18 700	$\sigma(Ru\text{–}Cl)\rightarrow\pi^*(Ru_2)$, ($5a_{2u}\rightarrow 6e_g$)	*x*,*y*	[49,59,67]
17 500	–	$\delta^*(Ru_2)\rightarrow\sigma^*(Ru\text{–}O)$, ($2b_{1u}\rightarrow 5b_{1g}$ or $4b_{2u}$)	–	[73]
		$\pi^*(Ru_2)\rightarrow\sigma^*(Ru\text{–}O)$, ($6e_g\rightarrow 5b_{1g}$ or $4b_{2u}$)		
15 900	–	$\delta(Ru_2)\rightarrow\pi^*(Ru_2)$, ($2b_{2g}\rightarrow 6e_g$)	–	[73]
9000–10 400	8600–8800	$\delta(Ru_2)\rightarrow\delta^*(Ru_2)$, ($2b_{2g}\rightarrow 2b_{1u}$)	*z*	[59,66,72]
10 000 (soln.)				
6900	–	$\pi^*(Ru_2)\rightarrow\delta^*(Ru_2)$, ($6e_g\rightarrow 2b_{1u}$)	*x*,*y*	[72]
5048, 1600	–	"spin-flip" transitions	–	[72]

[a] Unless otherwise stated measurements are for samples in the solid state.
[b] Calculated by Norman *et al.* [59] for $[Ru_2(\mu\text{-}O_2CH)_4Cl_2]^-$.

with analogies to the corresponding ruthenium complexes. The main band at 25 500 cm^{-1} (Os_2^{6+}) and 26 300 cm^{-1} (Os_2^{5+}) was assigned to an O (π)→Os_2 (π^*) transition possibly with some contribution from an X^-→Os_2 (π^*) charge transfer. No intervalence bands were observed in the near-IR and it was concluded that the mixed-valent Os_2^{5+} species were completely delocalized, similar to their Ru_2^{5+} counterparts.

Subsequent resonance Raman studies on $Os_2(\mu\text{-}O_2CCH_3)_4Cl_2$ confirmed an axially polarized band at 26 100 cm^{-1} to be due to a Cl^- (π)→Os_2 (π^*) transition [74,75]. A band at ~11 750 cm^{-1} (δ→δ^*) was also detected and a room-temperature configuration of $\sigma^2\pi^4\delta^2\delta^{*1}\pi^{*1}$ was proposed. Exchange of the Cl^- with Br^- brings about a reduction of the peak at ~25 500 cm^{-1} and an increase in the band at 21 900 cm^{-1} which is presumably due to a Br^- (π)→Os_2 (π^*) transition [44].

6. Vibrational spectroscopy

Infrared and Raman spectroscopic data, along with full coordinate analyses, have been studied and compiled for many Ru_2 and Os_2 complexes. References are given in Appendix A. General trends will be discussed in this section.

Early resonance Raman (RR) studies on $Ru_2(\mu\text{-}O_2CCH_3)_4Cl$ and $Ru_2(\mu\text{-}O_2CPr^n)_4Cl$ indicated weak to medium intensity ν(Ru–O) bands in the 340–380 cm^{-1} region with strong IR active bands at 400–450 cm^{-1}. A very intense band around 330 cm^{-1} has been assigned to ν(Ru–Ru) and a weak band at 180 cm^{-1} to ν(Ru–Cl) [67]. A later RR study [71] supported the earlier work on $Ru_2(\mu\text{-}O_2CCH_3)_4Cl$ and assigned a band at 327.3 cm^{-1} to ν(Ru–Ru) and one at 369.2 cm^{-1} to ν(Ru–O). As well, for $Ru_2(\mu\text{-}O_2CPr^n)_4Cl$ a ν(Ru–Ru) at 330.8 cm^{-1} and ν(Ru–O) at 376.5 cm^{-1} were determined. Single crystal data from Gray *et al.* [72] showed a ν(Ru–Ru) for both the propionate and butyrate derivatives at ~300 cm^{-1} and ν(Ru–O) at ~400 and 430 cm^{-1} for the propionate and butyrate derivatives, respectively. The acetates showed strong progressions in both ν(Ru–Ru) and ν(Ru–O). Vibronic effects were attributed to strong ground-state coupling of the a_{1g} ν(Ru–O) and ν(Ru–Ru) modes in the acetates.

Detailed Raman and infrared studies have been carried out on $[Os_2(\mu\text{-}O_2CR)_4Cl_2]$ (where R = CH_3, CD_3 [74]; CH_2Cl, Et, Pr^n [75]) and have found ν(Os–Os) modes in the range 228–236 cm^{-1}, ν(Os–O) at 256–393 cm^{-1} and ν(Os–Cl) at 292–311 cm^{-1}. While ν(Os–Os) and ν(Os–Cl) show very little dependence on the nature of R, the ν(Os–O) is highly dependent, with the highest value of 393 cm^{-1} corresponding to the lightest R group (CH_3) and the value of 256 cm^{-1} corresponding to the heaviest R group (Pr^n).

The most diagnostic feature in any infrared spectrum of the diruthenium or diosmium tetracarboxylates is the symmetric and asymmetric bridging carboxylate stretching modes. The $\nu_{sym}(CO_2)$ usually occurs in the range 1330–1460 cm^{-1} and the $\nu_{asym}(CO_2)$ from 1440–1650 cm^{-1}. A selection of these values for a series of Ru_2(II,II), Ru_2(II,III) and Os_2(III,III) complexes is given in Table 3. The small separations ($\nu_{asym} - \nu_{sym}$) in most of these complexes suggest symmetrical bridging

Table 3
Selected carboxylate stretching frequencies for diruthenium and diosmium complexes

Compound	$\nu_{sym}(CO_2)$ (cm^{-1})	$\nu_{asym}(CO_2)$ (cm^{-1})	$\nu_{asym} - \nu_{sym}$ (cm^{-1})	Ref.
Ru_2(III,II) complexes				
$Ru_2(\mu\text{-}O_2CH)_4Cl$	1336	1480	144	[7]
$Ru_2(\mu\text{-}O_2CCH_3)_4Cl$	1394	1453	59	[7]
$Ru_2(\mu\text{-}O_2CPh)_4Cl$	1410	1470	60	[5]
$[Ru_2(\mu\text{-}O_2CCH_3)_4(H_2O)_2](BPh_4)$	1395	1440	45	[25]
$[Ru_2(\mu\text{-}O_2CCH_3)_4(THF)_2](BF_4)$	1400	1460	60	[22]
$[Ru_2(\mu\text{-}O_2CEt)_4(THF)_2](BF_4)$	1425	1460	35	[14]
$[Ru_2(\mu\text{-}O_2CPh)_4(THF)_2](BF_4)$	1350	1480	130	[14]
$[Ru_2(\mu\text{-}O_2CPh)_4(O_2CPh)] \cdot HO_2CPh$	bi-1409 uni-1230	bi-1517 uni-1720	bi-108 uni-490	[8] [8]
Ru_2(II,II) complexes				
$Ru_2(\mu\text{-}O_2CH)_4$	1347	1575	228	[30]
$Ru_2(\mu\text{-}O_2CCH_3)_4$	1440	1575	110	[30,72]
$Ru_2(\mu\text{-}O_2CEt)_4$	1432	1556	124	[30]
$Ru_2(\mu\text{-}O_2CPh)_4$	1408	1537	129	[30]
$Ru_2(\mu\text{-}O_2CCF_3)_4$	1457	1624	167	[31]
$[Ru_2(\mu\text{-}O_2CPh)_4(HO_2CPh)_2]$	bi-1405 uni-1271	bi-1541 uni-1665	bi-136 uni-394	[8] [8]
Os_2(III,III) complexes				
$[Os_2(\mu\text{-}O_2CCH_3)_4Cl_2]$	1380	1450	70	[43]
$[Os_2(\mu\text{-}O_2CEt)_4Cl_2]$	1375	1478	103	[43]

coordination of the carboxylate groups. In the acetate and formate cases the $\Delta\nu$ values are less than the corresponding ionic values which are 164 cm^{-1} for CH_3COO^- and 201 cm^{-1} for $HCOO^-$ [76]. Some of the $\Delta\nu$ values, in particular those for $Ru_2(\mu\text{-}O_2CCH_3)_4Cl$, $[Ru_2(\mu\text{-}O_2CCH_3)_4(H_2O)_2](BPh_4)$ and $[Ru_2(\mu\text{-}O_2CEt)_4(THF)_2](BF_4)$, are very small and close to values seen for chelating

bidentate carboxylates rather than bridging carboxylates [76]. This is believed to be a peculiarity of the $[Ru_2(\mu\text{-}O_2CR)_4X]_n$ systems. Both bidentate bridging and unidentate carboxylate modes are seen for the complex $Ru_2(\mu\text{-}O_2CPh)_4(HO_2CPh)_2$ with the large $\Delta\nu$ of 394 cm^{-1} being characteristic of unidentate coordination [76].

In general, both $\nu_{asym}(CO_2)$ and $\nu_{sym}(CO_2)$ increase from the mixed-valent Ru_2^{5+} species to the corresponding reduced Ru_2^{4+} species. This is rather surprising given the fact that the average $Ru–O_{eq}$ bond length increases by 0.03 to 0.05 Å. On the other hand, the electrostatic attraction (between carboxylate and diruthenium centre) decreases from the mixed-valent to the reduced compounds which may more than compensate for the relatively small change in bond length.

7. Electron spin resonance (ESR)

Early ESR measurements [77] on $[Ru_2(\mu\text{-}O_2CPr^n)_4]^+$ were consistent with the magnetic susceptibility data. Frozen solution X-band spectra at 77 K and 4.2 K revealed a quartet ground-state with $g_\parallel = g_\perp = 2.10 \pm 0.10$. No hyperfine splitting was seen at 77 K, however at 4.2 K weak splitting was seen yielding splitting parameters $|A_\perp| = 3.1 \times 10^{-3}$ cm^{-1} and $|A_\parallel| = 9 \pm 3 \times 10^{-3}$ cm^{-1} for ^{99}Ru. (The latter being a calculated value since no parallel signal was actually seen.) These spectra are consistent with a structure containing two equivalent ruthenium nuclei.

More detailed measurements by Telser and Drago [60] on the same compound in 1:1 toluene/CH_2Cl_2 at 3.4 K revealed fine structure that could be simulated using a program for powder pattern spectra of $S = 1/2$ systems. [It should be noted that ruthenium has five zero-spin nuclei (^{96}Ru, ^{98}Ru, ^{100}Ru, ^{102}Ru and ^{104}Ru) and two nuclei with $I = 5/2$: ^{99}Ru (12.72%) and ^{101}Ru (17.07%)]. The simulation yielded $g_\perp = 2.200(1)$, $g_\parallel = 1.9465(5)$, $A_\perp = 2.67 \times 10^{-3}$ cm^{-1} and $A_\parallel = 2.17 \times 10^{-3}$ cm^{-1}. The parameter values were solvent independent, however, the line widths did vary somewhat with the nature of the solvent. In all solvents the relative intensities of zero-spin to $I = 5/2$ signals are 45.9% to 54.1% which, again, is consistent with a delocalization over both rutheniums. The observation of a parallel signal with narrower line widths and larger hyperfine splittings than the perpendicular signal adds much greater support to this delocalization. A definite conclusion can only be reached if measurements are made on isotopically pure ($I = 5/2$) ruthenium which would show an 11 line spectrum for equivalent rutheniums or a sextet of sextets if they were not. This would be a prohibitive undertaking and has, as yet, not been performed.

Attempts have been made at measuring the ESR spectra of some reduced $Ru_2(II,II)$ carboxylates but none have met with any success. No spectra were observed for $Ru_2(\mu\text{-}O_2CCH_3)_4(THF)_2$ or $Ru_2(\mu\text{-}O_2CCF_3)_4(THF)_2$ at 77 K (in 2-methyltetrahydrofuran glass) probably due to large zero-field splittings [29–31].

An ESR spectrum was determined for $[Ru_2(\mu\text{-}O_2CEt)_4(DM\text{-}DCNQI)]_n$ at 15 K. Here, signals appear at $g = 4.31$ (i.e. $g_\perp = g_\parallel = 2.15$) and $g = 1.95$, consistent with those found earlier for the Ru_2^{5+} cores, along with an additional broad signal at $g = 2.02$ which is possibly due to a radical anion DM-DCNQI bridge [62].

ESR spectra were observed at 77 K for the cationic–anionic (Ru_2(II,III)) complexes $[RuCl(MeCN)_3(PPh_3)_2][Ru_2Cl_2(\mu\text{-}O_2CPh)_4]$, $[RuCl(MeCN)_3(PPh_3)_2]$-$[Ru_2Cl_2(\mu\text{-}O_2CMe)_4]$, $[RuCl(MeCN)_3(PPh_3)_2][Ru_2Cl_2(\mu\text{-}O_2CC_6H_4\text{-}p\text{-}Me)_4]$ and $[RuCl(MeCN)_4(PPh_3)][Ru_2Cl_2(\mu\text{-}O_2CC_6H_4\text{-}p\text{-}OMe)_4]$ [56]. In all cases $g_\perp \approx 2.16$ ($S=3/2$), similar to that found for $Ru_2(\mu\text{-}O_2CPr^n)_4Cl$.

Finally, an interesting spectrum was obtained for $[Ru_2(\mu\text{-}O_2CBu^t)_4$-$(tempo)_2][Ru_2(\mu\text{-}O_2CBu^t)_4(H_2O)_2](BF_4)_2$ (Fig. 10) [51]. Here we see an effective g value, $g^e_\perp = 4.40$ due to $[Ru_2(\mu\text{-}O_2CBu^t)_4(H_2O)_2]^+$ ($S=3/2$), consistent with previous measurements on Ru_2^{5+} cores. Additional signals seen at $g^e_\perp = 2.33$ and $g^e_\parallel = 1.92$ are due to the $[Ru_2(\mu\text{-}O_2CBu^t)_4(tempo)_2]^+$ moiety and are consistent with an $S=1/2$ ground-state due to the strong antiferromagnetic coupling between the diruthenium cores and the bridging nitroxide radical (tempo) (see Section 9 for further details).

For diosmium tetracarboxylates few ESR measurements have been made. Weak signals in the $g=2$ region were observed for the mixed-valent $[Os_2(\mu\text{-}O_2CCH_3)_4(Cl)(py)]$ at 100 K, possibly due to fast spin-lattice relaxations at this temperature [41]. No ESR signals were observed for $Os_2(\mu\text{-}O_2CR)_4Cl_2$ (R = Et, Pr^n or CH_2Cl) down to liquid nitrogen temperatures [43]. X-band ESR spectra of $[(\eta^5\text{-}C_5H_5)Co][Os_2(\mu\text{-}O_2CPr^n)_4Cl_2]$ and electrochemically generated $[Os_2(\mu\text{-}O_2CPr^n)_4(Cl)_2]^-$ recorded at 113 K in toluene/CH_2Cl_2 (5:2) were reported by Tetrick *et al.* [45] but not elaborated upon due to the weak signal intensities. They mention seeing virtually identical spectra for the redox pair with signals at 2460 and 2840 G and a weaker signal at 4600 G.

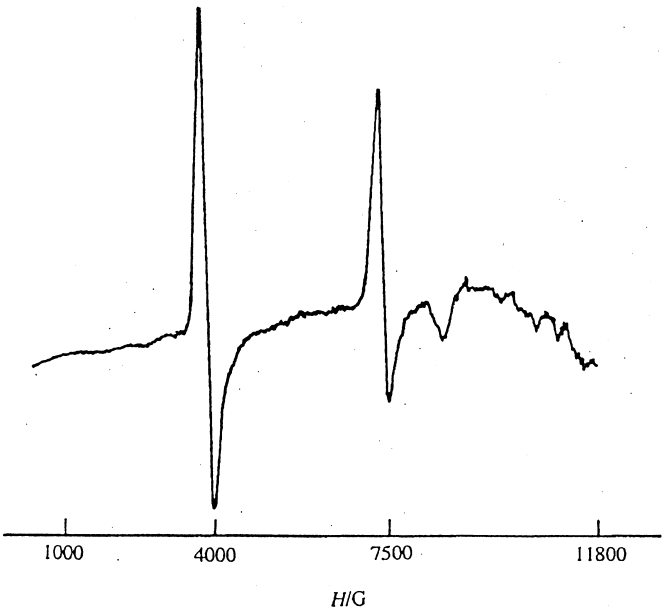

Fig. 10. ESR spectrum of $[Ru_2(\mu\text{-}O_2CBu^t)_4(tempo)_2][Ru_2(\mu\text{-}O_2CBu^t)_4(H_2O)_2](BF_4)$ at 5 K. Adapted from Ref. [51].

8. Electrochemistry

Early polarographic measurements by Mukaida *et al.* on the $[Ru_2(\mu\text{-}O_2CCH_3)_4]^{+/0}$ couple showed a mostly reversible wave, $E_{1/2} = +0.06$ V vs SCE [7]. Wilson and Taube [66] and Earley *et al.* [78] also reported a value of $+0.060$ V vs SCE (0.292 V vs NHE) for this couple, the former measured in 0.1M sulphuric acid and the latter in 0.9M $LiCF_3SO_3$/0.1M CF_3SO_3H using cyclic voltammetry. An anode to cathode peak separation of 83 mV was observed by Taube and 75 mV by Earley and the process was classified as quasi-reversible. More extensive measurements on $Ru_2(\mu\text{-}O_2CPr^n)_4Cl$ by Cotton and Pederson [77] involving rotating-disk electrode polarography and cyclic voltammetry at platinum, gold and carbon electrodes showed either a two-step or one-step reduction. These reductions were independent of electrode type, but were medium dependent. A two-step reduction is seen in 0.1M tetrabutylammonium perchlorate (TBAP) containing dichloromethane for $Ru_2(\mu\text{-}O_2CPr^n)_4Cl$ where both $Ru_2(\mu\text{-}O_2CPr^n)_4Cl$ and $[Ru_2(\mu\text{-}O_2CPr^n)_4]^+$ exist in equilibrium (Scheme 1).

The value of $E_{1/2} = 0.00$ vs SCE corresponds well to the values determined by Mukaida [7] and Wilson and Taube for $[Ru_2(\mu\text{-}O_2CCH_3)_4]^{+/0}$. In solvents without chloride in the electrolyte, but where the solvent can act as a ligand, single reductions are observed, albeit shifted slightly cathodically.

A summary of reduction potentials for a series of diruthenium tetracarboxylates in acetonitrile and tetrahydrofuran is listed in Table 4. Cyclic voltammograms in THF and MeCN solutions [30] for $Ru_2(\mu\text{-}O_2CR)_4$ (R = H, Me, CH_2Cl, Et and Ph) show a single quasi-reversible couple, with the THF adducts being slightly easier to oxidize than the MeCN adducts (as might be expected since THF is a better donor ligand). When NBu^n_4Cl is used as the electrolyte in MeCN a cathodic shift to -0.45 V vs SCE is seen for the $Ru_2(\mu - O_2CCH_3)_4^{0/+}$ couple. This is probably due to formation of $[Ru_2(\mu\text{-}O_2CCH_3)_4Cl_2]^{2-}$ which would be expected to be harder to reduce than its neutral precursor. Varying the R group also has an effect on $E_{1/2}$ in both THF and MeCN, although the data set is small. The greater the electron-withdrawing nature of R, i.e. CH_2Cl versus Me or Et, the more difficult the oxidations become and the easier the irreversible reductions.

Successive substitution of $[Ru_2(\mu\text{-}O_2CCH_3)_4(H_2O)_2]^+$ with Cl^- leads to a drop in the $E_{1/2}$ (vs SCE) value [79] (Scheme 2).

Electrochemical measurements on mixed carboxylates have also been performed

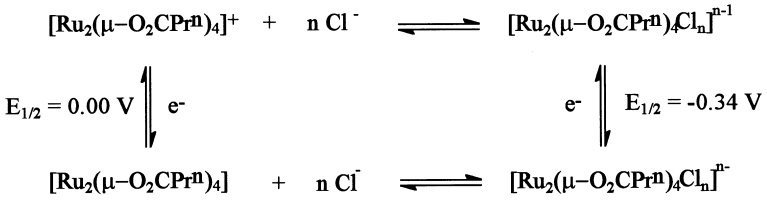

Scheme 1. Oxidation-reduction in the presence of Cl^-.

Table 4
Selected reduction potentials for a series of diruthenium adducts in MeCN and THF (adapted from Ref. [30])

$[Ru_2(\mu\text{-}O_2CR)_4]^{0/+}$	$E_{1/2}$ (V)[a]	$E_{1/2}$ (V)
R	MeCN[b]	THF[c]
H	+0.25 (−1.23)	+0.23 (−2.02)
Me	0.00 (−1.84) −0.45[d]	−0.05
CH_2Cl	+0.34 (−1.55)	+0.29
Et	−0.02 (−1.99)	−0.03
Ph	+0.13 (−1.41)	+0.07 (−2.08)

[a] Values are for the redox couple $Ru_2^{6+/5+}$, values in parentheses indicate an irreversible reduction, all $E_{1/2}$ values measured at 295 K vs SCE with ferrocene oxidized at +0.34 V.
[b] Electrolyte solution 0.2M $NBu_4^nPF_6$–MeCN.
[c] Electrolyte solution 0.2M $NBu_4^nPF_6$–THF.
[d] Electrolyte solution 0.2M NBu_4^nCl–MeCN.

$$[Ru_2(\mu\text{–}O_2CCH_3)_4(H_2O)_2]^+ + e^- \underset{}{\overset{E_{1/2} = 0.007\ V}{\rightleftharpoons}} [Ru_2(\mu\text{–}O_2CCH_3)_4(H_2O)_2]$$

$$[Ru_2(\mu\text{–}O_2CCH_3)_4(H_2O)(Cl)] + e^- \underset{}{\overset{E_{1/2} = -0.015\ V}{\rightleftharpoons}} [Ru_2(\mu\text{–}O_2CCH_3)_4(H_2O)(Cl)]^-$$

$$[Ru_2(\mu\text{–}O_2CCH_3)_4(Cl)_2]^- + e^- \underset{}{\overset{E_{1/2} = -0.055\ V}{\rightleftharpoons}} [Ru_2(\mu\text{–}O_2CCH_3)_4(Cl)_2]^{2-}$$

Scheme 2. Reductions of successively chlorinated species.

in great detail [10,31]. $[Ru_2(\mu\text{-}O_2CCH_3)_4(O_2CCF_3)]_n$ in MeCN shows a two-step reduction, +0.05 and −0.14 V vs SCE in the absence of Cl^- [using $NBu_4^nPF_6$ as the electrolyte] but only a one-step reduction at −0.45 V vs SCE when the electrolyte is NBu_4^nCl (Fig. 11). This is in line with what was observed in dichloromethane by Cotton and Pederson [77].

Cyclic voltammetry studies on $Ru_2(\mu\text{-}O_2CCF_3)_4$ were found to be very solvent dependent [31], with a reversible one-electron oxidation at +1.17 V in CH_2Cl_2 becoming less reversible and smaller (1.03 V) in acetone and totally irreversible in THF, the strongest donor solvent studied. It appears that the stronger the interaction between axial donor groups and the ruthenium centres the more easily they become oxidized. However, $Ru_2(\mu\text{-}O_2CCF_3)_4(CH_3CN)_2$ is still significantly more difficult to oxidize than $Ru_2(\mu\text{-}O_2CCH_3)_4(THF)_2$ (1.03 V versus −0.05 V) due to the strong electron-withdrawing CF_3 groups. In fact, for $Ru_2(\mu\text{-}O_2CCF_3)_4(THF)_2$, the reduction to a Ru_2^{3+} species at −1.15 V is completely reversible.

Cyclic voltammetry studies on $Ru_2(\mu\text{-}O_2CC_2H_5)_4(NO)_2$, which has formally been classified as a Ru_2^{2+} complex (see Section 3), in $CH_2Cl_2/NBu_4^nPF_6$ show a one-

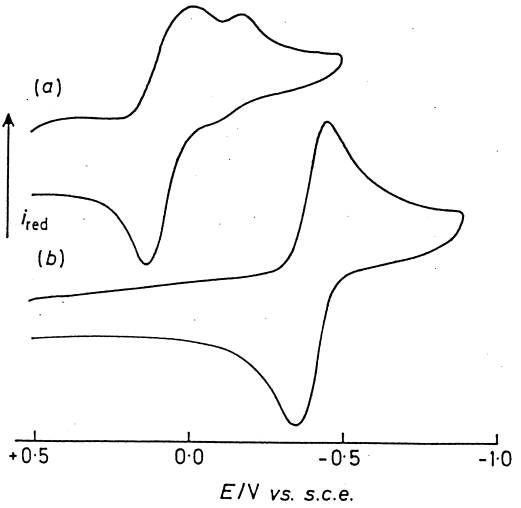

Fig. 11. Cyclic voltammograms in 0.2M $NBu^n_4PF_6$/MeCN at a scan rate of 100 mV s^{-1}. (a) $[Ru_2(\mu\text{-}O_2CCH_3)_4(O_2CCF_3)]_n$, (b) in the presence of a 10-fold excess of NBu^n_4Cl. Reproduced with permission from Ref. [31].

electron oxidation at +1.15 V to the Ru_2^{3+} mixed-valent species [31]. However, no oxidation process is observed for $Ru_2(\mu\text{-}O_2CCF_3)_4(NO)_2$ for similar reasons to those discussed above.

Early reports of a Ru_2^{6+} species, $[Ru_2(\mu\text{-}O_2CCH_3)_4(O_2CCH_3)_2]\cdot H_2O$ [38], showed two reversible one-electron reductions at 0.182 and −0.240 V vs Ag/AgCl in methanol. This was thought to be due to the consecutive reductions from Ru_2^{6+} to Ru_2^{5+} to Ru_2^{4+}. A follow-up study by Cotton *et al.* [11] failed to reproduce these results and only one one-electron reduction ($Ru_2^{5+/4+}$) at −0.010 V vs Ag/AgCl was observed and the compound reformulated as $Ru_2(\mu\text{-}O_2CCH_3)_4(O_2CCH_3)_2H\cdot 0.7H_2O$ (see Section 3).

A number of electrochemical measurements, mainly cyclic voltammetric determinations of reduction potentials, have been made on the $[Ru_2(\mu\text{-}O_2CR)_4(L)_2]^{+/0}$ couple since 1988. In all cases where R is not strongly electron withdrawing (e.g. CF_3, CH_2Cl) the $E_{298}{}^\circ$ for this couple was found to be in the range −0.060 to 0.250 V vs SCE and was reversible or quasi-reversible [9,12,24,25,27,55,103].

Electrochemical studies and, for that matter, most solution studies on diosmium tetracarboxylates are hampered by low solubility in the majority of solvents. Two compounds that are sufficiently soluble are the propionate and *n*-butyrate complexes. $Os_2(\mu\text{-}O_2CEt)_4Cl_2$ and $Os_2(\mu\text{-}O_2CPr^n)_4Cl_2$ each display a reversible one-electron reduction at $E_{1/2}=0.29$ and 0.30 V (vs SCE) respectively in $CH_2Cl_2/Bu^n_4NPF_6$ [45]. This corresponds to the $Os_2^{6+/5+}$ couple. (Earlier reports [42,43] stating that this process was due to an oxidation to an Os_2^{7+} core were shown to be incorrect [80]). An additional one-electron oxidation at $E_{1/2}\approx +1.75$ V was assigned to the $Os_2^{7+/6+}$ couple.

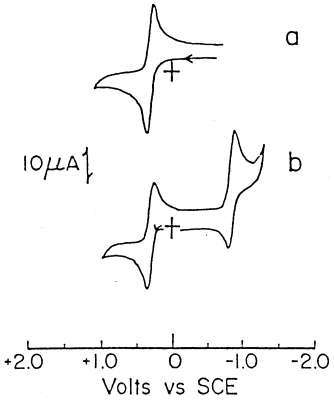

Fig. 12. Cyclic voltammograms in 0.2M $NBu^n_4PF_6/CH_2Cl_2$ at a scan rate of 200 mV s^{-1}. (a) $Os_2(\mu\text{-}O_2CPr^n)_4Cl_2$, (b) $[(\eta^5\text{-}C_5H_5)_2Co][Os_2(\mu\text{-}O_2CPr^n)_4Cl_2]$. Reproduced with permission from Ref. [45].

Controlled potential electrolysis at +0.20 V generates a solution containing a stable monoanion. Chemically, the monoanion can be formed by using cobaltocene as the reductant (−0.94 V vs SCE in CH_3CN) and $[(\eta^5\text{-}C_5H_5)_2Co]$-$[Os_2(\mu\text{-}O_2CR)_4Cl_2]$ (R = Et, Pr^n) isolated. Cyclic voltammetry measurements on these complexes revealed the peaks at 0.29 V (R = Et) and 0.30 V ($R = Pr^n$) as expected along with a reduction at −0.90 V vs SCE due to cobaltocene (Fig. 12). Unlike the ruthenium carboxylates, in which the mixed-valent Ru_2^{5+} species are more stable than Ru_2^{6+} (in fact, the latter have not yet been isolated), for osmium the Os_2^{6+} is the more stable core. This is a good example of the increased stability of higher oxidation states upon descending the periodic table.

Cyclic voltammetry on the equivalent bromide salts $Os_2(\mu\text{-}O_2CR)_4Br_2$ (R = Et, Pr^n) in CH_2Cl_2 yielded $E_{1/2} = 0.43$ and 0.40 V vs Ag/AgCl (ferrocene at 0.47 V) respectively [44], similar to the chloride salts discussed above. $Os_2(\mu\text{-}2\text{-}PBZ)_4Cl_2$ shows a reversible reduction at 0.602 V vs Ag/AgCl (ferrocene at 0.715 V) in CH_2Cl_2 [58].

9. Kinetics and thermodynamics

The determination of rate and equilibrium constants for electron transfer and ligand substitution reactions of ruthenium and osmium carboxylates has received little attention.

Ti(III) reduces the $[Ru_2(\mu\text{-}O_2CCH_3)_4]^+$ cation at 25 °C in 1M $LiCF_3SO_3/HCF_3SO_3$ by a two-term rate law involving both Ti^{3+} and $TiOH^{2+}$ [78]a

$$k = \frac{(k_1[H^+] + k_2K_a)}{([H^+] + K_a)} \tag{3}$$

where under pseudo-first-order conditions $k = k_{obs}/[Ti(III)]$, k_1 and k_2 are second-

order rate constants for the reactions of Ti^{3+} and $TiOH^{2+}$, and K_a is the acidity constant of Ti^{3+}. Values of $k_1 = 2.3 \times 10^2 M^{-1} s^{-1}$ and $k_2 = 3.4 \times 10^3 M^{-1} s^{-1}$ were obtained. It was concluded that base catalysis of the dimer reduction resulted from deprotonation of the reductant, i.e. $Ti(H_2O)_6 \rightarrow Ti(H_2O)_5(OH)$, rather than deprotonation of $[Ru_2(\mu\text{-}O_2CCH_3)_4]^+$. A base-catalyzed reaction mechanism was also implicated in the second-order outer-sphere reduction of $[Ru_2(\mu\text{-}O_2CCH_3)_4]^+$ by $Ti(C_2O_4)^-$ in 1.0M $LiCF_3SO_3$ media at 25 °C and $[H^+] = 0.15M$. The value of $k_1 = 4.17 \times 10^3 M^{-1} s^{-1}$ [78]b.

Axial anation reactions of $[Ru_2(\mu\text{-}O_2CCH_3)_4(H_2O)_2]^+$ by chloride ion have been investigated by Dema and Bose [79]a. The substitution is by successive anations.

$$[Ru_2(\mu-O_2CCH_3)_4(H_2O)_2]^+ + Cl^- \overset{K_1}{\rightleftharpoons} [Ru_2(\mu-O_2CCH_3)_4(H_2O)(Cl)]$$

$$[Ru_2(\mu-O_2CCH_3)_4(H_2O)(Cl)] + Cl^- \overset{K_2}{\rightleftharpoons} [Ru_2(\mu-O_2CCH_3)Cl_2]^-$$

The values of K_1 and K_2 were determined spectrophotometrically to be 15 ± 1 and $3.7 \pm 0.3 M^{-1}$, respectively. Attempts to measure the rates of chloride anation proved unsuccessful since 95% of the reaction was over within the time of mixing ($\sim$4 ms) of their stopped-flow apparatus. A lower limit of $10^4 M^{-1} s^{-1}$ was thus estimated.

In the same study the reduction of $[Ru_2(\mu\text{-}O_2CCH_3)_4Cl_2]^-$ was also accomplished with Ti(III).

$$[Ru_2(\mu-O_2CCH_3)_4Cl_2]^- + Ti^{3+} \rightarrow [Ru_2(\mu-O_2CCH_3)_4Cl_2]^{2-} + Ti^{4+}$$

This reaction obeys an identical, pH dependent, rate law as for the reduction of $[Ru_2(\mu\text{-}O_2CCH_3)_4]^+$ (Eq. (3)) given above and is consistent with the following mechanism

$$[Ti(H_2O)_6]^{3+} + H_2O \overset{K_a}{\rightarrow} [Ti(H_2O)_5(OH)]^{2+} + H_3O^+$$

$$[Ti(H_2O)_6]^{3+} + [Ru_2(\mu-O_2CCH_3)_4Cl_2]^- \overset{k_1}{\rightarrow} \text{products}$$

$$[Ti(H_2O)_5OH]^{2+} + [Ru_2(\mu-O_2CCH_3)_4Cl_2]^- \overset{k_2}{\rightarrow} \text{products}$$

where $K_a = 2.3 \times 10^{-3} M$, $k_1 = 75 M^{-1} s^{-1}$ *and* $k_2 = 1.1 \times 10^3 M^{-1} s^{-1}$. Chloride does not usually serve as a bridging ligand for Ti(III) reductants and an outer-sphere mechanism was therefore postulated. Displacement of the equatorial carboxylates has only briefly been investigated [79]b. When $[Ru_2(\mu\text{-}O_2CEt)_4]^+$ is reacted with oxalate ion in an acidic aqueous medium (0.10M $LiCF_3SO_3$, $[H^+] = 0.01M$) a three-step process is seen. There is initial rapid substitution of one propionate followed by a slower second-order displacement of a second propionate ($k = 1.3 M^{-1} s^{-1}$, $K_f > 2 \times 10^4 M^{-1}$). This is followed by an even slower decomposi-

Table 5
Enthalpies of 1:1 adduct formation for $Ru_2(\mu\text{-}O_2CPr^n)_4Cl$ with a series of Lewis bases[a] (adapted from Ref. [61])

Base	$-\Delta H_{exp}$	$-\Delta H^b_{EC}$
N-methylimidazole	18.5	18.6
Pyridine	18.1	17.1
4-Picoline *N*-oxide	17.1	16.8
Dimethyl sulphoxide	13.9	14.0
Tetrahydrothiophene	12.8	12.6
Acetone	10.6	10.6
Acetonitrile	9.7	8.5

[a] All values in kcal mol^{-1}.
[b] Where $E_A = 7.73 \pm 0.10$, $C_A = 1.27 \pm 0.02$ and E_B and C_B are as tabulated for the particular base [81].

tion step. To date there have been no kinetic investigations of diosmium tetracarboxylates.

A detailed calorimetric study was undertaken by Drago *et al.* [61] to determine the enthalpies of adduct formation for the reaction of $Ru_2(\mu\text{-}O_2CPr^n)_4Cl$ with the Lewis bases acetone, *N*-methylimidazole, tetrahydrothiophene, dimethylsulphoxide, 4-picoline *N*-oxide, acetonitrile and pyridine

$$Ru_2(\mu\text{-}O_2CPr^n)_4Cl + base \rightarrow Ru_2(\mu\text{-}O_2CPr^n)_4Cl(base) \quad (-\Delta H)$$

The experimentally determined values, $-\Delta H_{exp}$, are summarized in Table 5 for the 1:1 adduct formation reaction along with calculated values using an *E* and *C* parameter fitting of the data, $-\Delta H = E_A E_B + C_A C_B$, where E_A and C_A are intrinsic to the solvent system used and E_B and C_B depend on the base added [81]. It was concluded that the $Ru_2(\mu\text{-}O_2CPr^n)_4Cl$ complex is a stronger Lewis acid than both $Rh_2(\mu\text{-}O_2CPr^n)_4$ and $Mo_2(\mu\text{-}O_2CPr^n)_4$ and that this could be attributed to the higher overall oxidation state, i.e. 5+ versus 4+. It should be noted that the poorer fits of the *E* and *C* model to the data for pyridine and acetonitrile adduct formation (see Table 5) were proposed to be due to significant π backbonding from the partially filled metal π* orbitals to these moderate π-acceptor bases.

10. Other physical measurements

Other techniques which have seen limited application, such as mass spectrometry (MS), nuclear magnetic resonance (NMR), photoelectron spectroscopy (PES) and circular dichroism (CD) deserve some coverage.

Mass spectrometry has been used as a characterization tool for both diruthenium and diosmium complexes. Diruthenium examples include the reduced $Ru_2(\mu\text{-}O_2CR)_4$ where $R = CH_3$, Et, and Ph and the $Ru_2(\mu\text{-}O_2CEt)_4(THF)_2$ adduct [29,30], as well as the mixed-valent $[Ru_2(\mu\text{-}O_2CR)_4X]$ complexes where $R = CHEt_2$, CHMeEt, CHMePh and $X = Cl^-$ and SCN^- [28]. In these latter com-

plexes not only are monomolecular peaks seen but also peaks corresponding to dimeric units of the form $[Ru_2(\mu\text{-}O_2CR)_4XRu_2(\mu\text{-}O_2CR)_4]^+$. The formation of dimer fragments was proposed to be due to association during the fragmentation process (a phenomenon not uncommon in fast atom bombardment mass spectrometry or FAB-MS), since many of the complexes had previously been characterized by X-ray crystallography and found to be monomolecular.

A comparison of two different MS techniques, FAB-MS and desorption–chemical ionization electron-capture (DCI-EC), was undertaken on $Ru_2(\mu\text{-}O_2CPr^n)_4Cl$ [82]. No evidence of higher order fragments was seen. In the DCI mode a stable reduced fragment corresponding to $[Ru_2(\mu\text{-}O_2CPr^n)_4Cl]^-$ was observed. In the FAB experiment, only the dechlorinated $[Ru_2(\mu\text{-}O_2CPr^n)_4]^+$ species was seen along with its lower molecular weight fragments. It was concluded that the DCI-EC method was better at generating molecular ions for complexes exhibiting stable lower oxidation states.

Mass spectral characterizations have been undertaken on some diosmium compounds, in particular $Os_2(\mu\text{-}O_2CR)_4Cl_2$ ($R=CH_3$, Et, Pr^n and CH_2Cl) [43]. In all cases a parent ion peak is seen corresponding to $[Os_2(\mu\text{-}O_2CR)_4Cl_2]^+$ followed by peaks for successive Cl^- fragmentation, i.e. $[Os_2(\mu\text{-}O_2CR)_4Cl]^+$ and $[Os_2(\mu\text{-}O_2CR)_4]^+$. More extensive follow-up studies [57] derived detailed fragmentation maps for all of the above except where $R=CH_2Cl$ and they revealed distinctive peak patterns due to seven naturally occurring isotopes of osmium. In addition to the fragmentation of the chlorides, a pathway involving loss of $RCO^{\cdot}$ radical or an RCH=C=O fragment is also seen. There was no evidence of fragmentation to a mononuclear Os complex.

A technique that has not seen much use, due to the paramagnetic nature of the complexes, is NMR. A ^1H NMR was run on $[Ru_2(\mu\text{-}O_2CCH_3)_4(OPPh_3)_2]X\cdot CH_2Cl_2$, $X=BF_4^-$ or PF_6^-, and revealed the presence of the dichloromethane of solvation ($\delta=5.23$ ppm) as well as the methyl protons, which were shifted upfield due to the paramagnetic centre, at $\delta=-5.29$ ppm, and the phenyl protons at $\delta=5.74$–6.12 [22]. The THF adduct, $[Ru_2(\mu\text{-}O_2CCH_3)_4(THF)_2]BF_4$, showed signals at $\delta=1.85$ and 3.75 ppm due to free THF that had been exchanged by the solvent DMSO-d_6 molecules [14].

The presence of a diamagnetic Ru(II) centre and a paramagnetic diruthenium core in the cationic–anionic complexes of the form $[RuCl(MeCN)_3(PPh_3)_2]_x[Ru_2Cl_2(\mu\text{-}O_2CR)_4]$ ($x=1$, $R=CH_3$; $x=2$, $R=p$-MePh) [56] leads to ^1H resonances ranging from -45 to $+34$ ppm (Fig. 13). Peaks near 32 ppm were assigned to ortho-protons on the bridging carboxylates while peaks in the range of 3 to -3 ppm were due to the *cis* and *trans* CH_3CN. The acetate protons are observed at -44.26 ppm and the multiple peaks in the range 4.5 to 7.4 ppm are due to phenyl ring protons on the PPh_3 groups. Single peaks from -3.2 to 5.6 ppm were assigned to the methyl of the phenyl group.

A detailed study of the modes of axial ligation to various Ru_2^{4+} and Ru_2^{5+} cores using both ^1H and ^{13}C NMR was recently performed by Chisholm and coworkers [55]. Investigation of diruthenium tetra-*n*-octanoate, $Ru_2(\mu\text{-}O_2C(CH_2)_6CH_3)_4$, in non-coordinating solvents showed a ^1H NMR spectrum containing broad and

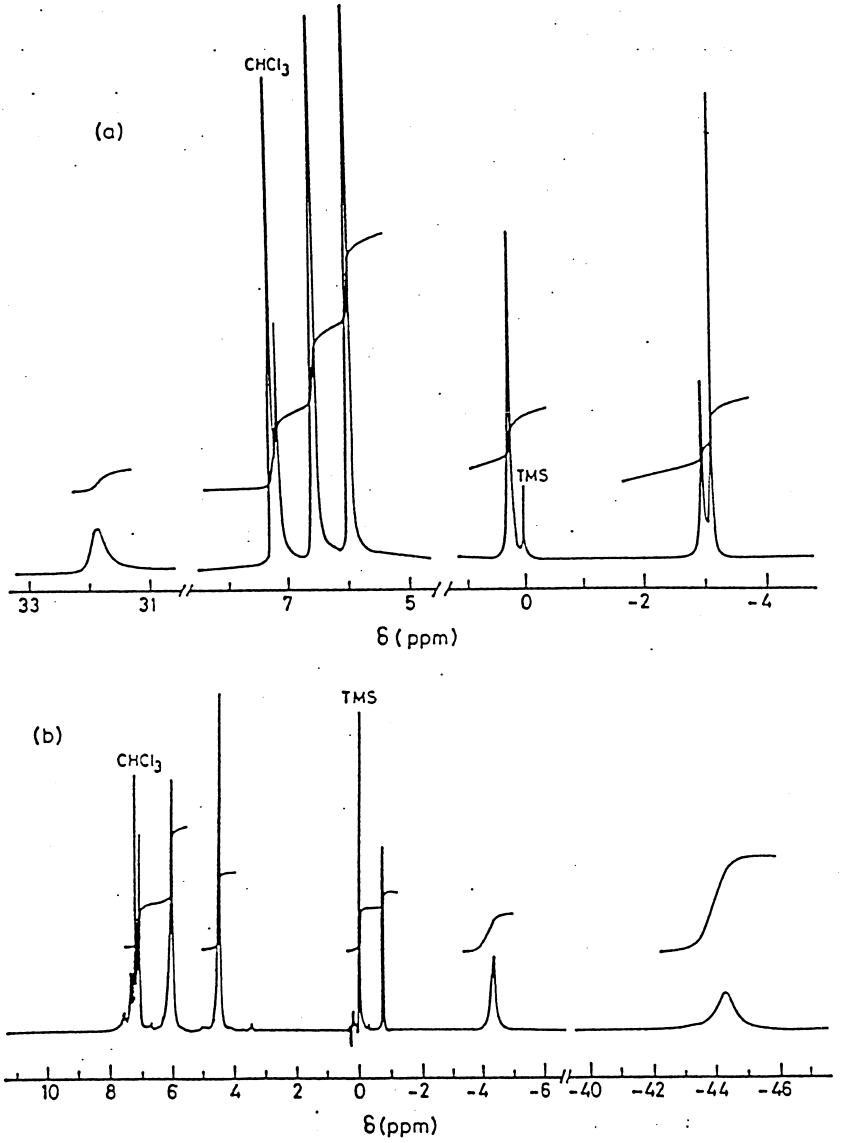

Fig. 13. ^{1}H NMR spectra of the cationic–anionic complexes: (a) $[RuCl(MeCN)_3(PPh_3)_2]_2[Ru_2Cl_2(\mu\text{-}O_2CC_6H_4\text{-}p\text{-}CH_3)_4]$ and (b) $[RuCl(MeCN)_3(PPh_3)_2]$-$[Ru_2Cl_2(\mu\text{-}O_2CCH_3)_4]$. Reproduced with permission from Ref. [56].

unresolvable signals, whereas its spectrum in coordinating solvents, such as THF or methanol, showed sharp, well-resolved peaks. This latter observation is characteristic of a diamagnetic species, however, all resonances were shifted to much lower field. The mixed-valent $[Ru_2(\mu\text{-}O_2C(CH_2)_6CH_3)]X$ ($X=Cl^-$ or BF_4^-) complexes showed

similar well-resolved spectra in both types of solvent. The reason for the spectral differences in the former case was proposed to be due to the formation of oligomers in non-coordinating solvents where the ruthenium of one dimer is coordinated to an acetate oxygen of the next dimer and so on (see Fig. 14). In coordinating solvents this does not happen and monomolecular $Ru_2(\mu\text{-}O_2CR)_4L_2$ (L = solvent) species are formed. UV/vis, resonance Raman and cyclic voltammetry studies supported this proposal [55]. Extensive peak assignments using the 1D NMR spectra (and 2D COSY spectra in THF-d_8 for the Ru_2^{4+} complex) for the well-resolved reduced and oxidized species were undertaken. Both dipolar and contact mechanisms were determined to contribute to the paramagnetic shifts for both axial and equatorial ligands. The dipolar mechanism leads to a downfield shift of the resonances on the equatorial ligands and an upfield shift of those on the axial ligands. An enhanced upfield shift of the axial ligand protons on the pyridine, pyrazine and picoline derivatives is indicative of some degree of π-delocalization from metal to ligand. π-contact shifts are also seen equatorially in $Ru_2(\mu\text{-toluate})_4$ and $Ru_2(\mu\text{-benzoate})_4$ species.

Contact-shifted resonances were also observed in the ^1H and ^{13}C NMR spectra of $Os_2(\mu\text{-}O_2CPr^n)_4Cl_2$ and $Os_2(\mu\text{-}O_2CR)_4Br_2$ (R = Et, Pr^n). Displacements to lower frequency are seen for all protons with those closest to the Os_2^{6+} core experiencing the greatest shift [19,43].

Photoelectron spectroscopy (PES) was performed on $Ru_2(\mu\text{-}O_2CCF_3)_4$ and $Ru_2(\mu\text{-}O_2CCF_3)_4(NO)_2$ and the results compared to the ionization energies of the model systems $Ru_2(\mu\text{-}O_2CH)_4$ and $Ru_2(\mu\text{-}O_2CH)_4(NO)_2$ determined by configuration interaction calculations and subsequent extended Hückel, Fenske–Hall and *ab initio* calculations [35]. The experimental spectra for $Ru_2(\mu\text{-}O_2CCF_3)_4$ were consistent with either a $\sigma^2\pi^4\delta^2\pi^{*2}\delta^{*2}$ or a $\sigma^2\pi^4\delta^2\pi^{*3}\delta^*$ ground-state configuration, however, the theoretical calculations on $Ru_2(\mu\text{-}O_2CH)_4$ of the ionization energies were more in line with a $\sigma^2\pi^4\delta^2\pi^{*2}\delta^{*2}$ configuration which was consistent with Cotton's earlier assessment [69]. When the axial NO ligands are present the complex is

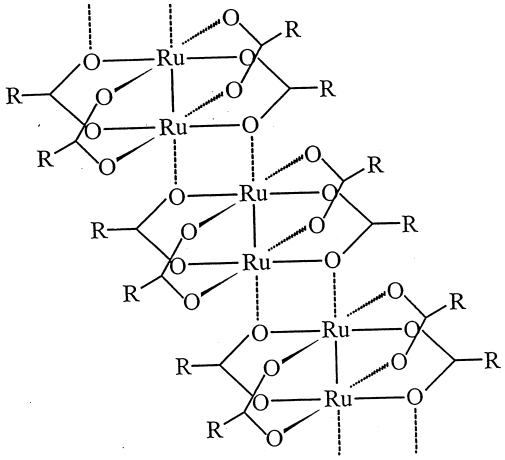

Fig. 14. Proposed oligomeric structure of $Ru_2(\mu\text{-}O_2CR)_4$ in non-coordinating solvents.

diamagnetic with a ground-state configuration of $\sigma^2\pi^4\delta^2\pi^{*4}\delta^{*2}$ [recall its formal assignment as a $Ru_2(I,I)$ complex]. The axial ligands also serve to destabilize the metal–metal σ bonding orbital and the lowest ionization energy now corresponds to a σ electron (from calculations on $Ru_2(\mu\text{-}O_2CH)_4(NO)_2$) instead of a δ^* electron as in the unligated complexes.

There has been only one example of circular dichroism being used as a characterization tool. This was for the chiral $Ru_2(\mu\text{-L-mandelate})_4 \cdot 2H_2O$ complex [33]. Three bands are seen in the CD spectrum. The one at 450 nm is the same as that seen in the electronic spectrum and assigned to a Ru–O, Ru_2 $\pi \rightarrow Ru_2$ π^* transition while one of the two exclusively CD bands was proposed to be due to a magnetically allowed Ru_2 $\sigma \rightarrow Ru_2$ π^* transition. No further analysis was given.

11. Magnetic susceptibility

11.1. Diruthenium(II,III) systems

We consider magnetic susceptibility, in particular variable-temperature magnetic susceptibility (VTMS), in more detail at this point (see also Section 4) in the review for two reasons. Firstly, we would like to contrast the behaviour of the discrete mixed-valent $[Ru_2(\mu\text{-}O_2CR)_4L_2]X$ and the reduced $Ru_2(\mu\text{-}O_2CR)_4$ or $Ru_2(\mu\text{-}O_2CR)_4L_2$ species with the bent and linear chain complexes of the form $[Ru_2(\mu\text{-}O_2CR)_4X]_n$ (X = bridging ligand). Secondly, we want to highlight current attempts at exploiting the $S = 3/2$ ground-state in the mixed-valent species in order to create chains (and potentially networks) displaying significant interdimer magnetic exchange, i.e. potential molecular magnetic wires.

Two early VTMS studies [60,77] on the mixed-valent, bent chain complex, $Ru_2(\mu\text{-}O_2CPr^n)_4Cl$, showed that Curie–Weiss behaviour explained the data over the temperature range 35–300 K but at temperatures below 35 K significant deviations occurred [60]. Because of the polymeric nature of these complexes both intra- and intermolecular effects were thought to be operating to lead to these deviations. These effects could be manifested either as intermolecular antiferromagnetic exchange *between* Ru_2^{5+} dimers and/or zero-field splitting (ZFS) *within* the Ru_2^{5+} dimer (where $S = 3/2$). This latter splitting was termed an "intramolecular antiferromagnetic" effect by Drago [60]. Five separate models were used to fit the data and two were deemed to be reasonably good. In both cases no intermolecular exchange was invoked, only a large ZFS.

The first model is based on the full spin Hamiltonian for an $S = 3/2$ system

$$\mathcal{H} = \beta(g_x \boldsymbol{H}_x \boldsymbol{S}_x + g_y \boldsymbol{H}_y \boldsymbol{S}_y + g_z \boldsymbol{H}_z \boldsymbol{S}_z) + D[\boldsymbol{S}_z^2 - (1/3)S(S+1)] + E(\boldsymbol{S}_x^2 - \boldsymbol{S}_y^2) \tag{4}$$

where D and E are scalar crystal field splitting parameters. The matrix elements for this Hamiltonian are given in Ref. [60]. The second model involves the exponential form for the zero-field susceptibility of an O_h, $S = 3/2$, complex with axial zero-field

splitting, originally derived by O'Connor [83]

$$\chi_{\parallel} = \frac{Ng_{\parallel}^2\beta^2}{kT}\,\frac{1+9\exp(-2D/kT)}{4[(1+\exp(-2D/kT)]} \tag{5}$$

$$\chi_{\perp} = \frac{Ng_{\perp}^2\beta^2}{kT}\,\frac{4+(3kT/D)[1-\exp(-2D/kT)]}{4[1+\exp(-2D/kT)]} \tag{6}$$

where an orientational average, χ_{av}, was used.

$$\chi_{av} = (\chi_{\parallel} + 2\chi_{\perp})/3 \tag{7}$$

The parameters obtained in the fitting process for both of these models are given in Table 6. The results from the fitting to Eqs. (4) and (7) are similar and were favoured by the authors over the other three models. The fitted curves (Eq. (4)) are shown in (Fig. 15). Whereas Cotton's earlier study [77] had implicated weak intermolecular antiferromagnetic exchange, Drago's results did not. In fact, the models that did incorporate exchange parameters gave decidedly poorer fits.

The value of D (a direct measure of ZFS), 77 cm^{-1}, is large but not unexpected when one considers the presence of two second row transition metals with closely spaced electronic states. Eq. (7), while fitting the data reasonably well, gave g values which differed considerably from those determined by ESR and thus were not entirely favoured. It was concluded that the $[Ru_2(\mu\text{-}O_2CPr^n)_4]^+$ units, despite being linked into a polymeric chain by bridging chlorides, could be treated as isolated $S = 3/2$ systems.

All mixed-valent complexes whether they are distinct adducts or chain complexes show room-temperature values of μ_{eff} in the range 3.6 to 4.4 B.M., consistent with an $S = 3/2$ ground-state. Many recent studies have looked at magnetic behaviour down to 70 K [14,18,19,22,23,28] and in all cases Curie–Weiss behaviour was observed. Unfortunately, none of these studies went below 70 K.

It may seem surprising at first that no intermolecular exchange was observed in the polymeric chloro-bridged complex, $Ru_2(\mu\text{-}O_2CPr^n)_4Cl$, but as mentioned earlier (see Section 3) the X-ray structure shows that these chains are significantly bent with an Ru–Cl–Ru angle of 125° and hence overlap of magnetic orbitals is certainly not optimized. Linear chains ($\angle$ Ru–X–Ru = 180°) are seen in $Ru_2(\mu\text{-}O_2CCH_3)_4Cl$ [49] and $Ru_2(\mu\text{-}O_2CEt)_4Cl$ [20], however, VTMS measurements have not been

Table 6
Parameters obtained from the fitting of the magnetic susceptibility data for $Ru_2(\mu\text{-}O_2CPr^n)_4Cl$ to Eqs. (4) and (7) (adapted from Ref. [60])

Equation used	D (cm^{-1})	$g_{\parallel}$	$g_{\perp}$	g_{av}	SE[a]
Eq. (4)	76.8	2.02	2.14	2.10	0.0038
Eq. (7)	70.6	–	2.11	2.09	–

[a] Goodness of fit: $SE = \{\Sigma_{i=1}^{n}[(\mu_{eff})_i^{obsd} - (\mu_{eff})_i^{calc}]^2/(n-k)\}^{1/2}$ where n = number of data points and k = number of varying parameters.

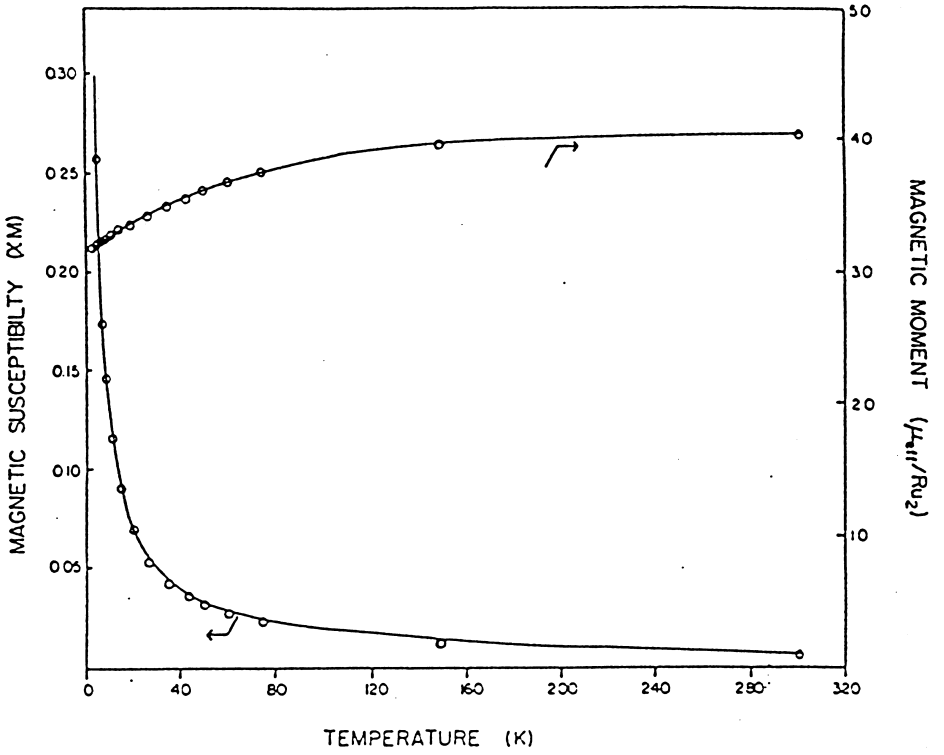

Fig. 15. Plots of molar magnetic susceptibility and effective magnetic moment versus temperature for $Ru_2(\mu\text{-}O_2CPr^n)_4Cl$. The solid lines correspond to least-squares fits to Eq. (5). Reproduced with permission from Ref. [60].

performed on these complexes. Instead, Cotton *et al.* [16] looked at $Ru_2(\mu\text{-}O_2CCMePh_2)_4Cl$ in 1993. The choice of bulkier R group was to eliminate any possibility of *interchain* interactions. Measurements were made over the range 2–300 K and the plot of χ_M vs T clearly shows a turning point at 70 K which is indicative of antiferromagnetic coupling (Fig. 16). Fitting of the data to a 1D Ising model revealed a J value of $-10.9\,cm^{-1}$. A small but definite degree of coupling; thus showing that geometry does appear to play a role.

Another way to induce a linear alignment of ruthenium dimers is to use linear bidentate ligands that can bridge the dimers axially. This has been achieved recently with interesting magnetic results. The first example involves a bridging phenazine between $[Ru_2(\mu\text{-}O_2CEt)_4]^+$ units [21]. The Ru–phenazine–Ru angle is, surprisingly, only 147.6°. Linearity is not achieved and the magnetic measurements over the range 5 to 300 K were inconclusive, although the deviations from the earlier results of the magnetically isolated $Ru_2(\mu\text{-}O_2CPr^n)_4Cl$ system are significant enough to imply some antiferromagnetic coupling. Though no fitting was attempted, and hence no J value determined, the coupling was thought to be quite small.

A similar system, $\{[Ru_2(\mu\text{-}O_2CCH_3)_4pyz](BPh_4)\}_n$, pyz = pyrazine, was studied by

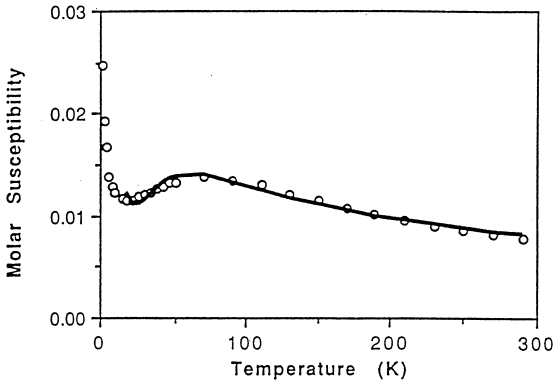

Fig. 16. Plot of molar magnetic susceptibility versus temperature for $Ru_2(\mu\text{-}O_2CCMe(Ph)_2)_4Cl$. The solid line corresponds to a least-squares fit of the data to an Ising model (see text). Reproduced with permission from Ref. [16].

Cukiernik *et al.* [26] and an extensive fitting process employed. Measurements of the susceptibility over the 6 to 300 K range for the polymer were contrasted with those obtained for the diadduct, $[Ru_2(\mu\text{-}O_2CCH_3)_4(H_2O)_2](BPh_4)$. The two compounds show distinctly different behaviour. The magnetic data for the diaquo adduct could readily be fit to O'Connor's exponential model for zero-field susceptibility (Eqs. (5)–(7)) with a large ZFS term, $D=71.8\ cm^{-1}$, and no intermolecular coupling. The polymer data, on the other hand, could not be fit to this model. The assumption made was that there was still a significant amount of intramolecular antiferromagnetism (i.e. a large ZFS) but also a small amount of interdimer antiferromagnetism. A molecular field approximation (Eq. (8)), also based on O'Connor's work [83], was therefore employed

$$\chi'_{av}=\frac{\chi_{av}}{1-(2zJ/N^2g^2\beta^2)\chi_{av}} \tag{8}$$

where χ_{av} is derived from a modified form of Eq. (7) which includes corrections for temperature independent paramagnetism (TIP) and the mole fraction of any paramagnetic impurity, ρ, (Eq. (9)) and zJ is the exchange energy J multiplied by the number of interacting neighbours, z.

$$\chi_{av}=(1-\rho)[(\chi_{\parallel}+2\chi_{\perp})/3+\mathrm{TIP}]+\rho N\beta^2g^2/4kT \tag{9}$$

The fitted data is shown in Fig. 17. The zJ value of $-2.3\ cm^{-1}$ indicates, again, a small but non-negligible interdimer antiferromagnetic coupling. The parameters determined from the fitted data are presented in Table 7. A recent extension of this work by Beck *et al.* [94] included 4,4′-dipyridyl (dipy) and 1,4-diazabicyclo[2.2.2]octane (dabco) as bridging ligands and also found Eq. (8) to be appropriate in fitting the data. The coupling in these cases is attenuated with respect to the pyrazine-bridged system as may be expected due to the larger distance between metal centres. For $\{[Ru_2(\mu\text{-}O_2CCH_3)_4(dabco)](PF_6)\}_n$, $zJ=-0.59\ cm^{-1}$

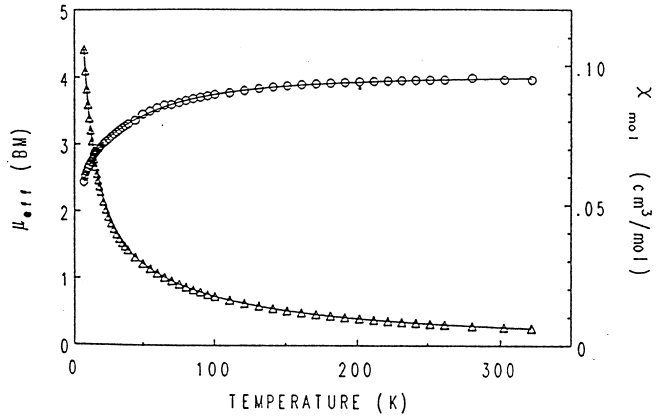

Fig. 17. Plots of molar magnetic susceptibility and effective magnetic moment versus temperature for $\{[Ru_2(\mu\text{-}O_2CCH_3)_4pyz](BPh_4)\}_n$. The solid lines correspond to least-squares fits to Eq. (8). Adapted from Ref. [26].

Table 7
Parameters obtained from the fitted magnetic data for $[Ru_2(\mu\text{-}O_2CCH_3)_4(H_2O)_2](BPh_4)$ (1) and $\{[Ru_2(\mu\text{-}O_2CCH_3)_4(pyz)](BPh_4)\}_x$ (2) using Eqs. (7) and (8) (adapted from Ref. [26])

Complex	g	D (cm^{-1})	TIP ($cm^3\ mol^{-1}$)	zJ (cm^{-1})	ρ (%)	σ^{2a}
1	2.190	71.8	$<10^{-6}$	–	0.11	7.1×10^{-6}
2	2.098	62.9	$<10^{-6}$	−2.3	0.61	3.7×10^{-5}

[a] $\sigma^2=\Sigma(\chi_{calc}-\chi_{exp})^2/\Sigma\chi^2_{exp}$.

and for $\{[Ru_2(\mu\text{-}O_2CCH_3)_4(dipy)]X\}_n$, $zJ=-1.0\ cm^{-1}$ for $X=PF_6^-$ and $zJ=-0.65\ cm^{-1}$ for $X=BPh_4^-$. The ZFS ranged from 63 to 70 cm^{-1}.

A promising direction for this work was to move from a diamagnetic to paramagnetic (or radical) bridging ligand [63]. Preliminary studies on $[Ru_2(\mu\text{-}O_2CR)_4(DM\text{-}DCNQI)]_n$, $R=p\text{-}CH_3Ph$, reveal antiferromagnetic behaviour with $T_{Neel}=46$ K at field strengths of $H=0.1$ T and $H=1$ T (Fig. 18(a)). The magnetization is field dependent, as one would expect for a 1D system, and the inverse susceptibility has a non-linear dependence on temperature below T_{Neel} but for $T>T_{Neel}$ it extrapolates to a negative Curie temperature. It was concluded that interchain or intrachain coupling was occurring, but no further analysis was undertaken. The complex $[Ru_2(\mu\text{-}O_2CCH_3)_4(DM\text{-}DCNQI)]_n$ was also studied and showed $T_{Neel}=27$ K at $H=1$ T but an additional maxima occurred at 17 K for $H=0.1$ T (Fig. 18(b)). The inverse susceptibility plot suggested both antiferromagnetic (for $T>150$ K) and ferromagnetic ($T<150$ K) correlations. The field dependence suggests a possible mixture of inter- and intrachain effects with the size of the R group possibly playing a role. Further study is underway [63,65].

The final category of mixed-valent magnetic materials involves diruthenium units incorporating the nitroxide radicals, tempo and nitph (shown below) [51,52]. The

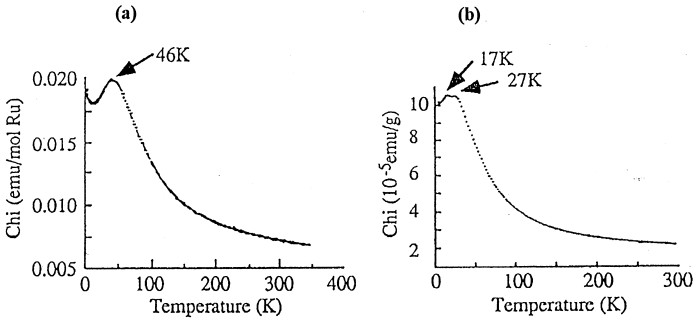

Fig. 18. Plots of magnetic susceptibility versus temperature for $[Ru_2(\mu\text{-}O_2CR)_4(DM\text{-}DCNQI)]_n$ at 0.1 T. (a) R = tolyl, (b) R = Me. Adapted from Ref. [63].

dicationic complex $[Ru_2(\mu\text{-}O_2CCMe_3)_4(tempo)_2][Ru_2(\mu\text{-}O_2CCMe_3)_4(H_2O)_2](BF_4)_2$ [51] displays significant antiferromagnetic coupling between the diruthenium core and the nitroxide radical (tempo). $J_2 = -130\ cm^{-1}$, in the $[Ru_2(\mu\text{-}O_2CCMe_3)_4(tempo)_2]^+$ cation with no coupling observed between nearest neighbour nitroxides ($J_1 = 0$) (see Fig. 19).

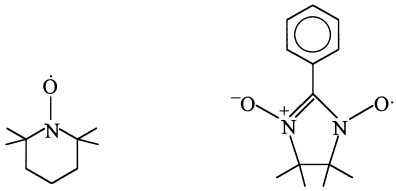

A chain complex (Fig. 4) incorporating a dinitroxide bridge (nitph) has also been studied [52] but again only a strong antiferromagnetic interaction ($J_2 = -100\ cm^{-1}$) was seen between the $S = 3/2\ Ru_2^{5+}$ core and the $S = 1/2$ nitroxide. No coupling between nearest neighbour nitroxides was observed. One may have expected *ferrimagnetic* behaviour to be manifested in these systems but the authors explain that significant inequalities in the two Ru–O(nitph) bond lengths (2.264 and 2.236 Å) and the two Ru–O–N angles (131.7° and 147.5°) is probably the cause of the localized coupling.

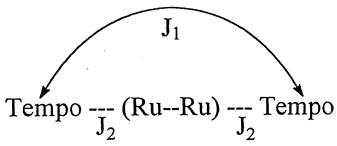

Fig. 19. Schematic showing two types of coupling interactions possible in the $[Ru_2(\mu\text{-}O_2CBu^t)_4(tempo)_2]^+$ ion. Adapted from Ref. [51].

11.2. Diruthenium(II,II) systems

Since the first Ru_2(II,II) complexes were not synthesized until the mid-1980s, and in most cases are quite air-sensitive, only limited VTMS measurements have been undertaken. Early room-temperature measurements were consistent with two unpaired electrons [12,29–31] in a triplet ground-state, $\mu_{eff}=1.9$–2.2 B.M. per Ru. The first VTMS measurement in 1986 by Spohn *et al.* [8] for $[Ru_2(\mu\text{-}O_2CC_6H_5)_4(C_6H_5COOH)_2]$ showed a decrease in μ_{eff} from 2.04 B.M. at $+160$ °C to 1.52 B.M. at -120 °C. This was consistent with Curie–Weiss behaviour and $\theta=-120$ K was calculated.

The first major magnetic study was performed three years later by Maldivi and coworkers [32,84] on a series of long-chain alkyl carboxylate derivatives that displayed liquid-crystal properties (see Section 11). Measurements were made over the range 6–400 K on the palmitate, laurate and butyrate derivatives. Using O'Connor's equations for D_{4h}, $S=1$, systems [similar to those mentioned in context with the mixed-valent Ru_2(II,III) complexes discussed earlier] good fits were obtained for all three species by incorporating very large zero-field splitting parameters ($D\sim300\ cm^{-1}$). This was consistent with the presence of a ground-state with a singlet component and a thermally accessible triplet excited state. Differentiation between $\sigma^2\pi^4\delta^2\pi^{*2}\delta^{*2}$ and $\sigma^2\pi^4\delta^2\pi^{*3}\delta^{*1}$ ground-state configurations could not be made. It is of interest to note that a distinct discontinuity in μ_{eff} occurs at the transition temperature from crystalline solid to columnar liquid-crystal mesophase at 370 K for the diruthenium(II,II) tetrapalmitate derivative (Fig. 20).

Cotton *et al.* [33] looked at the magnetic properties of $Ru_2(\mu\text{-}O_2CPh)_4$ and $Ru_2(\mu\text{-}O_2CCH_3)_4$ from 6 to 298 K and concluded that a $\sigma^2\pi^4\delta^2\pi^{*2}\delta^{*2}$ ground-state configuration was applicable. They found that the μ_{eff}/Ru_2 dropped from ~3.0 B.M.

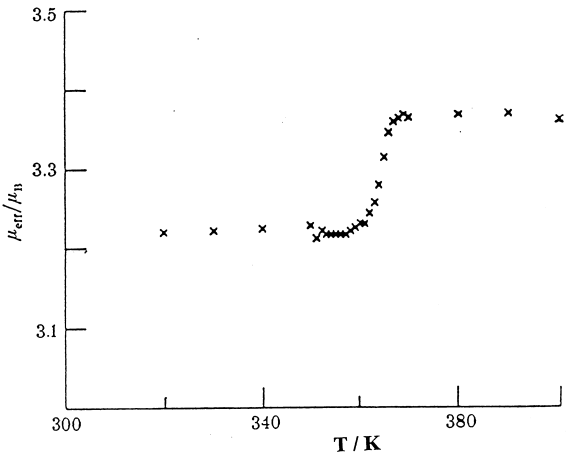

Fig. 20. Plot of effective magnetic moment versus temperature for the diruthenium(II,II) tetrapalmitate derivative about the solid→liquid crystal phase transition. Adapted from Ref. [84].

at 298 K to an extrapolated value of 0 B.M. at 0 K. This implied a nonmagnetic ground-state even though there are two unpaired electrons present at room temperature. A model was derived whereby the degenerate states $^1A_{1g}$, $^1B_{1g}$ and $^1B_{2g}$ and the $^3A_{2g}$ state derived from the $\sigma^2\pi^4\delta^2\pi^{*2}\delta^{*2}$ configuration are split further (second order) to yield, for the $^3A_{2g}$ state, an $S=0$ (A_{1g}) state and an $S=\pm1$ (E_g) state separated by D, the ZFS energy (Fig. 21). D can be estimated from Eq. (10)

$$D=\frac{8\lambda^2}{E_S-E_T} \tag{10}$$

where λ is the effective value of the spin–orbit coupling and E_S-E_T are the energies of the first-order singlet and triplet states, respectively. Fits to the appropriate equation (Eq. (11)) were found to be quite good

$$(\mu_{eff})^2=2g^2\,\frac{e^{-x}+(2/x)(1-e^{-x})}{1+2e^{-x}} \tag{11}$$

where g is the effective isotropic gyromagnetic ratio and $x=D/kT$ (D as in Fig. 21). The D values determined were $244\pm10\ cm^{-1}$ for $Ru_2(\mu\text{-}O_2CCH_3)_4$ and $215\pm25\ cm^{-1}$ for $Ru_2(\mu\text{-}O_2CPh)_4$.

Based on Cotton's assessment that the ground-state was indeed $\sigma^2\pi^4\delta^2\pi^{*2}\delta^{*2}$ a more recent study of the magnetic properties of Ru_2(II,II) metallomesogens by Maldivi *et al.* [85] could be performed in greater detail than their earlier study [32]. They looked at $Ru_2(\mu\text{-fatty acid})_4$ complexes (where fatty acid = lauric, citronellic and undecenoic) and the $[Ru_2(\mu\text{-fatty acid})_4(pyz)]_n$ (fatty acid = lauric) polymer. Using a model similar to O'Connor's mentioned earlier for $[Ru_2(\mu\text{-}O_2CCH_3)_4(H_2O)_2](BPh_4)$ (Eqs. (5)–(7)), only this time for an $S=1$ system with ZFS, reasonable fits were derived for both the nonpolymeric and the polymeric mesogens. As with the mixed-valent $\{[Ru_2(\mu\text{-}O_2CCH_3)_4pyz](BPh_4)\}_n$ polymer the pyrazine-bridged lauric acid derivative was also fitted to a model incorporating weak intermolecular exchange. In this case however, no improvements were found over the unmodified model and it was inconclusive whether any intermolecular antiferromagnetic coupling was occurring. It is possible, in this case, that due to the strong ZFS leading to the only populated level at room temperature being $S_z=0$, no anisotropic coupling is observed. A summary of the fitting results is given in Table 8.

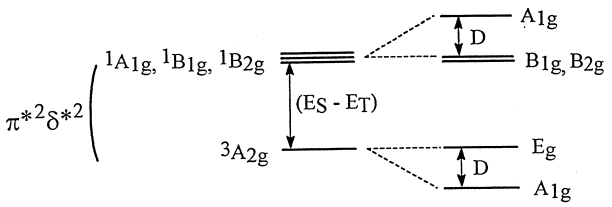

Fig. 21. Diagram showing the states derived from a $\sigma^2\pi^4\delta^2\delta^{*2}\pi^{*2}$ configuration with a large singlet–triplet separation (E_S-E_T) and a small second-order splitting (D) of the $^3A_{2g}$ state. Adapted from Ref. [33].

Table 8
Parameters obtained from the fitted magnetic data for Ru_2(μ-fatty acid)$_4$ complexes and Ru_2(μ-fatty acid)$_4$ pyrazine polymer (adapted from Ref. [85])

Fatty acid	D (cm^{-1})	$g_{\parallel}$	$g_{\perp}$	TIP ($cm^3\ mol^{-1}$)	ρ (%)	σ ($\times 10^2$)[a]
Citronellic	283	1.93	2.22	7×10^{-4}	4.3	2.2
Undecenoic	313	1.90	2.13	5×10^{-4}	3.5	1.7
Lauric	270	1.92	2.11	6×10^{-4}	0.3	0.5
Lauric/pyz	291	2.07	2.13	2.3×10^{-3}	1.0	0.47

[a] $\sigma=[\Sigma(\chi_{exp}-\chi_{calc})^2]^{1/2}/(\Sigma\chi^2_{exp})^{1/2}$.

Two reduced complexes involving the tempo ligand have been studied [36]. Ru_2(μ-O_2CCF_3)$_4$(tempo)$_2$ and Ru_2(μ-$O_2CC_6F_5$)$_4$(tempo)$_2$ exhibit strong antiferromagnetic coupling between the $S=1$, Ru_2^{4+} core and the $S=1/2$ tempo ligands. Magnetic data over the temperature range 5–300 K was fitted to a complicated expression (for details see Ref. [36]) which incorporated the ZFS within the dimetal core, interactions between nearest neighbour nitroxides (J_1) as well as coupling between metal and nitroxide (J_2) (see Fig. 19). It was found that $J_2=-263$ and $-234\ cm^{-1}$ for Ru_2(μ-O_2CCF_3)$_4$(tempo)$_2$ and Ru_2(μ-$O_2CC_6F_5$)$_4$(tempo)$_2$ respectively, with $J_1=0$ in both cases. The inter-nitroxide coupling is zero, as for the mixed-valent analogues mentioned earlier, but the nitroxide–metal coupling is stronger than them. Mechanistically, it was postulated that there was significant overlap between the partially occupied π* orbital on the Ru_2^{4+} core and the π* of the NO of the tempo ligand.

11.3. Diosmium(III,III) and (II,III) systems

Diosmium carboxylates have far more complex magnetic behaviour, as has already been alluded in Section 4. For the Os_2(III,III) complexes of the type Os_2(μ-O_2CR)$_4Cl_2$ there appears to be significant contributions from triplet states derived from $\sigma^2\pi^4\delta^2\pi^{*2}$ or $\sigma^2\pi^4\delta^2\pi^{*1}\delta^{*1}$ configurations and a $\sigma^2\pi^4\delta^2\delta^{*2}$ singlet ground-state.

When Os_2(μ-O_2CR)$_4Cl_2$ is reduced to its monoanion, its magnetic moment increases. For [(η^5-C_5H_5)$_2$Co][Os_2(μ-O_2CPr^n)$_4Cl_2$], for example [45], $\mu_{eff}=$ 2.73 B.M. at 298 K and increases to 2.84 B.M. at 209 K. This was suggested to be in line with contributions from a quartet $\sigma^2\pi^4\delta^2\pi^{*2}\delta^{*1}$ configuration and two doublet configurations $\sigma^2\pi^4\delta^2\delta^{*2}\pi^{*1}$ or $\sigma^2\pi^4\delta^2\pi^{*2}$. Solution magnetic studies on electrochemically generated [Os_2(μ-O_2CR)$_4Cl_2$]$^-$ species (R = Et, Pr^n) revealed similar behaviour to the above with $\mu_{eff}=2.65$ B.M. at 240 K and 2.88 B.M. at 190 K for R = Pr^n. Compared with the isoelectronic Ru_2(μ-O_2CPr^n)$_4$Cl species ($\mu_{eff}\sim4$ B.M. at 300 K) the Os_2^{5+} complexes appear to have a larger π*/δ* separation and a more populated doublet state (although a significant contribution from the quartet state is present).

The most recent, and only, detailed VTMS study on diosmium complexes by

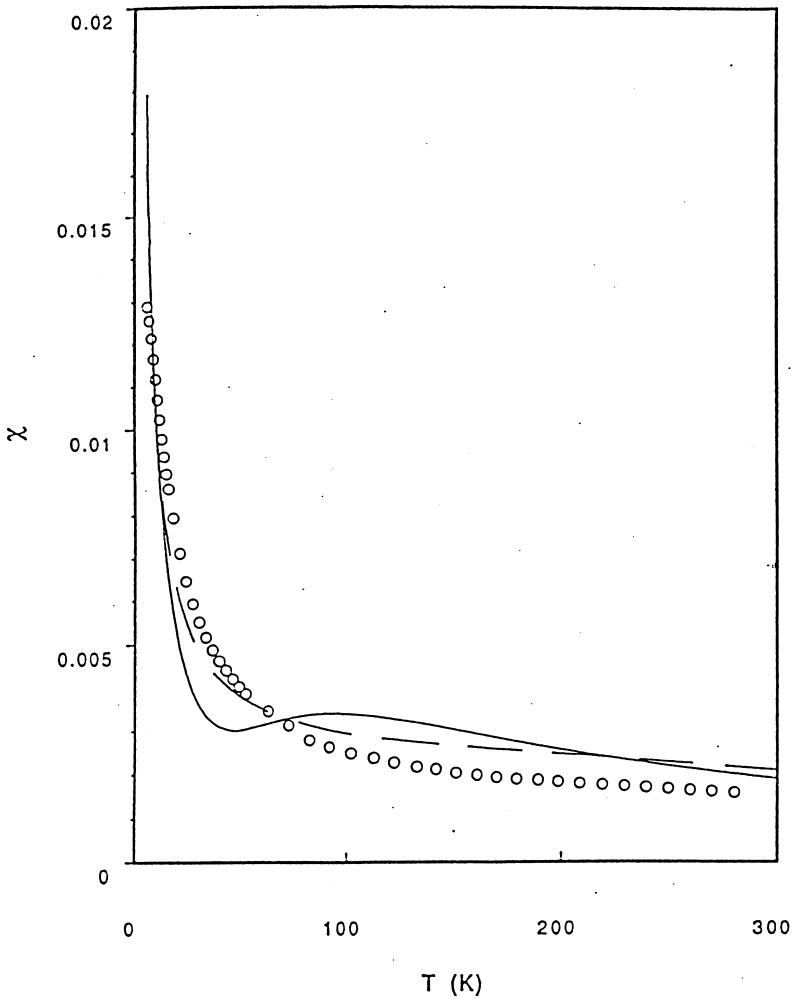

Fig. 22. Plot of magnetic susceptibility versus temperature for $Os_2(\mu\text{-}2\text{-}PBZ)_4Cl_2$. The solid line and the dashed line represent fits to the data using the Bleaney–Bowers model and the ZFS model, respectively. Reproduced with permission from Ref. [58].

Cotton and coworkers [58] on $Os_2(\mu\text{-}2\text{-}PBZ)_4Cl_2$, PBZ = 2-phenylbenzoate, over the temperature range 1.5 to 304 K showed slightly higher absolute moments than earlier Os_2(III,III) complexes. Their data was fitted to both a Bleaney–Bowers equation and a ZFS model with neither being particularly successful (Fig. 22). It was concluded that, because of the small energy differences between the three possible contributing states, the large spin–orbit coupling usually associated with the heavy osmium, and the possibility of weak ferro- or antiferromagnetic exchange via stacked phenyl rings, no satisfactory model could be established for this complicated system

until further information was gained regarding the exact states involved and their relative contributions.

12. Mesogenic properties

One of the primary areas of application for diruthenium tetracarboxylates is as mesogenic materials. Modification of the carboxylate bridge in the reduced, $Ru_2(O_2CR)_4$ type complexes to long-chain fatty acids, such as pelargonic [32], caprylic [86], lauric [32,86] and palmitic [32,84] acids, yielded complexes that displayed columnar liquid-crystalline phases. Similar properties have also been observed in Cu, Rh, Cr and Mo tetracarboxylates.

The synthetic procedure in most cases is straight forward and involves dissolution of $Ru_2(\mu\text{-}O_2CPr^n)_4$ in the neat fatty acid, under argon, followed by either heating to 100 °C for approximately 15 min or stirring at room temperature for two or more days. The precipitated product is recrystallized from heptane. Characterization of the mesophase uses three techniques: differential scanning calorimetry (DSC), variable temperature polarizing optical microscopy and X-ray powder diffraction (XRD). Endotherms observed in the DSC will often correspond to crystal (K)→liquid crystal (LC) and liquid crystal (LC)→isotropic liquid (I) phase transitions with the former being larger in most cases.

Table 9 lists a series of $Ru_2(\mu\text{-}O_2CR)_4$ complexes with varying chain length and their corresponding phase-transition temperatures and enthalpies. It should be noted that in all cases a "clearing" temperature corresponding to the LC→I transition was not observed due to sample decomposition. It can readily be seen that the transition temperatures vary significantly with chain length. The T_c decreases from 160 °C for $n=4$ to 96 °C for $n=9$ (where n is the total number of carbons in the carboxylate chain). Subsequent values for $n=10$ to $n=20$ remain relatively constant at around 100 °C.

For the complexes with short alkyl chains it is the cohesion of the metallic cores that appears to govern crystal stability. This cohesion is disturbed as the chains get longer which leads to an initial decrease in $T_{K\rightarrow LC}$. In the longer chain compounds crystal stability is dictated by the packing of the fatty acid side chains and $T_{K\rightarrow LC}$ decreases until stability is entirely overtaken by these chain interactions. Further chain extension does not influence $T_{K\rightarrow LC}$ to any great extent. The trend in enthalpy values, while apparently increasing with length of the chain, is more complicated and further elaboration has not been made.

In most cases direct observation of the mesophase using polarizing optical microscopy was not possible due to thermal decomposition of the Ru_2(II,II) complex from air oxidation (even under a constant flow of Ar). The final major characterization tool used for mesophase identification was X-ray powder diffraction. High temperature (above $T_{K\rightarrow LC}$) measurements were made for the $n=7$, 9, 10, 12, 14 and 16 compounds. Several reflections with spacings consistent with a hexagonal columnar mesophase were obtained and intercolumnar spacings were obtained for all but two of them [32,85] (see Table 9). Room-temperature measurements for the same

Table 9
Phase-transition temperatures (°C), ΔH values (kJ mol^{-1}), intercolumnar D_{Col} (LC phase) and interlamellar D_{Lam} (crystalline phase) distances (Å) for $Ru_2(\mu\text{-}O_2CR)_4$ compounds (n = number of carbon atoms in the carboxylate chain)

n	$T_{K\rightarrow LC}$	ΔH	D_{Col}	D_{Lam}	Ref.
4	160	17.2	–	–	[32]
5	158	20	–	–	[85]
7	113	54	–	–	[85]
8	103	48	–	–	[85]
	107	50.2	–	–	[86]
9	96	40	17.6	24.5	[32,85]
10	98	76	18.2	26.6	[85]
11	97	78	–	–	[85]
12	91	41	19.4	31.7	[32]
	99	66	–	–	[85]
	103	72	–	–	[86]
14	98	66	22.0	35.4	[85]
16	99.5	73	–	–	[32]
	102	149	–	42.3	[85]
18	98	145	–	–	[85]
	103	136	–	–	[86]
20	104	155	–	–	[85]
11[a]	52.7	32	–	–	[85,87]
10[b]	79.2	54	–	–	[85,87]

[a] R = CH_2=$CH(CH_2)_8$–.
[b] R = $(CH_3)_2C$=$CHCH_2CH_2CH(CH_3)CH_2$–.

series of compounds show the Ru_2(II,II) compounds to be analogous to their Cu_2(II,II) cousins and assume a lamellar structure. The interlamellar spacings are included in Table 9. A packing order within the columns was also observed leading to a stacking period of the binuclear ruthenium cores of 4.6–4.7 Å.

Modification of the side chain in these $Ru_2(\mu\text{-}O_2CR)_4$ liquid crystals to unsaturated or branched chain fatty acids leads to a substantial decrease in the $T_{K\rightarrow LC}$. For R = CH_2=$CH(CH_2)_8$– and R = $(CH_3)_2C$=$CH(CH_2)_2CH(CH_3)CH_2$– the $T_{K\rightarrow LC}$ values are 52.7 and 79.2 °C, respectively (Table 9) [85,87]. It was concluded that "packing" would be less efficient when branching and/or unsaturation was present and that this results in a less stable crystalline phase compared to the linear chain analogues. The mesophase is therefore manifested at lower temperatures and requires less energy to create; compare ΔH for $Ru_2(O_2CR)_4$, R = CH_2=$CH(CH_2)_8$, at 32.0 kJ mol^{-1} versus R = –$(CH_2)_9CH_3$ at 78.0 kJ mol^{-1}. These compounds are promising because they display a columnar mesophase near room temperature. Unfortunately, the air-sensitivity of all $Ru_2(\mu\text{-}O_2CR)_4$ complexes makes them unlikely candidates for practical application.

A more promising route would be to use the oxidized mixed-valent $[Ru_2(\mu\text{-}O_2CR)_4]X$ salts or $[Ru_2(\mu\text{-}O_2CR)_4L_2]X$ diadducts to create air-stable liquid crystals. Oddly, the fatty-acid derivatives of these complexes have hardly been investigated. Only a short communication by Maldivi *et al*. has outlined the potential

of these as liquid crystals [88]. The syntheses of $Ru_2(\mu\text{-}O_2CR)_4X$ complexes where $R = -n\text{-}C_8H_{17}$ and $-n\text{-}C_{11}H_{23}$ and $X = Cl^-$ and $RCOO^-$ were reported and both of the polymers in which $X = RCOO^-$ displayed a crystal to liquid crystal phase transition at 149 °C with decomposition occurring at 170 °C before any clearing to an isotropic liquid was observed. X-ray diffraction confirmed the mesophase as columnar and therefore established the compounds as the first examples of mixed-valent metallomesogens. The two $Ru_2(\mu\text{-}O_2CR)_4Cl$ derivatives did not display any mesomorphism. It was suggested that the structure of the chloride-bridged species would be similar to the $Ru_2(\mu\text{-}O_2CPr^n)_4Cl$ complex where bridging is not linear [46], i.e. the Ru_2 units are canted with respect to each other. This is not a good precursor for a columnar mesophase where column axes are, ideally, parallel. Linear bridging was therefore postulated to be the case for the derivatives where $X = RCOO^-$ in which the *interdimer* bridging carboxylate "lines up" the Ru_2 units and a relatively linear column results. Evidence for this linearity comes from the structure of $Ru_2(\mu\text{-}O_2CPh)_4(O_2CPh)$ where the fifth interdimer bridging carboxylate bridges in such a way as to lead to linear chains [8]. In any case, the liquid-crystalline properties of the mixed-valent derivatives appear to vary significantly with the bulk of the equatorial R group and the nature of the anion, X [95–97]. Further investigation of these mixed-valent metallomesogens is needed and is ongoing in our laboratory [106] and others [89].

13. Antitumour properties

Diruthenium tetracarboxylates have received far less attention as potential antitumour drugs than their neighbouring dirhodium(II,II) tetracarboxylates [90]. The only "major" study involving ruthenium carboxylates in the context of ruthenium complexes in general was performed by Keppler *et al.* [91] in 1989 on $Ru_2(\mu\text{-}O_2CR)_4Cl$ ($R = CH_3$ and Et) because of their moderate water-solubility. Both compounds showed a small but significant activity towards a P388 leukaemia system with T/C ratios of 125% for $R = CH_3$ and 133% for R = Et. [T/C represents the median survival time per tumour weight of treated (T) animals versus the median survival time per tumour weight of control (C) animals multiplied by 100.] The results are summarized in Table 1010. Efforts to improve the water and ether-solubility

Table 10
Antitumour activity of diruthenium tetracarboxylates (adapted from Ref. [91])

Complex	Dose/mmol kg^{-1} (mg kg^{-1})	Days of treatment	T/C[a] (%)	Tumour system
$Ru_2(\mu\text{-}O_2CCH_3)_4Cl$	0.21 (100)	1	125	P388
$Ru_2(\mu\text{-}O_2CEt)_4Cl$	0.16 (85)	1	125	P388
	0.06 (32)	1,5,9	133	P388

[a] For definition, see text.

of these compounds have been undertaken [25], but no further activity studies have been documented.

Recently Dunbar and coworkers have investigated the binding of guanine bases to various dimetal carboxylates including Ru_2^{5+} species [92,93]. The reaction of two

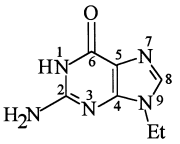

9-EtGH

equivalents of 9-ethylguanine (9-EtGH)to a methanol solution containing the product isolated from a refluxing solution of $Ru_2(\mu\text{-}O_2CCH_3)_4Cl$, $Ag(O_2CCF_3)$ and CF_3CO_2H yielded a complex structure with the formula $[Ru_2(\mu\text{-}O_2CCH_3)_{2-x}(\mu\text{-}O_2CCF_3)_x(9\text{-EtGH})_2(MeOH)_2]\,[O_2CCF_3]_2 \cdot 2MeOH \cdot 0.5\ Et_2O$, where $x = 0.18$. The crystal structure is given in Fig. 23. The 9-EtGH displaces two of the bridging acetates and coordinates (in a bridging fashion) through O^6 and N^7. The two 9-EtGH ligands are situated *cis* to each other in a head-to-tail fashion. No conclusions regarding potential binding to DNA were drawn.

Adenine and adenosine derivatives of $[Ru_2(O_2CCH_3)_4]^+$ have recently been synthesized and characterized by UV–visible, IR, NMR and EPR spectroscopy and magnetic susceptibility, however no crystal structures were reported [104]. The adenine derivative takes the form of a polymer, $[Ru_2(\mu\text{-}O_2CCH_3)_4(adenine)]$, in which the anionic adenine bridges adjacent diruthenium dimers through N^9 and N^3 (or N^1). The adenosine complex is a distinct diadduct, $[Ru_2(\mu\text{-}O_2CCH_3)_4(adenosine)_2]Cl$, in

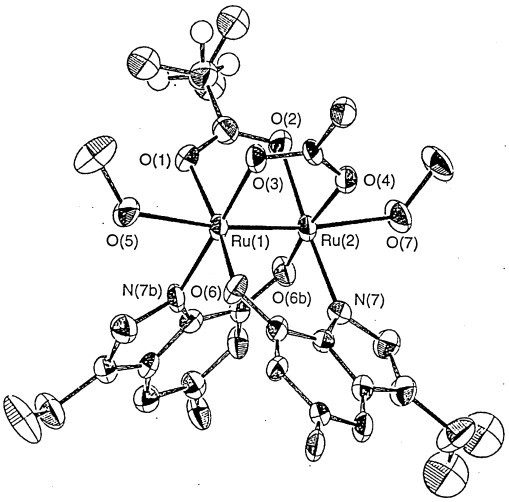

Fig. 23. Structure of the $[Ru_2(\mu\text{-}O_2CCH_3)_{2-x}(\mu\text{-}O_2CCF_3)_x(9\text{-EtGH})_2(MeOH)_2]^+$ cation. Adapted from Ref. [93].

which the adenosines are coordinated through N^7. Both complexes were found to be less toxic than other ruthenium complexes and could potentially form stable complexes by binding at the poly-A region of DNA through the N^7 of adenosine.

14. Catalytic applications

Early studies on $Ru_2(\mu\text{-}O_2CCH_3)_4Cl$ and $Ru_2(\mu\text{-}O_2CCH_3)_4$ [107] showed these complexes to be protonated when treated with fluoroboric acid. While they were not found to be catalytically active by themselves the protonated forms, in the presence of PPh_3, were highly active for the hydrogenation of alkenes and alkynes. Catalytic activity was also displayed if the $Ru_2(II,III)$ complex was dechlorinated prior to protonation and addition of PPh_3. Full characterization of any of the catalytically active species was not undertaken and it seems doubtful, particularly in the case of $Ru_2(\mu\text{-}O_2CCH_3)_4$ that the lantern structure remains intact in the presence of PPh_3. In fact it has been postulated that the active system appears to involve $[Ru(PPh_3)_2(alkene)]^{2+}$ [6].

A more recent study [108] has found $Ru_2(\mu\text{-}O_2CCH_3)_4$ to be a catalyst precursor for these same hydrogenations in methanol under ambient conditions. No acids, phosphines or elevated temperatures were required. Hydrogenation of terminal and cyclic monoenes and terminal alkynes occurred at room temperature and 1 atm of H_2. The reactivity order was: cyclic alkene > terminal alkene > terminal alkyne. The following hydrogenation cycle was postulated.

$$Ru_2(\mu-O_2CCH_3)_4 + H_2 \rightarrow HRu_2(\mu-O_2CCH_3)_3 + H^+ + CH_3CO_2^-$$

$$HRu_2(\mu-O_2CCH_3)_3 + \text{alkene} \rightarrow Ru_2(\mu-O_2CCH_3)_3(\text{alkyl})$$

$$Ru_2(\mu-O_2CCH_3)_3(\text{alkyl}) + H^+ + CH_3CO_2^- \rightarrow Ru_2(\mu-O_2CCH_3)_4 + \text{alkane}$$

These processes proceed without isomerization, which suggests that alkyl formation is irreversible.

Hydrogenation using $Ru_2(\mu\text{-}O_2CCF_3)_4$ was significantly slower than with $Ru_2(\mu\text{-}O_2CCH_3)_4$, presumably due to the slower addition of hydrogen to the electron-poor trifluoroacetate complex.

$Ru_2(\mu\text{-}O_2CCH_3)_4$ has also been found to be effective as a catalyst for the cyclopropanation and cross-metathesis of alkenes [109]. These reactions are carried out by adding ethyldiazoacetate to a mixture containing $Ru_2(\mu\text{-}O_2CCH_3)_4$ and an alkene mixture such as norbornene and styrene. Yields of cyclopropanated styrene and norbornene were 40% and 2%, respectively. The authors proposed that a carbene intermediate, $Ru{=}CHCO_2Et$, was responsible for initiating the reaction and a subsequent reaction with the olefin forms a metallacyclobutane. This intermediate can then react in two ways. It could then undergo metathesis in the usual way or demetalate to form a cyclopropane. The metal can then add ethyldiazoacetate to regenerate the carbene initiator and begin the cycle anew.

15. Conclusion

While diruthenium (and diosmium) tetracarboxylates are relative late-comers to the field of dimetal tetracarboxylates, little time has been lost in investigating their structural and physical properties and exploiting their interesting magnetic and electronic properties to create potential molecular materials and liquid crystals. For diruthenium, the fundamental studies are reaching their peak but the areas of application, in particular their potential as antitumour drugs, are still in their infancy. Diosmium complexes have received very little attention, in part due to their low solubility, a problem we are currently trying to rectify in our laboratory. Both diruthenium and diosmium also have a vast reaction chemistry in which various non-carboxylate-containing products are formed; a field that could warrant its own review. Much work is yet to be done on these unique complexes, the surface has only been scratched. I hope this review will serve as a starting point for further fruitful studies.

16. Addendum

During the preparation of this review a paper by Wesemann and Chisholm appeared [105] detailing the reactions of Ru_2(μ-octanoate)$_4$, octanoate = $^{-}O_2C(CH_2)_6CH_3$, with the potential bridging ligands pyrazine and 4-cyanopyridine (4-cp) and the redox active ligands tetracyanoethylene (TCNE) and *p*-benzoquinone. The increased solubility imparted by the longer chain R group allowed solution studies to be carried out and evidence was found in the pyrazine reaction for three species in equilibrium: Ru_2(μ-octanoate)$_4$(pyz)$_2$, [Ru_2(μ-octanoate)$_4$]$_2$(pyz) and the predominant species (the only one isolated from solution), the [Ru_2(μ-octanoate)$_4$(pyz)]$_n$ polymer. No polymer was formed with 4-cyanopyridine and the major species here was Ru_2(μ-octanoate)$_4$(4-cp)$_2$ with some evidence of weak nitrile coordination in solution. Enhanced π interactions with the pyridine moiety were proposed to be due to the electron-withdrawing nature of the CN group. A redox reaction occurs with TCNE leading to displacement of at least one carboxylate (octanoate) but with no evident Ru–Ru bond cleavage. The exact nature of the product was not determined. *p*-Benzoquinone also undergoes a redox reaction with Ru_2(μ-octanoate)$_4$ but only after it has coordinated. It was postulated to form the somewhat unstable salt, [Ru_2(μ-octanoate)$_4$]$^{+}$[SQ^{-}], SQ^{-} = semiquinone.

A comprehensive article by Miskowski and Gray [110] has recently appeared that covers in detail the variable-temperature magnetic susceptibility and electronic spectral properties of various $Os_2(O_2CR)_4Cl_2$ compounds (R = CH_3, $C(CH_3)_3$, Pr^n). From these measurements it was concluded that the ground-state of these complexes is $^3E_u(\delta^*\pi^*)$ with an accidental near-degeneracy of the δ* and π* similar to what is seen for [$Ru_2(O_2CR)_4$]$^{+}$ complexes. Electronic transitions at 850 nm (δ→δ*), 1200 nm (spin-forbidden δ*→π*) and 394 nm (spin-allowed π(Cl)→π*(Os_2)) were also assigned.

Appendix A

Summary of references for diruthenium and diosmium tetracarboxylates

Complex and L	n	Prep.	Colour	Vib. spec.	Elec. spec.	Mag. susc.	Other[a]
Ru_2(II,III) compounds							
$M[Ru_2(\mu\text{-}O_2CH)_4L_n]X$							
–	0						SCF-Xα-SW [68]
Cl^-	1	[7,71,72,98]	black-brown	[7,71,72,98]	[7]	[7,98]	SCF-Xα-SW [59,68]
Cl^- ($M=K^+$)	2	[20]	brown-black				SCF-Xα-SW [68]
Br^-	1	[7,47]			[7]	[7]	
$M[Ru_2(\mu\text{-}O_2CMe)_4L_n]X$							
–	0	[78,99]					Kinetics [78]
Cl^-	1	[5–7,48,49]	red-brown	[5,7,67,71,72]	[5,7,11,49, 66,71,73]	[5,7]	Echem. [7,66] Catalysis [107]
$Cl^- \cdot 2H_2O$	1	[20]	dark red				
Cl^- ($M=Cs^+$)	2	[20]	red-brown	[72]			Kinetics and Echem. [79]
Br^-	1	[23]		[79]	[23,79]	[23]	
I^-, SCN^-, NO_3^-	1	[7]	brown (NO_3^-)		[7] (NO_3^-)	[7]	Polarography [7] (NO_3^-)
$CH_3CO_2^-$	1	[7]	brown		[7]	[7]	
$CH_3CO_2^- \cdot 0.7H_2O$ ($M=H^+$)	2	[10,11,38]	red	[10,38]	[10,11,38]	[10,38]	Echem. [10,11,38]
$CF_3CO_2^- \cdot 2H_2O$	1	[10,31]	red-brown	[10,31]	[10,31]	[10,31]	Echem. [10,31]
$CF_3CO_2^- \cdot 2CH_3OH$	1	[11]	brown		[11]		Echem. [11]
$C_6H_5C{\equiv}CCO_2^- \cdot H_2O$	1	[25]	orange-brown	[25]	[25]	[25]	Echem. [25]
$HPhPO_2^-$ ($M=H^+$)	2	[24]	brown	[24]	[24]	[24]	Echem. [24]
$PhPO_3^-$ ($M=H^+$)	2	[24]	brown	[24]	[24]	[24]	Echem. [24]
H_2O ($X=BF_4^-$)	2	[20]	red-brown	[71]	[71]		Kinetics, Thermo. and Echem. [69]
H_2O ($X=SO_4^{2-}$)	2	[25,101]	yellow-brown	[25]	[25]	[25]	Echem. [25]
H_2O ($X=BPh_4^-$)	2	[25,26]	orange-brown	[25,26]	[25,26]	[25,26]	Echem. [25]
$H_2O \cdot 3H_2O$ ($X=PF_6^-$)	2	[27]	red-orange	[27]	[27]	[27]	Echem. [27]
D_2O ($X=BF_4^-$)	2	[102]			[102]		
THF ($X=BF_4^-$)	2	[22]	red	[22]	[22]	[22]	
DMSO ($X=PF_6^-$)	2	[27]	red	[27]	[27]	[27]	Echem. [27]
DMF ($X=PF_6^-$)	2	[27]	orange-red	[27]	[27]	[27]	Echem. [27]
$DMF \cdot DMF$ ($X=PF_6^-$)	2	[27]	orange-red	[27]	[27]	[27]	Echem. [27]
$OPPh_3 \cdot CH_2Cl_2$ ($X=PF_6^-$, BF_4^-)$OPPh_3 \cdot CH_2ClCH_2Cl$	2	[22,23]	red-brown	[22,23]	[23]	[22,23]	NMR [22]
$O{=}P(C_6H_4\text{-}p\text{-}F)_3$ ($X=PF_6^-$)	2	[23]	brown-yellow	[23]	[23]	[23]	
$O{=}P(C_6H_4\text{-}p\text{-}Cl)_3$ ($X=PF_6^-$)	2	[23]	brown-yellow	[23]	[23]	[23]	

$O{=}P(C_6H_4\text{-}p\text{-}OCH_3)_3$ ($X{=}PF_6^-$)	2	[23]	yellow	[23]	[23]	[23]	
(+)–PHOS · $5H_2O$;((+)–PHOS)((−)–PHOS) · H_2O	2	[103]	brown	[103]	[103]	[103]	Echem. [103]
pyz ($X{=}BPh_4^-$)	1	[26]	green-grey	[26]		[26]	
adenine	1	[104]	pink	[104]	[104]	[104]	NMR, ESR [104]
adenosine	2	[104]		[104]	[104]	[104]	NMR, ESR [104]
$[RuCl(MeCN)_3(PPh_3)_2][Ru_2Cl_2(\mu\text{-}O_2CMe)_4]$		[56]	purple		[56]	[56]	NMR, ESR [56]
$M[Ru_2(\mu\text{-}O_2CEt)_4L_n]X$							
Cl^-	1	[5,14,20]	dark-brown	[5,71,72]	[5,71–73]	[5]	
Br^- ($M{=}NBu_4^{n+}$)	2	[72]	orange	[72]	[72]		
$CH_3CH_2CO_2^-$	1	[11,31]	red-brown	[31]	[11,31]	[31]	Echem. [11,31]
H_2O ($X{=}BF_4^-$)	2	[21]	brown	[21]	[21]		
THF ($X{=}BF_4^-$)	2	[14]	orange	[14]	[14]	[14]	NMR [14]
$OPPh_3 \cdot CH_2Cl_2$ ($X{=}BF_4^-$)	2	[14]	brown	[14]	[14]	[14]	
$py \cdot CH_2Cl_2$ ($X{=}BF_4^-$)	2	[14]		[14]	[14]	[14]	
phz ($X{=}BF_4^-$)	1	[21]	red-brown	[21]		[21]	
$[Ru_2(\mu\text{-}O_2CPr^n)_4L_n]X$							
–	0	[55]		[55]	[55]		NMR [55]
Cl^-	1, (2)	[5,46,55]	dark brown	[5,55,60,67,71,72]	[5,55,61,71–73]	[5,60,77]	NMR [55], ESR [77,60], Echem. [77,61], MS [82], calorimetry [61], theory [60]
Br^-	1, (2)	[72]	green (?)	[72]	[72,73]		
$[Ru_2(\mu\text{-}O_2C\text{-}n\text{-}C_7H_{15})_4L_n]X$							
–	0	[55]		[55]			NMR [55]
Cl^-	1	[55]		[55]			NMR [55]
$[Ru_2(\mu\text{-}O_2C(n\text{-}C_pH_q))_4L_n]X$							
Cl^- (p=8, q=17); (p=11, q=23)	1	[88]					DSC, Mic., XRD [88]
$n\text{-}C_pH_qCO_2^-$ (p=8, q=17); (p=11, q=23)	1	[88]					DSC, Mic., XRD [88]
$Ru_2(\mu\text{-}O_2CCH{=}CH_2)_4Cl$	1	[15]	brown	[15]	[15]	[15]	
$[Ru_2(\mu\text{-}O_2CCH{=}CHCH_3)_4L_n]X$							
–	0	[55]		[55]			NMR [55]
Cl^-	1	[55]		[55]			NMR [55]
$Ru_2(\mu\text{-}O_2CCH_2CH{=}CH_2)_4Cl$	1	[15]	dark brown	[15]	[15]	[15]	
$Ru_2(\mu\text{-}O_2C(CH_3)C{=}CH_2)_4Cl$	1	[15]	dark brown	[15]	[15]	[15]	
$[Ru_2(\mu\text{-}O_2CCH{=}C(CH_3)_2)_4L_n]X$							
–	0	[55]		[55]			NMR [55]
Cl^-	1	[55]		[55]			NMR [55]
I^-	1				[73]		
$[Ru_2(\mu\text{-}O_2CBu^t)_4L_n]X$							
Cl^-	1	[18,28]	brown	[18]	[28]	[18]	MS [28]
SCN^-	1	[28]	red	[28]	[28]	[28]	MS [28]

Complex and L	n	Prep.	Colour	Vib. spec.	Elec. spec.	Mag. susc.	Other[a]
Cl^-, H_2O	2	[18]	red-brown	[18]		[18]	
Cl^-, THF	2	[18]	red	[18]		[18]	
Cl^-, $OPPh_3$	2	[28]	red	[28]	[28]	[28]	MS [28]
SCN^-, $OPPh_3$	2	[28]		[28]	[28]	[28]	MS [28]
THF	2	[28]	dark brown	[28]	[28]	[28]	
$[Ru_2(\mu\text{-}O_2CBu^t)_4(tempo)_2][Ru_2(\mu\text{-}O_2CBu^t)_4(H_2O)_2](BF_4)_2$	–	[51]				[51]	ESR [51]
$[Ru_2(\mu\text{-}O_2CBu^t)_4(nitPh)]_n(BF_4)_n$	–	[52]				[52]	
$[Ru_2(\mu\text{-}O_2CCHMe_2)_4L_n]X$							
Cl^-	1	[18,28,100]	brown	[18]	[28]	[18]	
Cl^-, H_2O	2	[18]	red-brown	[18]		[18]	
Cl^-, THF	2	[18]	red	[18]		[18]	
Cl^-, $OPPh_3$	2	[28]	dark red	[28]	[28]	[28]	MS [28]
THF ($X=BF_4^-$)	2	[28]	dark brown	[28]		[28]	
$OPPh_3$ ($X=BF_4^-$)	2	[28]	red	[28]	[28]	[28]	
THF, $OPPh_3$ ($X=BF_4^-$)	2	[28]		[28]		[28]	
$[Ru_2(\mu\text{-}O_2CCHMeEt)_4L_n]X$							
Cl^-	1	[28]	red	[28]		[28]	
Cl^-, $OPPh_3$	2	[28]	red	[28]		[28]	
$[Ru_2(\mu\text{-}O_2CCHMePh)_4L_n]X$							
Cl^-	1	[28]	red	[28]	[28]	[28]	MS [28]
SCN^-	1	[28]	red	[28]	[28]	[28]	
Cl^-, $OPPh_3$	2	[28]	red	[28]	[28]	[28]	
SCN^-, $OPPh_3$	2	[28]		[28]		[28]	
$[Ru_2(\mu\text{-}O_2CCHEt_2)_4L_n]X$							
Cl^-	1	[28]	red	[28]	[28]	[28]	MS [28]
SCN^-	1	[28]	red	[28]	[28]	[28]	MS [28]
Cl^-, $OPPh_3$	2	[28]	brown	[28]	[28]	[28]	
SCN^-, $OPPh_3$	2	[28]		[28]	[28]	[28]	
$Ru_2(\mu\text{-}O_2CCMePh_2)_4Cl$	1	[16]	brown	[16]	[16]	[16]	
$Ru_2(\mu\text{-}O_2CCH_2Cl)_4Cl\cdot 2H_2O$	1	[7]	brown	[7]	[7]	[7]	
$Ru_2(\mu\text{-}O_2CCF_3)_4(CF_3CO_2)$	1	[11,31]	orange-brown	[31]	[11,31]	[31]	Echem. [11,31]
$[Ru_2(\mu\text{-}O_2CPh)_4L_n]X$							
–	0	[55]		[55]			NMR [55]
Cl^-	1	[7,9,10,14,53,55,100]	brown	[9,10,12,53,55]	[9,55]	[7,9]	Echem. [9], NMR [55]
Br^-	1	[7]				[7]	
$CF_3CO_2^-\cdot 2H_2O$	1		red-orange	[10,12]	[10]	[10]	Echem. [10]
$PhCO_2^-\cdot PhCO_2H$	1	[8]	red	[8]		[8]	TGA [8]
THF ($X=BF_4^-$)	2	[14]	orange	[14]	[14]	[14]	

$OPPh_3$ ($X=BF_4^-$)	2	[14]	yellow-brown	[14]	[14]	[14]	
py ($X=BF_4^-$)	2	[14]		[14]	[14]	[14]	
C_2H_5OH, HSO_4^- (double-salt)	2, 2	[25]	dark red	[25]	[25]	[25]	Echem. [25]
$[RuCl(MeCN)_3(PPh_3)_2][Ru_2Cl_2(\mu\text{-}O_2CPh)_4]$		[56]	brown		[56]	[56]	NMR, ESR [56]
$[Ru_2(\mu\text{-}O_2C(\text{cyclo-}C_6H_{11})_4L_n]X$							
Cl^-	1	[14]	brown	[14]	[14]	[14]	
THF ($X=BF_4^-$)	2	[14]	orange	[14]	[14]	[14]	
$OPPh_3$ ($X=BF_4^-$)	2	[14]	yellow-brown	[14]	[14]	[14]	
py ($X=BF_4^-$)	2	[14]		[14]	[14]	[14]	
$[Ru_2(\mu\text{-}O_2CC_6H_4\text{-}p\text{-}Me)_4L_n]X$							
–	0	[55]					NMR [55]
Cl^-	1	[55]		[55]	[55]		NMR [55]
THF ($X=BF_4^-$)	2	[55]		[55]	[55]		NMR [55]
$[RuCl(MeCN)_3(PPh_3)_2][Ru_2Cl_2(\mu\text{-}O_2CC_6H_4\text{-}p\text{-}Me)_4]$		[56]	black		[56]	[56]	NMR, ESR [56]
$[Ru_2(\mu\text{-}O_2CC_6H_4\text{-}p\text{-}Bu^t)_4L_n]X$							
Cl^-	1	[13]	brown	[13]	[13]	[13]	
THF ($X=BF_4^-$, OH^-)	2	[13]	red-brown	[13]	[13]	[13]	
$Ru_2(\mu\text{-}O_2CC_6H_4\text{-}p\text{-}OMe)_4Cl$	1	[9,54]		[9]	[9]	[9]	Echem. [9]
$[RuCl(MeCN)_4PPh_3][Ru_2Cl_2(\mu\text{-}O_2CC_6H_4\text{-}p\text{-}OMe)_4]$		[56]	purple		[56]	[56]	NMR, ESR [56]
$[Ru_2(O_2CC_6H_4\text{-}\sigma\text{-}Cl)_4L_n]X$							
Cl^-	1	[14]	brown	[14]	[14]	[14]	
THF ($X=BF_4^-$)	2	[14]	orange	[14]	[14]	[14]	NMR [14]
$OPPh_3$ ($X=BF_4^-$)	2	[14]	brown	[14]	[14]	[14]	
py ($X=BF_4^-$)	2	[14]		[14]	[14]	[14]	
$[Ru_2(\mu\text{-}O_2CC_6H_4\text{-}\sigma\text{-}OH)_4L_n]X$							
Cl^-	1	[14]	brown	[14]	[14]	[14]	
THF ($X=BF_4^-$)	2	[14]	orange	[14]	[14]	[14]	NMR [14]
$OPPh_3$ ($X=BF_4^-$)	2	[14]	brown	[14]	[14]	[14]	
$[Ru_2(\mu\text{-asp})_4L_n]X$ (asp = 2-acetoxybenzene)							
Cl^-	1	[12]	red-brown	[12]		[12]	Echem. [12]
$CF_3CO_2^-$	1	[12]	orange	[12]		[12]	Echem. [12]
NO_3^-	1	[12]	orange	[12]		[12]	Echem. [12]
$Ru_2(\mu\text{-}O_2CC_7H_9)_4Cl$ ($-C_7H_9$ = endo-bicyclo[2.2.1]-hept-5-ene)	1	[15]	beige	[15]	[15]	[15]	
$Ru_2(\mu\text{-}O_2CC_8H_{11})_4Cl$ ($-C_8H_{11}$ = bicyclo[2.2.1]hept-5-ene-2-methyl)	1	[15]	light brown	[15]	[15]	[15]	
$Ru_2(\mu\text{-}O_2CC_4H_4N)_4(THF)(Cl)$ ($-C_4H_4N$ = 2-pyrrole)	2	[17]	brown	[17]	[17]	[17]	
$[Ru_2(\mu\text{-}O_2CR)_4L_n]X$ (R = N-methyl-2-pyrrole; 2-furyl; 2-thienyl)							

Complex and L	n	Prep.	Colour	Vib. spec.	Elec. spec.	Mag. susc.	Other[a]
Cl^-	1	[19]	brown	[19]		[19]	
THF ($X=BF_4^-$)	2	[19]	red-brown	[19]		[19]	
$OPPh_3$ ($X=BF_4^-$)	2	[19]	red	[19]		[19]	
(R = 2-indolyl)							
Cl^-, THF	2	[19]	brown	[19]		[19]	
(R = 2-benzofuryl)							
–	0	[19]	red-brown	[19]		[19]	
Cl^-	1	[19]	brown	[19]		[19]	
$OPPh_3$ ($X=BF_4^-$)	2	[19]	red	[19]		[19]	
Mixed Ru_2(II,III) carboxylates							
$Ru_2(\mu\text{-}O_2CMe)_2(\mu\text{-}O_2CCF_3)_2(O_2CCF_3)$	1	[10]	red	[10]	[10]	[10]	Echem. [10]
$[Ru_2(\mu\text{-}O_2CMe)_2(\mu\text{-}O_2CBu^t)_2L_n]Cl^-$; SCN^-Cl^- and $OPPh_3$	12	[28,28]		[28,28]	[28,28]	[28,28]	MS [28] (SCN^-)
$Ru_2(\mu\text{-}O_2CPh)_2(\mu\text{-}O_2CCF_3)_2(O_2CCF_3)$	1	[10]	red	[10]	[10]	[10]	Echem. [10]
$Ru_2(\mu\text{-asp})_2(\mu\text{-}O_2CPh)_2Cl$	1	[12]	orange	[12]		[12]	Echem. [12]
Ru_2(II,II) complexes							
$Ru_2(\mu\text{-}O_2CH)_4L_n$							
–	0	[30]	orange-brown	[30]	[30]	[30]	Echem. [30], PES [35], theory [59]
DM-DCNQI	1	[62]	blue	[62]	[62]		EPR [62]
H_2O	2	[30]	dark red	[30]	[30]	[30]	Echem. [30]
THF	2	[30]	red-orange	[30]	[30]	[30]	Echem. [30]
$Ru_2(\mu\text{-}O_2CCH_3)_4L_n$							
–	0	[30]	orange-brown	[30]	[30]	[30]	Echem. [30], Catalysis [108,109]
H_2O	2	[30,85]	brown	[30]	[30]	[30]	Echem. [30]
THF	2	[29,30]	yellow-brown	[29,30]	[29,30]	[29,30]	Echem. [30]
MeOH; Me_2CO; MeCN	2	[30]	brown	[30]	[30]	[30]	Echem. [30]
$Ru_2(\mu\text{-}O_2CEt)_4L_n$							
–	0	[30]	dark brown	[30]	[30]	[30]	Echem., MS [30]
THF; Me_2CO	2	[30]	brown	[30]	[30]	[30]	Echem. [30]
$Ru_2(\mu\text{-}O_2CPr^n)_4$	–	[32,55]		[55]		[32]	DSC, XRD [32]; NMR [55]
$Ru_2(\mu\text{-}O_2C(CH)_2CH_3)_4$	–	[55]		[55]			NMR [55]
$Ru_2(\mu\text{-}O_2CBu^n)_4$	–	[85]	brown	[85]		[85]	DSC, Mic., XRD [85]
$Ru_2(\mu\text{-}O_2C(CH)C(CH_3)_2)_4$	–	[55]		[55]			NMR [55]
$Ru_2(\mu\text{-}O_2C\text{-}n\text{-}C_6H_{13})_4$	–	[85]		[85]		[85]	DSC, Mic., XRD [85]
$Ru_2(\mu\text{-}O_2C\text{-}n\text{-}C_7H_{15})_4$	–	[55,85,86]		[55,85]	[55]	[55,85]	DSC, Mic., XRD [85,86]; NMR, Echem. [55]
$Ru_2(\mu\text{-}O_2C\text{-}n\text{-}C_8H_{17})_4$	–	[32]				[32]	DSC, Mic., XRD [32]
$Ru_2(\mu\text{-}O_2C\text{-}n\text{-}C_9H_{19})_4$	–	[85]	brown	[85]		[85]	DSC, Mic., XRD [32]
$Ru_2(\mu\text{-}O_2C\text{-}n\text{-}C_{10}H_{21})_4$	–	[85]	brown	[85]		[85]	DSC, Mic., XRD [32]

$Ru_2(\mu\text{-}O_2C\text{-}n\text{-}C_{11}H_{23})_4L_n$							
–	0	[32,85,86]	yellow-brown	[85]		[32,85]	DSC, Mic., XRD [32,85]
pyz	1	[85]	dark purple	[85]		[85]	DSC, Mic., XRD [85]
$Ru_2(\mu\text{-}O_2C\text{-}n\text{-}C_{13}H_{27})_4$	–	[85]		[85]		[85]	DSC, Mic., XRD [85]
$Ru_2(\mu\text{-}O_2C\text{-}n\text{-}C_{15}H_{31})_4$	–	[32,84,85]	brown	[85]		[32,84,85]	DSC, Mic., XRD [32,85]
$Ru_2(\mu\text{-}O_2C\text{-}n\text{-}C_{17}H_{31})_4$	–	[85,86]	brown	[85]		[85]	DSC, Mic., XRD [85,86]
$Ru_2(\mu\text{-}O_2C\text{-}n\text{-}C_{19}H_{39})_4$	–	[85]	yellow-brown	[85]		[85]	DSC, Mic., XRD [85]
$Ru_2(\mu\text{-}O_2CCH_2{=}CH(CH_2)_8)_4$	–	[85,87]	brown	[85]		[85]	DSC, Mic., XRD [85,87]
$Ru_2(\mu\text{-}O_2CCH_2CH(CH_3)(CH_2)_2CH{=}C(CH_3)_2)_4$	–	[85,87]	brown	[85]		[85]	DSC, Mic., XRD [85,87]
$Ru_2(\mu\text{-}O_2CCF_3)_4L_n$							
–	0	[31]	orange	[31]	[31]	[31]	Echem. [31]; PES [35], Catalysis [108]
THF	2	[31]	orange	[31]	[31]	[31]	Echem. [31]
tempo	2	[36]	dark brown			[36]	
$Ru_2(\mu\text{-}O_2C\text{-}n\text{-}C_7F_{15})_4$	–	[85]	red	[85]		[85]	DSC, Mic., XRD [85]
$Ru_2(\mu\text{-}O_2CH_2Cl)_4L_n$							
–	0	[30]	golden-brown	[30]	[30]	[30]	Echem. [30]
THF	2	[30]	yellow-orange	[30]	[30]	[30]	Echem. [30]
$Ru_2(\mu\text{-}O_2CPh)_4L_n$							
–	0	[30,55]	dark red	[8,30,55]	[30]	[30]	Echem. [30], NMR [55]
THF; Me_2CO	2	[30]	brown	[30]	[30]	[30]	Echem. [30]
HO_2CPh	2	[8]	black	[8]		[8]	TGA [8]
$Ru_2(\mu\text{-}O_2CC_6H_4\text{-}p\text{-}Me)_4$	–	[55]		[55]			NMR [55]
$[RuCl(MeCN)_3(PPh_3)]_2[Ru_2(\mu\text{-}O_2CC_6H_4\text{-}p\text{-}Me)_4Cl_2]$	–	[56]	purple		[56]	[56]	NMR, ESR [56]
$Ru_2(\mu\text{-}O_2CC_6F_5)_4(tempo)_2$	–	[36]	dark brown			[36]	
$Ru_2(\mu\text{-}O_2CPh_3)_4(H_2O)(EtOH)\cdot 2EtOH$	–	[37]	yellow				
$Ru_2(\mu\text{-aspirinate})_4(NO)\cdot 4H_2O$	–	[12]	dark brown	[12]	[12]	[12]	Echem. [12]
$Ru_2(\mu\text{-adamantyl})_4(MeOH)_2$	–	[34]	light brown	[34]	[34]		
$Ru_2(\mu\text{-L-mandelate})_4(H_2O)_2$	–	[33]	yellow		[33]	[33]	CD [33]
"Ru_2(I,I) compounds"							
$Ru_2(O_2CH)_4(NO)_2$	–						Theory [48]
$Ru_2(O_2CCH_3)_4(NO)_2$	–	[31]	orange-red	[31]	[31]	[31]	MS, Echem. [31]
$Ru_2(O_2CEt)_4(NO)_2$	–	[31]	red	[31]	[31]	[31]	MS, Echem., NMR [31]
$Ru_2(O_2CPh)_4(NO)_2$	–	[31]		[31]	[31]	[31]	MS, Echem. [31]
$Ru_2(O_2CCF_3)_4(NO)_2$	–	[31]		[31]	[31]	[31]	MS, Echem., NMR [31]; PES [48]
Os_2(III,III) compounds							
$Os_2(\mu\text{-}O_2CCH_3)_4Cl_2$	–	[41,43]	brown-red	[41,43, 74,110]	[43,110]	[43,110]	ESR, NMR [41]; MS [43,57]
$Os_2(\mu\text{-}O_2CCD_3)_4Cl_2$	–	[74]	brown	[74]			

Complex and L	n	Prep.	Colour	Vib. spec.	Elec. spec.	Mag. susc.	Other[a]
$Os_2(\mu\text{-}O_2CEt)_4L_n$							
Cl^-	2	[42,43]	dark green	[43,75]	[43,75]	[42,43]	Echem. [42,43]; MS [43,57]
Br^-	2	[44]	red-brown		[44]	[44]	Echem., NMR [44]
$Os_2(\mu\text{-}O_2CPr^n)_4L_n$							
Cl^-	2	[42,43]	dark-green	[43,75,110]	[43,75,110]	[42,43,110]	Echem. [42,43], MS [43]; NMR [43,57]
Br^-	2	[44]	red-brown		[44]	[44]	Echem., NMR [44]
$Os_2(\mu\text{-}O_2CCMe_3)_4Cl_2$	–	[110]	green-brown	[110]	[110]	[110]	
$Os_2(\mu\text{-}O_2CCH_2Cl)_4Cl_2$	–	[42]	green	[43,75]	[43,75]	[43]	
$Os_2(\mu\text{-}2\text{-}PBZ)_4Cl_2$	–	[58]	brown		[58]	[58]	Echem. [58]
Os_2(II,III) compounds							
$Os_2(\mu\text{-}O_2CCH_3)_4L_n$							
Cl^-, py	2	[41]		[41]			
py	2	[41]	red	[41]			
$[(\eta^5\text{-}C_5H_5)_2Co]$ $[Os_2(\mu\text{-}O_2CEt)_4Cl_2]$	–	[45]	yellow-green		[45]	[45]	Echem., ESR [45]
$[(\eta^5\text{-}C_5H_5)_2Co]$ $[Os_2(\mu\text{-}O_2CPr^n)_4Cl_2]$	–	[45]	yellow-green		[45]	[45]	Echem., ESR [45]

[a] Abbreviations: SCF-Xα-SW = self-consistent field, Xα, scattered wave (calculations); Echem. = electrochemistry; Thermo. = thermodynamics; NMR = nuclear magnetic resonance; ESR = electron spin resonance; DSC = differential scanning calorimetry; XRD = X-ray diffraction; MS = mass spectrometry; TGA = thermal gravimetric analysis; PES = photoelectron spectroscopy; CD = circular dichroism.

References

[1] F.A. Cotton, G. Wilkinson, Advanced Inorganic Chemistry, 5th ed., Wiley Interscience, New York, 1988.
[2] F.A. Cotton, R.A. Walton, Multiple Bonds Between Metal Atoms, 2nd ed., Clarendon Press, Oxford, 1993.
[3] (a) A.R. Chakravarty, Proc. Indian Natl. Sci. Acad. 52A (1986) 749. (b) M.C. Barral, R. Jiménez-Aparicio, J.L. Priego, E.C. Royer, F.A. Urbanos, An. Quím. Int. Ed. 93 (1997) 277.
[4] E.A Seddon, K.R. Seddon, The Chemistry of Ruthenium, Elsevier, Amsterdam, 1984, p. 175.
[5] T.A. Stephenson, G. Wilkinson, J. Inorg. Nucl. Chem. 28 (1966) 2285.
[6] R.W. Mitchell, A. Spencer, G. Wilkinson, J. Chem. Soc., Dalton Trans. (1973) 846.
[7] M. Mukaida, T. Nomura, T. Ishimori, Bull. Chem. Soc. Jpn. 45 (1972) 2143.
[8] M. Spohn, J. Strähle, W. Hiller, Z. Naturforsch. 41B (1986) 541.
[9] B.K. Das, A.R. Chakravarty, Polyhedron 7 (1988) 685.
[10] P. Higgins, G.M. McCann, J. Chem. Soc., Dalton Trans. (1988) 661.
[11] F.A. Cotton, M. Matusz, B. Zhong, Inorg. Chem. 27 (1988) 4368.
[12] A. Carvill, P. Higgins, G.M. McCann, H. Ryan, A. Shiels, J. Chem. Soc., Dalton Trans. (1989) 2435.
[13] M.C. Barral, R. Jiménez-Aparicio, J.L. Priego, E.C. Royer, E. Gutiérrez-Puebla, C.R. Valero, Polyhedron 11 (1992) 2209.
[14] M.C. Barral, R. Jiménez-Aparicio, C. Rial, E.C. Royer, M.J. Saucedo, F.A. Urbanos, Polyhedron 9 (1990) 1723.
[15] M. McCann, A. Carvill, P. Guinan, P. Higgins, J. Campbell, H. Ryan, M. Walsh, G. Ferguson, J. Gallagher, Polyhedron 10 (1991) 2273.
[16] F.A. Cotton, Y. Kim, T. Ren, Polyhedron 12 (1993) 607.
[17] M.C. Barral, R. Jiménez-Aparicio, E.C. Royer, C. Ruíz-Valero, M.J. Saucedo, F.A. Urbanos, Inorg. Chem. 33 (1994) 2692.
[18] M.C. Barral, R. Jiménez-Aparicio, J.L. Priego, E.C. Royer, M.J. Saucedo, F.A. Urbanos, U. Amador, J. Chem. Soc., Dalton Trans. (1995) 2183.
[19] M.C. Barral, R. Jiménez-Aparicio, J.L. Priego, E.C. Royer, M.J. Saucedo, F.A. Urbanos, Polyhedron 14 (1995) 2419.
[20] A. Bino, F.A. Cotton, T.R. Felthouse, Inorg. Chem. 18 (1979) 2599.
[21] F.A. Cotton, Y. Kim, T. Ren, Inorg. Chem. 31 (1992) 2723.
[22] F.A. Urbanos, M.C. Barral, R. Jiménez-Aparicio, Polyhedron 7 (1988) 2597.
[23] M.C. Barral, R. Jiménez-Aparicio, E.C. Royer, C. Ruíz-Valero, F.A. Urbanos, E. Gutiérrez-Puebla, A. Monge, Polyhedron 8 (1989) 2571.
[24] M. McCann, E. Murphy, C. Cardin, M. Convery, Polyhedron 12 (1993) 1725.
[25] M. McCann, A. Carvill, C. Cardin, M. Convery, Polyhedron 12 (1993) 1163.
[26] F.D. Cukiernik, A.M. Giroud-Godquin, P. Maldivi, J.C. Marchon, Inorg. Chim. Acta 215 (1994) 203.
[27] K.D. Drysdale, E.J. Beck, T.S. Cameron, K.N. Robertson, M.A.S. Aquino, Inorg. Chim. Acta 256 (1997) 243.
[28] M.C. Barral, R. Jiménez-Aparicio, J.L Priego, E.C. Royer, F.A. Urbanos, U. Amador, J. Chem. Soc., Dalton Trans. (1997) 863.
[29] A.J. Lindsay, R.P. Tooze, M. Motevalli, M.B. Hursthouse, G. Wilkinson, J. Chem. Soc., Chem. Commun. (1984) 1383.
[30] A.J. Lindsay, G. Wilkinson, M. Motevalli, M.B. Hursthouse, J. Chem. Soc., Dalton Trans. (1985) 2321.
[31] A.J. Lindsay, G. Wilkinson, M. Motevalli, M.B. Hursthouse, J. Chem. Soc., Dalton Trans. (1987) 2723.
[32] P. Maldivi, A.M. Giroud-Godquin, J.C. Marchon, D. Guillon, A. Skoulios, Chem. Phys. Lett. 157 (1989) 552.
[33] F.A. Cotton, V.M. Miskowski, B. Zhong, J. Am. Chem. Soc. 111 (1989) 6177.
[34] F.A. Cotton, L. Labella, M. Shang, Inorg. Chim. Acta 197 (1992) 149.

[35] (a) D.L. Clark, J.C. Green, C.M. Redfern, G.E. Quelch, I.H. Hillier, M.F. Guest, Chem. Phys. Lett. 154 (1989) 326. (b) D.L. Clark, J.C. Green, C.M. Redfern, J. Chem. Soc., Dalton Trans. (1989) 1037. (c) G.E. Quelch, I.H. Hillier, M.F. Guest, J. Chem. Soc., Dalton Trans. (1990) 3075.
[36] A. Cogne, E. Belorizky, J. Laugier, P. Rey, Inorg. Chem. 33 (1994) 3364.
[37] F.A. Cotton, L.M. Daniels, P.A. Kibala, M. Matusz, W.J. Roth, W. Schwotzer, W. Wong, B. Zhong, Inorg. Chim. Acta 215 (1994) 9.
[38] M.G.B. Drew, P. Higgins, G.M. McCann, J. Chem. Soc., Chem. Commun. (1987) 1385.
[39] J.L. Bear, B. Han, S. Huang, J. Am. Chem. Soc. 115 (1993) 1175.
[40] C. Sudha, S.K. Mandal, A.R. Chakravarty, Inorg. Chem. 33 (1994) 4878.
[41] D.S. Moore, A.S. Alves, G. Wilkinson, J. Chem. Soc., Chem. Commun. (1981) 1164.
[42] T.A. Stephenson, D.A. Tocher, M.D. Walkinshaw, J. Organomet. Chem. 232 (1982) C51.
[43] T. Behling, G. Wilkinson, T.A. Stephenson, D.A. Tocher, M.D. Walkinshaw, J. Chem. Soc., Dalton Trans. (1983) 2109.
[44] T.W. Johnson, S.M. Tetrick, R.A. Walton, Inorg. Chim. Acta 167 (1990) 133.
[45] S.M. Tetrick, V.T. Coombe, G.A. Heath, T.A. Stephenson, R.A. Walton, Inorg. Chem. 23 (1984) 4567.
[46] M.J. Bennet, K.G. Caulton, F.A. Cotton, Inorg. Chem. 8 (1969) 1.
[47] T. Kimura, T. Sakurai, M. Shima, T. Togano, M. Mukaida, T. Nomura, Bull. Chem. Soc. Jpn. 55 (1982) 3927.
[48] T. Togano, M. Mukaida, T. Nomura, Bull. Chem. Soc. Jpn. 53 (1980) 2085.
[49] D.S. Martin, R.A. Newman, L.M. Vlasnik, Inorg. Chem. 19 (1980) 3404.
[50] R.E. Marsh, V. Schomaker, Inorg. Chem. 20 (1981) 299.
[51] M. Handa, Y. Sayama, M. Mikuriya, R. Nukada, I. Hiromitsu, K. Kasuga, Bull. Chem. Soc. Jpn. 68 (1995) 1647.
[52] M. Handa, Y. Sayama, M. Mikuriya, R. Nukada, I. Hiromitsu, K. Kasuga, Chem. Lett. (1996) 201.
[53] M. Abe, Y. Sasaki, T. Yamaguchi, T. Ito, Bull. Chem. Soc. Jpn. 65 (1992) 1585.
[54] B.K. Das, A.R. Chakravarty, Polyhedron 10 (1991) 491.
[55] M.H. Chisholm, G. Christou, K. Folting, J.C. Huffman, C.A. James, J.A. Samuels, J.L. Wesemann, W. H Woodruff, Inorg. Chem. 35 (1996) 3643.
[56] B.K. Das, A.R. Chakravarty, Inorg. Chem. 31 (1992) 1395.
[57] F.A. Cotton, A.R. Chakravarty, D.A. Tocher, T.A. Stephenson, Inorg. Chim. Acta 87 (1984) 115.
[58] F.A. Cotton, T. Ren, M.J. Wagner, Inorg. Chem. 32 (1993) 965.
[59] J.G. Norman Jr.,, G.E. Renzoni, D.A. Case, J. Am. Chem. Soc. 101 (1979) 5256.
[60] (a) J. Telser, R.S. Drago, Inorg. Chem. 23 (1984) 3114. (b) J. Telser, R.S. Drago, Inorg. Chem. 24 (1985) 4765.
[61] R.S. Drago, R. Cosmano, J. Telser, Inorg. Chem. 23 (1984) 4514.
[62] S.C. Huckett, C.A. Arrington, C.J. Burns, D.L. Clark, B.I. Swanson, Synth. Met. 414243 (1991) 2769.
[63] D. Li, S.C. Huckett, T. Frankcom, M.T. Paffet, J.D. Farr, M.E. Hawley, S. Gottesfeld, J.D. Thompson, C.J. Burns, B.I. Swanson, in: T. Bein (Ed.), Supramolecular Architecture: Synthetic Control in Thin Films and Solids, American Chemical Society Symposium Series 499, American Chemical Society, Washington, DC, 1992, chapter 4.
[64] K.R. Dunbar, J. Cluster Sci. 5 (1994) 125.
[65] X. Ouyang, C. Campana, K.R. Dunbar, Inorg. Chem. 35 (1996) 7188.
[66] C.R. Wilson, H. Taube, Inorg. Chem. 14 (1975) 2276.
[67] R.J.H. Clark, M.L. Franks, J. Chem. Soc., Dalton Trans. (1976) 1825.
[68] J.G. Norman Jr.,, H.J. Kolari, J. Am. Chem. Soc. 100 (1978) 791.
[69] F.A. Cotton, M. Matusz, J. Am. Chem. Soc. 110 (1988) 5761.
[70] F.A. Cotton, T. Ren, J.L. Eglin, Inorg. Chem. 30 (1991) 2552.
[71] R.J.H. Clark, L.T.H. Ferris, Inorg. Chem. 20 (1981) 2759.
[72] V.M. Miskowski, T.M. Loehr, H.B. Gray, Inorg. Chem. 26 (1987) 1098.
[73] V.M. Miskowski, H.B. Gray, Inorg. Chem. 27 (1988) 2501.
[74] R.J.H. Clark, A.J. Hempleman, D.A. Tocher, J. Am. Chem. Soc. 110 (1988) 5968.
[75] R.J.H. Clark, A.J. Hempleman, J. Chem. Soc., Dalton Trans. (1988) 2601.

[76] K. Nakamoto, Infrared and Raman Spectra of Inorganic and Coordination Compounds, Wiley Interscience, New York, 1986, p. 231.
[77] F.A. Cotton, E. Pedersen, Inorg. Chem. 14 (1975) 388.
[78] (a) J.E. Earley, R.N. Bose, B.H. Berrie, Inorg. Chem. 22 (1983) 1836. (b) A.O. Oyetunji, O. Olubuyide, J.F. Ojo, J.E. Earley, Polyhedron 10 (1991) 829.
[79] (a) A.C. Dema, R.N. Bose, Inorg. Chem. 28 (1989) 2711. (b) M. Everhart, J.E. Earley, Polyhedron 7 (1988) 1393.
[80] T. Behling, G. Wilkinson, T.A. Stephenson, D.A. Tocher, M.D. Walkinshaw, J. Chem. Soc., Dalton Trans. (1984) 305.
[81] R.S. Drago, Coord. Chem. Rev. 33 (1980) 251.
[82] E. Forest, P. Maldivi, J.C. Marchon, H. Virelizier, Spectrosc. Int. J. 5 (1987) 129.
[83] C.J. O'Connor, Prog. Inorg. Chem. 29 (1982) 203.
[84] J.C. Marchon, P. Maldivi, A.M. Giroud-Godquin, D. Guillon, A. Skoulios, D.P. Strommen, Philos. Trans. R. Soc. Lond. A 330 (1990) 109.
[85] L. Bonnet, F.D. Cukiernik, P. Maldivi, A.M. Giroud-Godquin, J.C. Marchon, M. Ibn-Elhaj, D. Guillon, A. Skoulios, Chem. Mater. 6 (1994) 31.
[86] R.G. Cayton, M.H. Chisholm, F.D. Darrington, Angew. Chem. Int. Ed. Engl. 29 (1990) 1481.
[87] P. Maldivi, L. Bonnet, A.M. Giroud-Godquin, M. Ibn-Elhaj, D. Guillon, A. Skoulios, Adv. Mater. 5 (1993) 909.
[88] F.D. Cukiernik, P. Maldivi, A.M. Giroud-Godquin, J.C. Marchon, M. Ibn-Elhaj, D. Guillon, A. Skoulios, Liq. Cryst. 9 (1991) 903.
[89] F.D. Cukiernik, private communication, 1996.
[90] N. Farrel, J. Inorg. Biochem. 14 (1981) 261 and references therein.
[91] B.K. Keppler, M. Henn, U.M. Juhl, M.R. Berger, R. Niebl, F.E. Wagner, Prog. Clin. Biochem. Med. 10 (1989) 41.
[92] K.R. Dunbar, J.H. Matonic, V.P. Saharan, C.A. Crawford, G. Christou, J. Am. Chem. Soc. 116 (1994) 2201.
[93] C.A. Crawford, E.F. Day, V.P. Saharan, K. Folting, J.C. Huffman, K.R. Dunbar, G. Christou, J. Chem. Soc., Chem. Commun. (1996) 1113.
[94] E.J. Beck, K.D. Drysdale, C.A. Murphy, L.K. Thompson, L. Li, M.A.S. Aquino, submitted for publication.
[95] L. Bonnet, F.D. Cukiernik, A.M. Giroud-Godquin, D. Guillon, M. Ibn-Elhaj, P. Maldivi, J.C. Marchon, A. Skoulios, M. Taylor, Proc. 3rd Int. Symp. on Metallomesogens, Pensicola, Spain, June 3–5, 1993, p. 36.
[96] P. Maldivi, J.C. Marchon, F.D. Cukiernik, M. Ibn-Elhaj, D. Guillon, A.M. Giroud-Godquin, N. Gon, M.C. Molina, A Skoulios, Proc. 9th Congress Argentino de Fisicoquimica, San Luis, Argentina, November 21–25, 1994, p. F22.
[97] E.H. Boubkari, M. Ibn-Elhaj, D. Guillon, P. Maldivi, J.C. Marchon, A.M. Giroud-Godquin, F.D. Cukiernik, Z. Chaia, Proc. 4th Int. Symp. on Metallomesogens, Cetraro, Italy, June 6–9, 1995, p. C4.
[98] M. Mukaida, T. Nomura, T. Ishimori, Bull. Chem. Soc. Jpn. 40 (1967) 2462.
[99] J.P. Collin, A. Jouaiti, J.P. Sauvage, W.C. Kaska, M.A. McLoughlin, N.L. Keder, W.T. Harrison, G.D. Stucky, Inorg. Chem. 29 (1990) 2238.
[100] E.B. Boyar, P.A. Harding, S.D. Robinson, C.P. Brock, J. Chem. Soc., Dalton Trans. (1986) 1771.
[101] A.N. Zhilyaev, T.A. Fomina, I.V. Kuz'menko, A.V. Rotov, I.B. Baranovskii, Russ. J. Inorg. Chem. 34 (1989) 532.
[102] I.V. Kuz'menko, A.N. Zhilyaev, T.A. Fomina, M.A. Porai-Koshits, I.B. Baranovskii, Russ. J. Inorg. Chem. 34 (1989) 1457.
[103] M. McCann, E. Murphy, Polyhedron 11 (1992) 2327.
[104] S. Gangopadhyay, P.K. Gangopadhyay, J. Inorg. Biochem. 66 (1997) 175.
[105] J.L. Wesemann, M.H. Chisholm, Inorg. Chem. 36 (1997) 3258.
[106] M.A.S. Aquino, E.J. Beck, J.F. Caplan, K.D. Drysdale, R. Lawrence, D. MacDonald, T.S. Cameron, K.N. Robertson, L.K. Thompson, Abstracts for 31st International Conference on Coordination Chemistry, Vancouver, Canada, August 18–23, 1996, p. 172.

[107] P. Legzdins, R.W. Mitchell, G.L. Rempel, J.D. Ruddick, G. Wilkinson, J. Chem. Soc. (A) (1970) 3322.
[108] A.J. Lindsay, G. McDermott, G. Wilkinson, Polyhedron 7 (1988) 1239.
[109] A.F. Noels, A. Demonceau, E. Carlier, A.J. Hubert, R.L. Márquez-Silva, R.A. Sánchez-Delgado, J. Chem. Soc., Chem. Commun. (1988) 783.
[110] V.M. Miskowski, H.B. Gray, in: H. Yersin (Ed.), Electronic and Vibronic Spectra of Transition Metal Complexes – Topics in Current Chemistry Vol. 191, Springer-Verlag, Berlin, 1997, p. 41.